Philipp Leser

Enlarged Higgs sectors as a window into flavor symmetric extensions of the standard model of particle physics

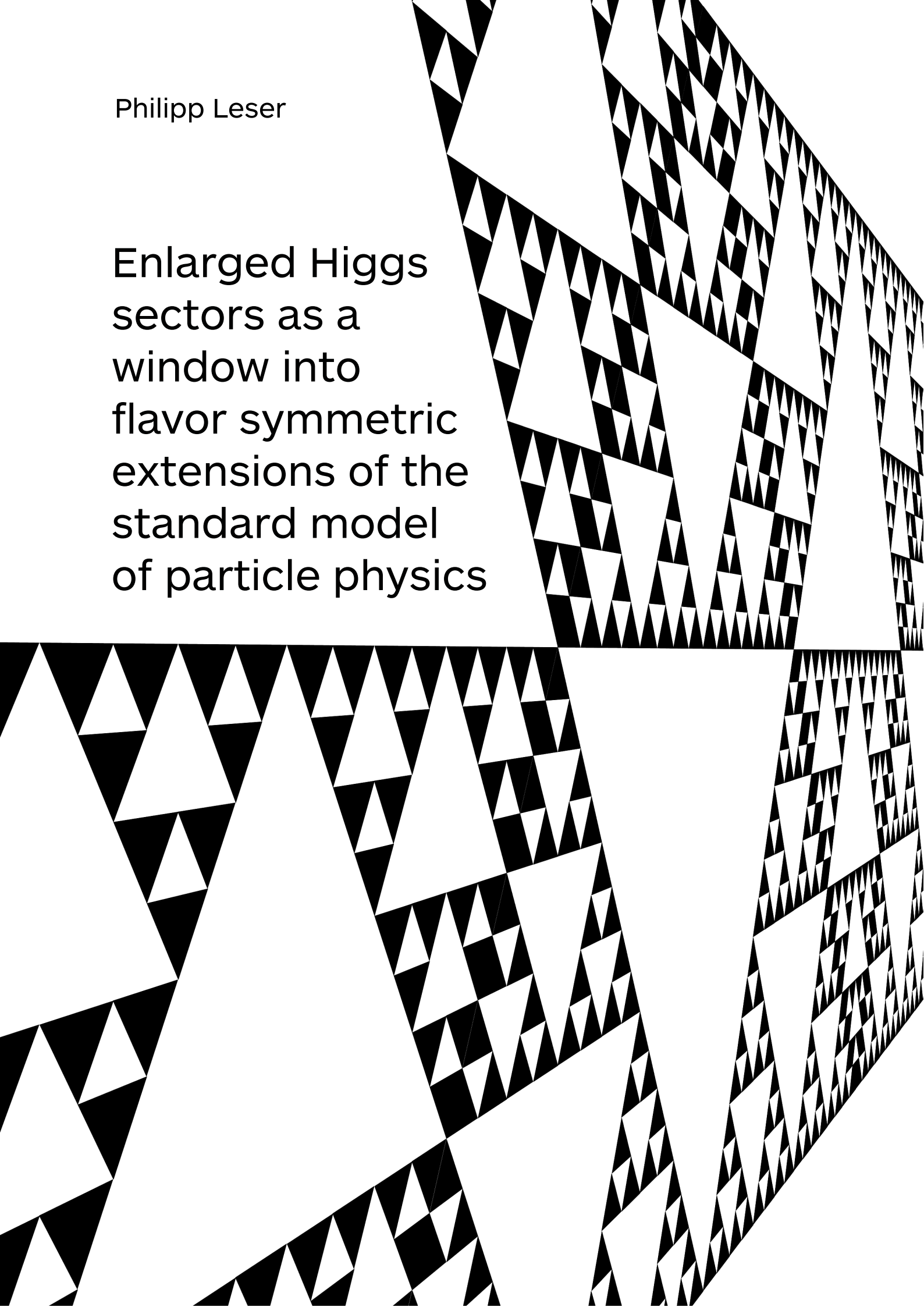

Enlarged Higgs sectors as a window into flavor symmetric theories beyond the standard model of particle physics

Dissertation zur Erlangung des akademischen Grades

Dr. rer. nat.
im Fach Physik

vorgelegt von

Philipp Leser

aus Herten

Fakultät Physik
Technische Universität Dortmund

Dortmund, im Dezember 2012

Gutachter dieser Arbeit sind
Herr Prof. Dr. Heinrich Päs und Frau Prof. Dr. Gudrun Hiller.
Datum der mündlichen Prüfung: 31. Januar 2013

This thesis contains work that has been previously published by the author:

- [1] G. Bhattacharyya, P. Leser, and H. Päs, "Exotic Higgs boson decay modes as a harbinger of S_3 flavor symmetry", Phys. Rev. **D83**, 011701(R), arXiv: 1006.5597 [hep-ph] (2011)

- [2] P. Leser and H. Päs, "Neutrino mass hierarchy and the origin of leptonic flavor mixing from the righthanded sector", Phys. Rev. **D84**, 017303, arXiv: 1104.2448 [hep-ph] (2011)

- [3] T. W. Kephart, P. Leser, and H. Päs, "Knotted strings and leptonic flavor structure", Mod. Phys. Lett. **A27**, 1250224, arXiv: 1106.6201 [hep-ph] (2012)

- [4] G. Bhattacharyya, P. Leser, and H. Päs, "Novel signatures of the Higgs sector from S_3 flavor symmetry", Phys. Rev. **D86**, 036009, arXiv: 1206.4202 [hep-ph] (2012)

- [5] I. d. M. Varzielas, D. Emmanuel-Costa, and P. Leser, "Geometrical CP violation from non-renormalisable scalar potentials", Phys. Lett. **B716**, 193, arXiv: 1204.3633 [hep-ph] (2012)

- [6] G. Bhattacharyya, I. d. M. Varzielas, and P. Leser, "Common origin of fermion mixing and geometrical CP violation, and its test through Higgs physics at the LHC", Phys. Rev. Lett. **109**, 241603, arXiv: 1210.0545 [hep-ph] (2012)

Summary

The flavor puzzle refers to the existence of three generations of quarks and leptons with identical gauge couplings but widely hierarchical masses. These generations mix among each other, but with very different mixing matrices in the quark and lepton sectors respectively. Flavor models used to address these issues often lack unique predictions and testability. Consequently, in this thesis we investigate phenomenological models that aim to solve parts of the flavor puzzle, but are testable using collider experiments. A neutrino mixing model based on the symmetry S_3 is analyzed which contains a Higgs sector potentially testable at the LHC through exotic decays. We also propose a model based on $\Delta(27)$, which for the first time provides a calculable, geometrical phase stable up to all orders as the only source of CP violation. The model can reproduce all CKM data while having a symmetry breaking sector testable at the LHC. Finally—as an alternative to discrete symmetries—using a class of generic seesaw models we investigate the consequences of a scenario in which all the neutrino mixing is generated in a heavy right-handed Majorana sector. We show that even in the generic class of models considered, common experimental predictions such as a normal neutrino mass hierarchy emerge.

Zusammenfassung

Das Flavorproblem beschreibt drei Generationen von Quarks und Leptonen, die zwar identische Eichkopplungen aber stark hierarchische Massen aufweisen. Diese Generationen mischen untereinander, allerdings sind die Strukturen der Mischungsmatrizen in den Quark- und Leptonsektoren sehr verschieden. Flavormodelle, die diese Probleme zu beheben versuchen, haben oft wenig eindeutige Vorhersagen und sind kaum testbar. Aus diesem Grund untersuchen wir phänomenologische Flavormodelle, die mit Beschleunigerexperimenten überprüfbar sind. Ein Neutrinomischungsmodell auf Basis der Gruppe S_3 wird vorgestellt, dessen Higgs-Sektor am LHC mithilfe von exotischen Zerfällen untersucht werden kann. Weiterhin postulieren wir ein Modell auf Basis der Gruppe $\Delta(27)$, das erstmalig eine berechenbare, geometrische Phase enthält, die in allen Ordnungen stabil bleibt, und die die einzige Quelle der CP-Verletzung darstellt. Das Modell reproduziert die CKM-Daten vollständig, wobei der symmetriebrechende Sektor überprüfbare LHC-Signale enthält. Als eine Alternative zu diskreten Symmetrien untersuchen wir mithilfe eines generischen Seesaw-Modells die Konsequenzen eines Szenarios, in dem die gesamte Neutrinomischung im schweren rechtshändigen Majorana-Sektor des Modells generiert wird. Wir zeigen, dass selbst in dieser generischen Klasse von Modellen experimentelle Vorhersagen wie eine *normale* Neutrinohierarchie enthalten sind.

Contents

1 Introduction

On July 4, 2012, a promising candidate for the last missing piece of the standard model of particle physics was discovered at the Large Hadron Collider (LHC), located at CERN in Geneva. As we will review in this chapter, this Higgs particle is of fundamental importance, yet its discovery nevertheless does not answer all open questions: Indeed, the field of particle physics in 2012 is at the crossroads. Although successful tests of the standard model of particle physics have been ongoing at various collider experiments for decades, especially the mechanism of spontaneous symmetry breaking (SSB), whose realization would lead to the existence of the Higgs boson has been mostly untested so far, with previous experiments only being able to give exclusion ranges for the mass of the particle. After the discovery of a Higgs-like particle it will now be important to pinpoint the exact mechanism of symmetry breaking involved through measurements of production rates, decays and thus ultimately of the fundamental couplings. The LHC is also the experiment that should finally shed a light onto large parts of the parameter space for supersymmetric extensions of the standard model, which have been proposed to solve several problems the theory has.

Among these problems—some of which we will discuss in section 1.3 of this work—the *flavor puzzle* is especially mesmerizing: It describes three almost identical generations of elementary particles for whose existence no explanation has yet been discovered. It also refers to the fact that the generations of particles are not perfect copies of each other, but exhibit strong mass hierarchies. Transitions from a particle of one generation to a particle of another generation are also possible, and the transition rates are governed by mixing matrices whose entries seem too patterned to be random.

Flavor models that address these issues often lack unique predictions and have limited testability. In this work we deal with the flavor puzzle and its possible connection to signals visible at the LHC. We propose discrete symmetries as the governing principle behind the observed patterns of particle mixing in the lepton and quark sectors. As an improvement of the experimental testability of these models, the symmetries are also responsible for extended electroweak symmetry breaking sectors, leading to signals involving Higgs-like particles that can be tested at the LHC. We thus promote the symmetry breaking sector to a window into the fundamental patterns that appear in the flavor puzzle.

Also, for the first time we propose a flavor model based on the discrete symmetry group $\Delta(27)$, which not only successfully reproduces the Cabbibo-Kobayashi-Maskawa (CKM) mixing, but also includes a geometrically calculable phase in the symmetry breaking vacuum which can act as the source of CP violation in the CKM sector. The model can also be extended to include the leptons and it features a scalar breaking sector at a low energy scale which can be tested at the LHC.

As an alternative to the approach based on discrete symmetries, we also investigate a generic seesaw model where the neutrino mixing matrix is generated by the heavy right-handed Majorana sector, a result of physics at the grand unified theory (GUT) scale. We show that even in this generic case without a specific flavor symmetry, predictions for the measurable neutrino data emerge.

1.1 The standard model of particle physics

The standard model of particle physics [7–10] is a framework that explains all basic interactions among particles. It is highly successful experimentally [11], yet cannot explain all of the observed phenomena, as will be more extensively explained in section 1.3. Because of this, extensions of the standard model have to be considered. An important key to evaluating these extensions is the symmetry breaking process, in which the mechanism of SSB is employed in order to mediate between an unbroken, fully symmetric energy scale of the theory and the obviously less symmetric lower scale at which our observations in experiments take place. The particular way in which this mechanism works, specifically which symmetry breaking fields are involved and what their couplings to the standard model sector are provides a window into physics models beyond the standard model. In light of the recent experimental results from the LHC [12, 13] hinting at the existence of a scalar particle that can play the role of the Higgs boson [14], this approach is highly relevant. As a starting point, it is prudent to list the basic building blocks of this mechanism:

1.2 Symmetry groups and the standard model

Interactions between subatomic particles are governed by the electromagnetic, weak, and strong forces. In the framework of quantum field theory these forces are described by the electroweak theory[1]—which is a unification of the electromagnetic and weak

[1] also called Glashow-Weinberg-Salam (GWS) theory.

forces—and quantum chromodynamics (QCD) respectively. The standard model consists of these dynamic theories understood as acting on a number of fundamental particles that are otherwise not predicted by theory. These fundamental matter particles can be found in the left half of figure 1.1. As an umbrella for most of modern particle physics the standard model has lead to highly detailed predictions and has been experimentally supported to an astonishing degree [11]. In the language of group theory the interaction content of the standard model can be written schematically as the product of three groups:

$$\mathsf{SU}(3)_C \times \mathsf{SU}(2)_L \times \mathsf{U}(1)_Y. \tag{1.1}$$

Each of these is a group of continuous local transformations, i.e. the parameters of the transformations depend on the Minkowski spacetime coordinate x. As a consequence of the locality of the transformations, gauge fields have to be introduced to keep the Lagrangian invariant at all points of spacetime. Physically the gauge fields have to be treated as dynamical variables and are usually interpreted as representing physical particles that serve as mediators of the force the local symmetry group describes. In figure 1.1 the gauge fields are displayed in the rightmost column.

The group $\mathsf{SU}(3)_C$ describes QCD, the theory of strong interactions. The index C stands for the *color* charge that is associated with QCD. The fundamental particles that take part in strong interactions—the *quarks* **u**p, **c**harm, **t**op, and **d**own, **s**trange, **b**ottom—are each assigned to the three-dimensional fundamental representation **3** of $\mathsf{SU}(3)_C$. Each of the three dimensions corresponds to one of the three different color charges, whimsically called *red*, *green*, and *blue*. The number of force mediators is given by the dimension of the adjoint representation of the gauge group. In the case of QCD the adjoint representation of $\mathsf{SU}(3)_C$ is the octect **8**. The eight mediators are the *gluons* and carry a color/anticolor charge.

The non-Abelian nature of $\mathsf{SU}(3)_C$ gives rise to the properties of *confinement* and *asymptotic freedom*: It is not possible to separate two quarks from each other, because the strength of the force does not diminish with distance. Quarks are thus confined into

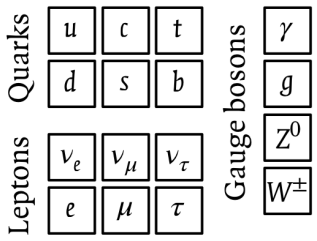

Figure 1.1: The particle content of the standard model.

mesons (quark–anti-quark) and baryons (three quarks), both in singlets of $\mathsf{SU}(3)_C$. As energy increases the force grows weaker which means that quarks can be considered asymptotically free. In the high energy regime QCD is thus accessible to being treated in the context of perturbation theory.

In equation (1.1) the remaining product group $\mathsf{SU}(2)_L \times \mathsf{U}(1)_Y$ represents the Glashow-Weinberg-Salam (GWS) theory, a unified theory of the weak interactions and quantum electrodynamics (QED). The models and consequences discussed in this dissertation belong to this electroweak sector of the standard model and to extensions thereof. The GWS gauge group has $3 + 1$ generators of which three are broken in the process of electroweak symmetry breaking, leading to three massive vector bosons $W^{\pm}, Z^0$ and one massless mediator, γ, listed in the rightmost column of figure 1.1.

As indicated by the index L of $\mathsf{SU}(2)_L$, only left-chiral fields take part in the weak interactions mediated by $\mathsf{SU}(2)_L$, where a left-chiral spinor field ψ_L is defined by $\gamma_5 \psi_L = -\psi_L$. This fact manifests itself in the assignments of the particles to representations of $\mathsf{SU}(2)_L$. The left-handed doublets of the standard model are

$$\begin{gathered} \begin{pmatrix} \nu_e \\ e^- \end{pmatrix}_L, \quad \begin{pmatrix} \nu_\mu \\ \mu^- \end{pmatrix}_L, \quad \begin{pmatrix} \nu_\tau \\ \tau^- \end{pmatrix}_L, \\ \begin{pmatrix} u \\ d \end{pmatrix}_L, \quad \begin{pmatrix} c \\ s \end{pmatrix}_L, \quad \begin{pmatrix} t \\ b \end{pmatrix}_L. \end{gathered} \tag{1.2}$$

In each doublet, the upper and lower entries differ by an electric charge of 1 (in units of the electron charge), i.e. the neutrinos are uncharged while electron, muon, and tau have charge -1. The up-type quarks have charge $+\frac{2}{3}$ and the down-type quarks have charge $-\frac{1}{3}$. Analogous to the treatment of spin in classical quantum mechanics—which is also described by an $\mathsf{SU}(2)$ symmetry—the third component of the *weak isospin* is $+\frac{1}{2}$ for the upper entries and $-\frac{1}{2}$ for the lower entries.

1.2.1 Mass generation of fermions and gauge bosons

The right-handed fields that appear in mass terms in the Lagrangian are singlets under $\mathsf{SU}(2)_L$:

$$\mathscr{L}_Y \supset -m_e \bar{e}_L e_R. \tag{1.3}$$

In this expression, m_e as a constant is uncharged under $\mathsf{SU}(2)_L$ as is the singlet e_R, while e_L belongs to the doublet of equation (1.2). The expression is thus not invariant

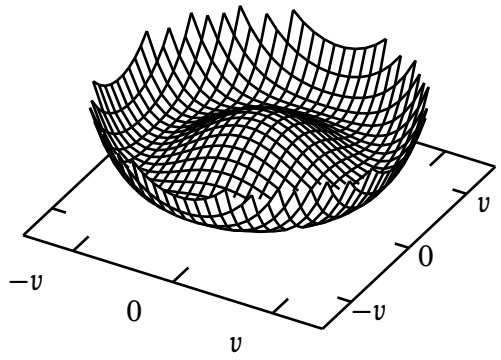

Figure 1.2: Illustration of the potential shown in equation (1.5). This is the so-called *Mexican hat–potential*.

under $\mathsf{SU}(2)_{\mathrm{L}}$ and therefore all mass terms with an equivalent structure are forbidden. The celebrated solution to this problem is to explain the origin of m_e dynamically. Instead of starting with the constant m_e, a new field ϕ, which is a doublet under $\mathsf{SU}(2)_{\mathrm{L}}$, is inserted into the expression:

$$\mathscr{L}_{\mathrm{Y}} \supset -y_e \phi \bar{e}_{\mathrm{L}} e_{\mathrm{R}}, \tag{1.4}$$

where y_e is a dimensionless coupling constant. As the group $\mathsf{SU}(2)_{\mathrm{L}}$ has a multiplication rule $\mathbf{2} \otimes \mathbf{2} = \mathbf{1}$, the expression is now invariant. The mass term of equation (1.3) is obtained when ϕ is replaced by its vacuum expectation value (VEV) $\langle \phi \rangle$, which breaks the $\mathsf{SU}(2)_{\mathrm{L}}$ symmetry spontaneously[2].

The field ϕ obtains a VEV that corresponds to the stable minimum of its potential. As an example, consider a scalar field φ with an associated scalar potential V_φ:

$$V_\varphi = -\frac{1}{2}\lambda^2 \left(|\varphi|^2 - \frac{1}{2}v^2 \right)^2 . \tag{1.5}$$

There are two classes of extremal points for this potential: It has an unstable maximum at the origin and a ring of stable minima with radius v. At the origin, the potential is invariant under $\mathsf{U}(1)$ rotations, as can be seen in figure 1.2. However, as soon as the potential acquires a VEV on the ring of stable minima, this symmetry is broken spontaneously. A remnant of the symmetry is left in the fact that each point along the ring of minima is equivalent, parametrized by a massless Goldstone boson, which can be understood as an excitation along the ring of minima. The excitation along the orthogonal axis corresponds to a massive physical scalar.

[2] As opposed to a nonspontaneous or explicit breaking by manual insertion of a noninvariant term. Such a noninvariant term, which has a coupling with a positive mass dimension is called *soft*.

The equivalent process in $\mathsf{SU}(2)_L \times \mathsf{U}(1)_Y$ involves the scalar field ϕ of equation (1.4), which has four degrees of freedom:

$$\phi = \begin{pmatrix} \phi^+ + i\chi^+ \\ \phi^0 + i\chi^0 \end{pmatrix}. \tag{1.6}$$

When the symmetry is broken, each field acquires a VEV. However, due to the spherical structure of the potential, the doublet can always be rotated in such a way that

$$\langle \phi \rangle = \begin{pmatrix} 0 \\ v + h \end{pmatrix}, \tag{1.7}$$

where v is the VEV and h is the real physical scalar field. Through this process, the mass term in equation (1.3) as well as the masses of the three massive gauge bosons $W^\pm$ and Z^0 are generated. The masses of the gauge bosons are not generated through Yukawa terms, but come into play as a consequence of the covariant derivative:

$$D_\mu \phi = \left[\partial_\mu - \frac{ig}{2} \tau^a W^a_\mu - ig' \frac{Y}{2} B_\mu \right] \phi. \tag{1.8}$$

Here, g and g' are electroweak coupling constants, the τ^a and Y are the generators of $\mathsf{SU}(2)_L$ and $\mathsf{U}(1)_Y$ respectively, and W^a_μ, B_μ are the gauge boson fields. After expanding the term $|D_\mu \phi|^2$ and inserting the VEV of equation (1.7), three massive gauge boson states and one massless state emerge. The massless state is identified as the photon γ, the massive states are $W^\pm$ and Z^0. It is reassuring although not trivial that breaking the symmetry spontaneously conserves the number of degrees of freedom: Three Goldstone bosons that should appear are absorbed in the process of making $W^\pm$ and Z^0 massive. This process of SSB in which the gauge boson and fermion masses are generated is commonly known as the *Higgs mechanism* [14]. The real physical scalar particle h is consequently called the *Higgs particle*[3].

1.2.2 Three generations of fermions

It is an experimental observation that quarks and leptons appear in three *generations* which differ in mass, but are identical with respect to charges under the gauge symmetries. In the picture of figure 1.1, the gauge symmetry that describes the standard

[3] This name is often applied without great consistency. Generally, when one encounters a *Higgs* particle in a model, it can be any scalar taking part in the process of electroweak SSB. It does not necessarily have to have the properties of the standard model Higgs particle.

model mediates only between the rows of the diagram, i.e. between the upper and lower entries of the $\mathsf{SU}(2)_\mathrm{L}$ doublets. However, transitions between the generations are nevertheless possible due to a mismatch of the symmetry basis and the mass basis of the fermions: $\mathsf{SU}(2)_\mathrm{L}$ transitions via the $W^\pm$ boson mediate for example between a u' and a d' quark in the weak eigenbasis, but expressed in terms of mass eigenstates which are also eigenstates of the QCD interactions, d' is a mixture of the mass eigenstates d, s, and b. This was first postulated by Nicola Cabbibo in 1963 for the case of the first two generations and thus the mixing angle describing the d/s mixing is called θ_C [15].

As QCD processes mediate between mass eigenstates and as those are observed in experiments, when writing u, c, t or d, s, b mass eigenstates are usually implied.

The matrix expressing the full mixing information between all three quark generations is called the CKM matrix. It is unitary and approximately diagonal, the largest off-diagonal element being the Cabbibo angle θ_C [16]:

$$\left|V_\mathrm{CKM}\right| = \begin{pmatrix} 0.97427 \pm 0.00015 & 0.22534 \pm 0.00065 & 0.00351^{+0.00015}_{-0.00014} \\ 0.22520 \pm 0.00065 & 0.97344 \pm 0.00016 & 0.0411^{+0.0011}_{-0.0005} \\ 0.00867^{+0.00029}_{-0.00031} & 0.0404^{+0.0011}_{-0.0005} & 0.999146^{+0.000021}_{-0.000046} \end{pmatrix}. \tag{1.9}$$

Note that although in this numerical representation of the magnitudes nine entries are given, there are only three real degrees of freedom and one complex, commonly expressed as three mixing angles and one complex phase. The CKM matrix is obtained by inspecting a charged, i.e. $W^\pm$, current and switching to the weak eigenbasis:

$$\begin{aligned} & W^+_\mu \bar{u}_\mathrm{L} \gamma^\mu d_\mathrm{L} \\ &= W^+_\mu \bar{u}_\mathrm{L} V_u^\dagger V_u \gamma^\mu V_d^\dagger V_d d_\mathrm{L} \\ &= W^+_\mu \bar{u}'_\mathrm{L} \left[V_u V_d^\dagger\right] \gamma^\mu d'_\mathrm{L}, \end{aligned} \tag{1.10}$$

where V_i is the matrix of eigenvectors that diagonalizes the product of mass matrices $m_i m_i^\dagger$ and $V_\mathrm{CKM} = V_u V_d^\dagger$.

In the leptonic sector there exists an equivalent mixing matrix, the Pontecorvo-Maki-Nakagawa–Sakata (PMNS) matrix, which encodes the neutrino mixing information between the weak eigenstates ν_e, ν_μ, ν_τ and the mass eigenstates ν_1, ν_2, ν_3. Numerically,

it is strikingly different from the CKM matrix in that it involves large mixing angles[4], instead of being almost diagonal. The current best fit values for the mixing angles are [18]

$$\theta_{12} = 33.3°, \tag{1.11a}$$

$$\theta_{23} = \begin{cases} 40.0° & \text{normal} \\ 50.4° & \text{inverted} \end{cases}, \tag{1.11b}$$

$$\theta_{13} = 8.6°, \tag{1.11c}$$

where the indices refer to the weak eigenstates and the angles θ_{12}, θ_{23}, and θ_{13} are commonly referred to as *solar*, *atmospheric*, and *reactor* angles. The angles are related to the entries of the PMNS matrix U via these equations: [19]

$$\theta_{13} = \arcsin\left(\left|U_{13}\right|\right), \tag{1.12a}$$

$$\theta_{12} = \begin{cases} \arctan\left(\frac{|U_{12}|}{|U_{11}|}\right) & \text{if } U_{11} \neq 0 \\ \frac{\pi}{2} & \text{else} \end{cases}, \tag{1.12b}$$

$$\theta_{23} = \begin{cases} \arctan\left(\frac{|U_{23}|}{|U_{33}|}\right) & \text{if } U_{33} \neq 0 \\ \frac{\pi}{2} & \text{else} \end{cases}. \tag{1.12c}$$

As it is currently not possible to accurately measure the neutrinos' masses, but only the mass squared differences, the mass hierarchy is not fixed. The data allows for a *normal* hierarchy, in which m_3^2—i.e. the mass associated with the third mass eigenstate—is the largest squared mass, and an *inverted* hierarchy, in which m_3^2 is the lightest squared mass.

The PMNS matrix can be expressed using unitary transformation matrices equivalent to the case of the CKM matrix in equation (1.10), with mass matrices for the charged leptons and neutrinos in place of the mass matrices for up- and down-type quarks. In most cases[5] the neutrino mass matrix is normal—i.e. $MM^\dagger = M^\dagger M$—and can thus be diagonalized using an eigenvalue decomposition yielding a unitary transformation matrix instead of using a singular value decomposition[6]. It is customary to transform the Lagrangian into the basis where the charged lepton mass matrix is diagonal. This basis is called *flavor basis*. In many models the natural *symmetry basis* as dictated by the model symmetry has a nondiagonal charged lepton mass matrix.

[4] A thorough review of the history of the neutrino can be found in reference [17].
[5] specifically, if Majorana neutrinos are assumed.
[6] This is the case in the seesaw mechanism introduced in the next section.

1.3 Two shortcomings of the standard model

While the standard model as a theory is in excellent agreement with the data, it has some shortcomings that have lead to the advent of a multitude of extensions. As an example, the *hierarchy problem*, which refers to the fact that the Higgs boson mass should be of GUT scale but electroweak precision data points to a Higgs at the electroweak scale, is unsolved in the framework of the standard model. Its solution is one of the prominent features of supersymmetry. At this point, we are going to elaborate on two shortcomings of the standard model that are of importance to this work:

1.3.1 Massive neutrinos

The existence of small neutrino masses is experimentally well-established [20–23] by the observance of neutrino oscillations and is encoded in the PMNS matrix introduced in the last section. The absolute scale of the neutrino masses can be deduced from cosmological experiments [24–33], given as the sum of all neutrino masses. The current bound is

$$\sum m_i^\nu < 0.5\,\mathrm{eV}, \tag{1.13}$$

where m_i^ν is the mass of the ith neutrino mass eigenstate. Generating this mass using a mass term like the one shown in equation (1.3) requires right-handed neutrinos, which do not exist in the standard model.

Adding neutrino masses to the theory involves two building blocks:

Dirac masses The most straightforward way to generate neutrino masses is to add right-handed neutrinos and construct a Dirac mass term as in equation (1.3). A disadvantage of this method is that even the highest possible neutrino mass allowed by the bound of equation (1.13) is many orders of magnitude smaller than the masses of the charged leptons and quarks, requiring unnaturally small Yukawa couplings.

Majorana masses As neutrinos are uncharged, they can be Majorana particles, i.e. they can be their own antiparticles [34]. In this case, it is possible to construct a *Majorana mass term*[7] [35]:

$$\mathscr{L}_\nu \supset \bar{\nu}_L M \nu_R^C. \tag{1.14}$$

The Majorana mass M is not generated by the standard model Higgs mechanism and is thus not required to lay at the TeV scale. A tell-tale sign for the Majorana nature of

[7] The position of the charge conjugation superscript C is important: $\bar{\nu}_L^C \nu_R$ is a Majorana mass term for a right-handed neutrino ν_R, the one given in equation (1.14) generates a left-handed Majorana mass.

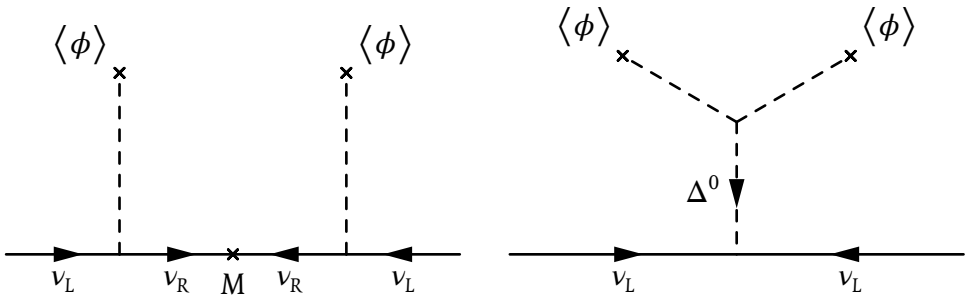

(a) Type I seesaw mechanism. **(b)** Type II seesaw mechanism.

Figure 1.3: Feynman diagrams for two different types of seesaw mechanism. In figure 1.3a the Dirac mass is generated by the VEV $\langle \phi \rangle$ and M is the Majorana mass. In figure 1.3b the heavy SU(2) triplet Δ^0 generates a mass term for the low-mass neutrinos.

the neutrino would be the discovery of neutrinoless double beta decay [36], which is a $|\Delta L| = 2$ process, i.e. the lepton number is changed by two units. Another effect of the Majorana nature is the existence of two additional CP-violating phases in the PMNS matrix.

There is a multitude of ways in which the two mass terms can be combined to give the observed neutrino masses. A very successful method is the *seesaw mechanism*, in which an electroweak scale Dirac mass and a GUT-scale right-handed Majorana mass are combined to generate a small effective neutrino mass. A renormalizable realization of the type I mechanism can be written as

$$\mathscr{L} \supset f \bar{\nu}_R \nu_L \left\langle \phi^0 \right\rangle + \frac{M}{2} \bar{\nu}_L^C \nu_R + \text{H.c.} \tag{1.15}$$

Note that that *right-handed* field ν_R receives a heavy Majorana mass M. The first part of the expression is an ordinary Dirac mass term involving the left- and right-handed neutrino fields and the vacuum expectation value of the Higgs field ϕ.

In a one-generation case the generation of a light neutrino mass can be easily seen: Consider a Dirac mass m_D and a right-handed Majorana mass M, where M is much larger than m_D. Diagonalizing the mass matrix

$$\begin{pmatrix} 0 & m_D \\ m_D & M \end{pmatrix}, \tag{1.16}$$

yields two eigenvalues, which can approximated as

$$m_1 = -\frac{m_D^2}{M}, \tag{1.17}$$

$$m_2 = M. \tag{1.18}$$

The mass m_1 can be seen as the light neutrino mass by virtue of suppression by the GUT scale mass M. A diagrammatic realization of this *seesaw type I mechanism* is displayed in figure 1.3a. When considering all three generations of neutrinos, the mass matrix can be written as

$$M_\nu^{\text{flv}} = m_D^T M^{-1} m_D, \tag{1.19}$$

where m_D now refers to the *matrix* of Dirac masses corresponding to the first part of equation (1.15) and M is now the *matrix* of Majorana masses, i.e. the second part of equation (1.15). This formula illustrates how masses that are very light compared to the charged leptons and quarks can be obtained for the neutrinos.

Another possible way to generate an effective neutrino mass operator is by coupling the left-handed neutrino to a heavy $\mathsf{SU}(2)$ triplet particle Δ^0, as shown in figure 1.3b. This is known as the *seesaw type II mechanism*. Both seesaw mechanisms can be seen as high-energy models that at the low scale generate a neutrino mass operator. This can be interpreted as integrating out the heavy right-handed neutrino ν_R in the type I realization or the heavy scalar Δ^0 in the type II model.

1.3.2 The flavor puzzle

The three generations of matter particles shown in figures 1.1 and 1.4 behave identically with respect to the gauge interactions introduced in this chapter. However, during the process of electroweak symmetry breaking every particle receives a different mass and nontrivial mixing relations between the generations emerge. These intergenerational differences are in contrast with the uniformity of their gauge interactions.

As illustrated in figure 1.4 the mass differences between the generations of quarks and leptons are large and can be considered clearly hierarchical. In the neutrino sector the absolute mass scale is not precisely known beyond the result shown in equation (1.13), except that it is at a very low energy compared to all other massive particles. It is also possible that the neutrino mass spectrum is close to being degenerate.

In summary, there are two types of hierarchies in the flavor sector that are unexplained as of now: The large hierarchy observed within the charged fermion sector and the enormous hierarchy between the charged fermion masses and the neutrino masses.

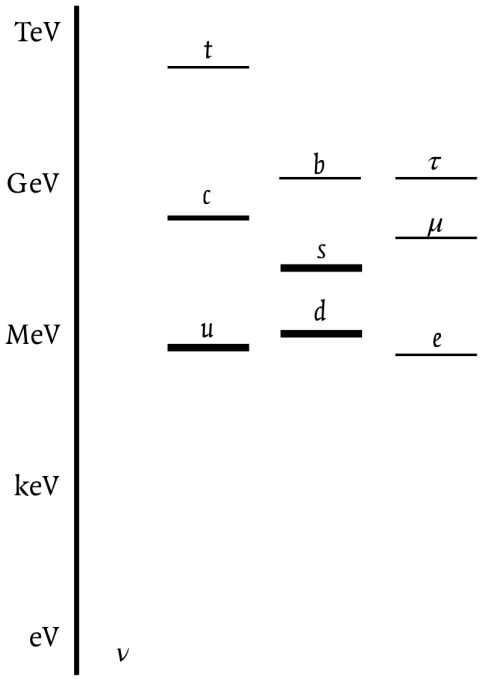

Figure 1.4: The mass hierarchy between the three generations of fermions. Based on data from reference [16].

The second piece of the flavor puzzle is the mixing information for quarks (equation [1.9]) and neutrinos (equations [1.11]), encoded in the CKM and PMNS matrices, respectively. The CKM matrix can be expressed as a small deviation from unity, as all the mixing angles are small. This view is taken in the *Wolfenstein parametrization* [37], where the deviation from unity is expressed as a series expansion in the Cabibbo angle $\lambda = \theta_C \approx 13.04°$:

$$V_{CKM} \approx \begin{pmatrix} 1 - \frac{\lambda^2}{2} & \lambda & A\lambda^3 \left(\rho - i\eta\right) \\ -\lambda & 1 - \frac{\lambda^2}{2} & A\lambda^2 \\ A\lambda^3 \left(1 - \rho - i\eta\right) & -A\lambda^2 & 1 \end{pmatrix}, \tag{1.20}$$

where λ, A, ρ, and η are the Wolfenstein parameters, representing the three real and one complex degrees of freedom.

Such a parametrization is not suitable for the PMNS matrix however, as it contains large mixing angles with θ_{23} being close to maximal, as can be seen in equation (1.11b). In fact, before the nonzero nature of the mixing angle θ_{13} (cf. equation [1.11c]) was

established by recent experiments [38–40], the mixing matrix was excellently described by the *tribimaximal pattern* [41, 42]:

$$\left(V_{\text{PMNS}}\right)^2 \approx \begin{pmatrix} \frac{2}{3} & \frac{1}{3} & 0 \\ \frac{1}{6} & \frac{1}{3} & \frac{1}{2} \\ \frac{1}{6} & \frac{1}{3} & \frac{1}{2} \end{pmatrix}. \tag{1.21}$$

Now that a nonzero θ_{13} is an experimental fact, the tribimaximal pattern can still function as a viable starting point from which to generate a nonzero θ_{13}.

Not included in the PMNS parametrization are complex phases. One such phase—called the *Dirac phase*—is the leptonic equivalent of the one complex degree of freedom contained in the CKM matrix. In addition, the possible Majorana nature of the neutrinos allows for two more CP-violating phases. The phases in the neutrino sector are currently unconstrained by experimental data [18].

All couplings that are responsible for the mixing matrices of quarks and leptons are free parameters in the standard model; it does not make any prediction.

2 Symmetry groups in model building

In chapter 1 the standard model was shown to be based on the mathematical foundation of the continuous local symmetry groups $\mathsf{U}(1)$, $\mathsf{SU}(2)$, and $\mathsf{SU}(3)$. The theoretical setup of the standard model is mostly concerned with the *vertical* direction of figure 1.1, i.e. with interactions involving gauge bosons and transitions between isospin states. Even though the CKM matrix is commonly discussed in the context of the standard model[1], its content is solely based on experimental input and cannot be predicted by the standard model.

The models discussed in this work employ discrete symmetry groups to constrain the possible textures of particle mixing and therefore explain the mixing patterns introduced in chapter 1. A short introduction into the group theoretical vocabulary needed follows at this point, a much more thorough treatment can be found in references [43, 44].

2.1 The vocabulary of group theory

A group is defined as a set G, where any two elements can be combined using an operation $\bullet$ to produce another element, which is also an element of G. The set G and the operation $\bullet$ used to combine the elements have to fulfill four requirements:

Closure $\forall a, b \in G : \; a \bullet b \in G$,

Associativity $\forall a, b, c \in G : \; (a \bullet b) \bullet c = a \bullet (b \bullet c)$,

Existence of an identity element $\exists e \in G : \; e \bullet a = a \bullet e = a$,

Existence of an inverse element $\forall a \in G, \exists b \in G : \; a \bullet b = b \bullet a = e$.

Note that while associativity is a requirement, commutativity is not. Groups whose elements can all be commuted are called *Abelian*, all other groups are consequently *non-Abelian*. Groups with a finite number of elements are called *finite groups*.

The elements $g^{-1}ag$ are called *conjugate elements* to $a \in G$. The set of these conjugate elements is called a *conjugacy class*.

[1] The PMNS matrix is not part of the standard model, as there is no canonical mechanism for neutrino mass generation.

Often, it is possible to express all elements of a group in terms of finite combinations of a subset of these elements and their inverse elements. This subset is called the *generating set* of the group, its elements are the *generators*.

A *representation* of a group G maps each element a of G onto a matrix $\mathsf{D}(a)$ homomorphically, i.e. while preserving the multiplication structure $\mathsf{D}(a)\mathsf{D}(b) = \mathsf{D}(a \bullet b)$, where b is another element of G. The vector space on which these matrices act is called the *representation space*. Its dimension is the *dimension of the representation*. We commonly deal with one-dimensional, two-dimensional, and three-dimensional representations in flavor models (often called singlet[2], doublet and triplet representations), but larger representations are common in GUTs.

If the representation space contains a subspace in which the operations $\mathsf{D}(a)v$ for any element $a \in G$ acting on a vector v in that subspace result in a vector that is also an element of the subspace, it is called an *invariant subspace*. Any representation that has an invariant subspace is called *reducible*. Consequently, an *irreducible* representation contains no such invariant subspace.

A very important result that is given without proof here is that the number of irreducible representations of a group is equal to the number of its conjugacy classes.

To construct larger groups it is possible to multiply groups in several ways. The simplest such construction is the *direct product*: For two groups A and B with elements a_i and b_i the product group $\mathsf{A} \times \mathsf{B}$ consists of the elements (a_i, b_i) and the group operation is performed in each component:

$$\left(a_i, b_i\right) \bullet \left(a_j, b_j\right) = \left(a_i \bullet a_j, b_i \bullet b_j\right). \tag{2.1}$$

A more complicated way to construct a larger group is by using the *semidirect product*. It is a generalization of the direct product and is usually written using the $\rtimes$ symbol. In the semidirect product group $\mathsf{A} \rtimes \mathsf{B}$, the new group elements are still the tuples (a_i, b_i), however the group operation is now defined as

$$\left(a_i, b_i\right) \bullet \left(a_j, b_j\right) = \left(a_i \bullet f_{b_i}(a_j), b_i \bullet b_j\right), \tag{2.2}$$

where f_{b_i} is a homomorphism mapping from B into the group of automorphisms of A. Note that the semidirect product is not commutative and also not unique, as different homomorphisms f produce different semidirect product groups.

A common special case that is used in this work is that of a large group G with a normal[3] subgroup N and a subgroup H. If every group element g of G can be written

[2] In this work *singlet* is only used for one-dimensional *invariants*.

[3] A *normal subgroup* N is invariant under conjugation with elements of its parent group G, i.e. $gng^{-1} \in \mathsf{N}$.

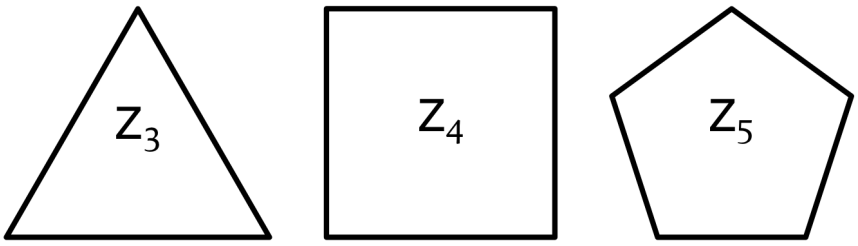

Figure 2.1: Geometric representation of the cyclic group Z_n for $n = 3, 4, 5$. The group elements are the rotations that leave the polygon invariant.

as $g = nh = hn$ and the groups H and N only have the identity element in common, then with the homomorphism

$$f_{h_i}(n_j) = h_i n_j (h_i)^{-1}, \tag{2.3}$$

the semidirect product $\mathsf{N} \rtimes \mathsf{H}$ is isomorphic to G. We will see this applied in the discussion of $\Delta(27)$ in section 2.2.3.

2.2 Groups used for model building

Generally, the effort of finding groups suitable for flavor models has been concentrated on subgroups of $\mathsf{SU}(3)$ as there are three families. A classification of the $\mathsf{SU}(3)$ subgroups with small order and their use in particle physics can be found in reference [45] and renewed interest in flavor symmetries has lead to more recent work, e.g. in reference [46]. Here, we concentrate on the discrete groups used to build the models discussed in the following chapters and introduce them in order of increasing complexity.

2.2.1 The cyclic group Z_n

A cyclic group Z_n is generated by one generator g and its powers:

$$\langle g \rangle = \left\{ g^0, g^1, g^2, \ldots, g^{n-1} \right\}. \tag{2.4}$$

In a finite cyclic group, when starting with an element a of the group and multiplying it with g iteratively one eventually ends up with the element a again, thus closing the cycle[4]. The groups Z_n are Abelian and have only one-dimensional irreducible representations.

A geometrical representation of the cyclic groups Z_n can be obtained by considering a regular n-gon, i.e. a polygon with n vertices, and is shown in figure 2.1. The elements of the group are then the rotations that leave the n-gon invariant[5].

The smallest nontrivial group Z_2—also called *parity*—is often used in particle physics to represent two distinct classes of particles that should not interact, where one class is assigned the representation $\mathbf{1}$ ($g\psi = \psi$) and the other is assigned to $\mathbf{1}'$, defined as $g\phi = -\phi$, where g is the group element. An interaction $\psi\phi$ is thus forbidden.

2.2.2 The symmetric group S_n

The symmetric group S_n is the group of all possible permutations of n objects. The elements are usually written as

$$\begin{pmatrix} a_1 & \dots & a_n \\ a_{\sigma(1)} & \dots & a_{\sigma(n)} \end{pmatrix}, \tag{2.5}$$

where the first row gives the original order of the elements a_i and the second row gives the new order after permuting the elements. The first row is often omitted when the original order is obvious (e.g. when it is $a_1, a_2, a_3, \dots$). The group S_n contains as many elements as there are permutations of n object, so there are $n!$ elements.

The smallest symmetric group, S_1, is trivial, containing only the identity element. The next-simplest example is S_2, which is simply the parity group Z_2, introduced in the previous section.

The symmetric group S_3

The smallest non-Abelian group is the permutation group of three objects, S_3. It contains $3! = 6$ elements and can be imagined as the symmetry group of an equilateral

[4] This is not true for the infinite cyclic group, which has infinitely many distinct elements and is isomorphic to the additive group of integers Z.

[5] It is interesting that the the infinite group of the natural numbers is a cyclic group under addition but the rotation group of the circle is not, even though it might seem to be a natural limit of a polygon with an ever-increasing number of vertices.

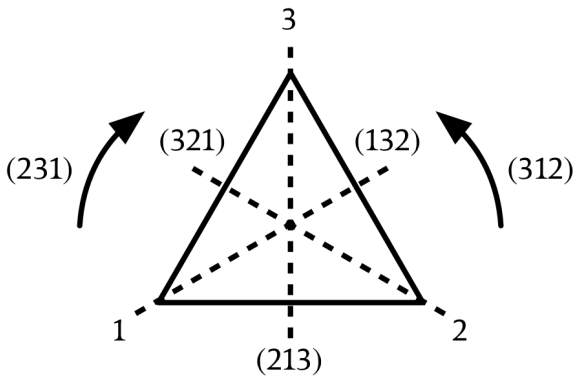

Figure 2.2: Geometric representation of the symmetric group S_3 including its elements. The identity element (123) is not shown.

triangle. In this geometrical image, the vertices of the equilateral triangle can be labeled 1, 2, 3 and the elements can be written as permutations:

$$\text{Identity } (e): \quad (123), \tag{2.6a}$$
$$\text{Reflections } (a_1, a_2, a_3): \quad (213), (321), (132), \tag{2.6b}$$
$$\text{Rotations } (a_4, a_5): \quad (312), (231). \tag{2.6c}$$

Interestingly, the group can be generated by just two elements: rotation by 120° and reflection along one axis. The set of all elements is then

$$\{e, a, b, ab, ba, aba\}, \tag{2.7}$$

where e is the identity, $a = (231)$ is a rotation by 120° and $b = (213)$ is a reflection along one of the axes shown in figure 2.2. Of course, other choices for a, b out of the elements shown in equation (2.6) are possible and equivalent.

The irreducible representations of S_3 To deduce the number of irreducible representations, the number of conjugacy classes has to be identified. In the case of S_3, the conjugacy classes are

$$\{e\}, \tag{2.8a}$$
$$\{ab, ba\}, \tag{2.8b}$$
$$\{a, b, aba\}. \tag{2.8c}$$

Consequently, S_3 has three irreducible representations, called **1**, **1′** and **2**. The existence of a doublet representation makes it suitable for nontrivial model building applications.

A real representation directly representing the vectors pointing to the vertices of the triangle of figure 2.2 can be chosen. In that case, the rotation and reflection matrices are a subset of the $\mathsf{O}(2)$ elements in an $\mathbb{R}^2$ representation. However, in order to accommodate complex fields in this work, a complex doublet representation $\mathsf{D}_{\mathbf{2}}^{\mathsf{C}} \equiv \mathsf{D}_{\mathbf{2}}$ is used [47]:

$$\begin{aligned}
\mathsf{D}_{\mathbf{2}}(e) &= \begin{pmatrix} 1 & 0 \\ 0 & 1 \end{pmatrix}, \\
\mathsf{D}_{\mathbf{2}}(a_1) &= \begin{pmatrix} 0 & 1 \\ 1 & 0 \end{pmatrix}, \quad \mathsf{D}_{\mathbf{2}}(a_2) = \begin{pmatrix} 0 & \omega^2 \\ \omega & 0 \end{pmatrix}, \quad \mathsf{D}_{\mathbf{2}}(a_3) = \begin{pmatrix} 0 & \omega \\ \omega^2 & 0 \end{pmatrix}, \\
\mathsf{D}_{\mathbf{2}}(a_4) &= \begin{pmatrix} \omega & 0 \\ 0 & \omega^2 \end{pmatrix}, \quad \mathsf{D}_{\mathbf{2}}(a_5) = \begin{pmatrix} \omega^2 & 0 \\ 0 & \omega \end{pmatrix},
\end{aligned} \tag{2.9}$$

where $\omega \equiv \exp(2\pi \mathrm{i}/3)$ is the third root of unity. The two one-dimensional representations can be distinguished by their behavior under reflections:

$$\mathsf{D}_{\mathbf{1}}(e) = \mathsf{D}_{\mathbf{1}}(a_1) = \mathsf{D}_{\mathbf{1}}(a_2) = \mathsf{D}_{\mathbf{1}}(a_3) = \mathsf{D}_{\mathbf{1}}(a_4) = \mathsf{D}_{\mathbf{1}}(a_5) = 1, \tag{2.10a}$$

$$\begin{aligned}
\mathsf{D}_{\mathbf{1}'}(e) = \mathsf{D}_{\mathbf{1}'}(a_4) = \mathsf{D}_{\mathbf{1}'}(a_5) = 1, \\
\mathsf{D}_{\mathbf{1}'}(a_1) = \mathsf{D}_{\mathbf{1}'}(a_2) = \mathsf{D}_{\mathbf{1}'}(a_3) = -1.
\end{aligned} \tag{2.10b}$$

Objects belonging to the one-dimensional $\mathbf{1}$ representation are invariants under S_3, i.e. all group elements are mapped to a multiplication with 1. It is therefore a true singlet representation[6]. The antisymmetric one-dimensional representation $\mathbf{1}'$ is characterized by a sign swap under the reflective group elements a_1, a_2 and a_3.

The tensor products of S_3 In order to construct invariant terms to be used in the Lagrangian of a field theory, the tensor products of the group have to be known.

To deduce the product of two doublets $\mathbf{2}$, consider[7] $(x_1, x_2)^{\mathsf{T}}_{\mathbf{2}}$ and $(y_1, y_2)^{\mathsf{T}}_{\mathbf{2}}$ and how all different combinations of the entries behave under transformation with a_1 and a_4.

[6] In this work, a *singlet* is always an invariant. The expression *one-dimensional representation* is used for the generic case.

[7] As in general there can be more than one representation of the same dimensionality, the representation is indicated by a subscript when using the component form. Where the representation is clarified using the $\in$-notation, this subscript is omitted.

In each case, the matrices $\mathsf{D}_2(a_1)$ and $\mathsf{D}_2(a_4)$ are applied to the doublets and then all combinations are considered. When applying the group element a_1 one gets:

$$\begin{aligned} x_1 y_1 &\xrightarrow{\mathsf{D}_2^{\mathsf{C}}(a_1)} x_2 y_2, \\ x_1 y_2 &\xrightarrow{\mathsf{D}_2^{\mathsf{C}}(a_1)} x_2 y_1, \\ x_2 y_1 &\xrightarrow{\mathsf{D}_2^{\mathsf{C}}(a_1)} x_1 y_2, \\ x_2 y_2 &\xrightarrow{\mathsf{D}_2^{\mathsf{C}}(a_1)} x_1 y_1. \end{aligned} \tag{2.11}$$

Applying the group element a_4 in its two-dimensional representation $\mathsf{D}_2(a_4)$ yields:

$$\begin{aligned} x_1 y_1 &\xrightarrow{\mathsf{D}_2^{\mathsf{C}}(a_4)} \omega^2 x_1 y_1, \\ x_1 y_2 &\xrightarrow{\mathsf{D}_2^{\mathsf{C}}(a_4)} x_1 y_2, \\ x_2 y_1 &\xrightarrow{\mathsf{D}_2^{\mathsf{C}}(a_4)} x_2 y_1, \\ x_2 y_2 &\xrightarrow{\mathsf{D}_2^{\mathsf{C}}(a_4)} \omega x_2 y_2. \end{aligned} \tag{2.12}$$

In both one-dimensional representations, the elements of the group are represented by multiplication with ± 1, so no factors of ω may remain in the tensor products. It is thus possible to combine the entries of the doublets $(x_1, x_2)^{\intercal}_{\mathbf{2}}$ and $(y_1, y_2)^{\intercal}_{\mathbf{2}}$ in the following ways:

$$x_1 y_2 + x_2 y_1 \in \mathbf{1}, \tag{2.13a}$$
$$x_1 y_2 - x_2 y_1 \in \mathbf{1}'. \tag{2.13b}$$

Note that for a complex doublet field $\phi = (\phi_1, \phi_2)^{\intercal} \in \mathbf{2}$ the Hermitian conjugate is given by $\phi^{\dagger} = (\phi_2^{\dagger}, \phi_1^{\dagger}) \in \mathbf{2}$. In this case, the tensor product with a second doublet field ψ is [48]

$$\phi_1^{\dagger}\psi_1 + \phi_2^{\dagger}\psi_2 \in \mathbf{1}, \tag{2.14a}$$
$$\phi_1^{\dagger}\psi_1 - \phi_2^{\dagger}\psi_2 \in \mathbf{1}'. \tag{2.14b}$$

It is also possible to form a new doublet out of two doublets:

$$\begin{pmatrix} \phi_1^{\dagger}\psi_2 \\ \phi_2^{\dagger}\psi_1 \end{pmatrix} \in \mathbf{2}. \tag{2.15}$$

The tensor products involving one-dimensional representations are somewhat simpler, for $v \in \mathbf{1}$ and $w \in \mathbf{1}'$:

$$vv \in \mathbf{1}, \tag{2.16a}$$
$$ww \in \mathbf{1}, \tag{2.16b}$$
$$vw \in \mathbf{1}'. \tag{2.16c}$$

In summary, the tensor products of S_3 are

$$\mathbf{2} \otimes \mathbf{2} = \mathbf{1} \oplus \mathbf{1}' \oplus \mathbf{2}, \tag{2.17a}$$
$$\mathbf{1} \otimes \mathbf{1}' = \mathbf{1}', \tag{2.17b}$$
$$\mathbf{1}' \otimes \mathbf{1}' = \mathbf{1}. \tag{2.17c}$$

The respective construction rules are listed in equations (2.13) and (2.16).

2.2.3 The group $\Delta(3n^2)$

The group $\Delta(3n^2)$ is a subgroup of $\mathsf{SU}(3)$ of order $3n^2$. It is the smallest non-Abelian subgroup with three-dimensional representations[8]. It can be expressed as the group product [43, 49]

$$\Delta(3n^2) \sim \left(\mathsf{Z}_n \times \mathsf{Z}_n'\right) \rtimes \mathsf{Z}_3. \tag{2.18}$$

All elements of the group can be written by combining its three generators, which are the generators of the product groups $\mathsf{Z}_n \times \mathsf{Z}_n$ and Z_3:

$$b^3 = 1, \tag{2.19}$$

for the Z_3 subgroup of $\Delta(3n^2)$ and

$$a^n = a'^n = 1, \tag{2.20a}$$
$$aa' = a'a, \tag{2.20b}$$

for the $\mathsf{Z}_n \times \mathsf{Z}_n'$ subgroup. These two subgroups are connected via the semidirect product, which in this case uses a conjugation as the homomorphism, as was introduced in section 2.1:

$$bab^{-1} = a^{-1}a'^{-1}, \tag{2.21a}$$
$$ba'b^{-1} = a. \tag{2.21b}$$

All elements of $\Delta(3n^2)$ can be expressed as a product of a, a', and b. The further treatment of $\Delta(3n^2)$ diverges for $n = 3\mathbb{Z}$ and $n \neq 3\mathbb{Z}$. As $\Delta(27)$ is extensively used in this work, only that case is considered from now on.

[8] The well-known group A_4 is $\Delta(12)$.

The irreducible representations of $\Delta(27)$ The number of irreducible representations is equal to the number of conjugacy classes of the group. For $n = 3\mathbb{Z}$, the conjugacy classes of $\Delta(3n^2)$ are [43]

$$C_1 : \left\{e\right\}, \tag{2.22a}$$

$$C_1^{(k)} : \left\{a^k a'^{-k}\right\}, k = \frac{n}{3}, \frac{2n}{3}, \tag{2.22b}$$

$$C_3^{(l,m)} : \left\{a^l a'^m, a^{-l+m} a'^{-l}, a^{-m} a'^{l-m}\right\}, (l,m) \neq \left(\frac{n}{3}, \frac{2n}{3}\right), \left(\frac{2n}{3}, \frac{n}{3}\right), \tag{2.22c}$$

$$C_{n^2/3}^{(1,p)} : \left\{ba^{p-n'-3m} a'^n | m = 0, 1, \ldots, \frac{n-3}{3}, n' = 0, 1, \ldots, n-1\right\}, p = 0, 1, 2, \tag{2.22d}$$

$$C_{n^2/3}^{(2,p)} : \left\{b^2 a^{p-n'-3m} a'^n | m = 0, 1, \ldots, \frac{n-3}{3}, n' = 0, 1, \ldots, n-1\right\}, p = 0, 1, 2. \tag{2.22e}$$

The total number of conjugacy classes is $9 + (n^2 - 3)/3$, consisting of two cases of equation (2.22b), $(n^2-3)/3$ cases of equation (2.22c) and three cases each of equations (2.22d) and (2.22e). This corresponds to nine one-dimensional representations—including one singlet—as well as $(n^2 - 3)/3$ triplets. Consequently $\Delta(27)$ has nine one-dimensional and two three-dimensional representations.

The conjugacy classes for $\Delta(27)$ are

$$C_1 : \left\{e\right\}, \tag{2.23a}$$

$$C_1^{(1)} : \left\{a, a'^2\right\}, \tag{2.23b}$$

$$C_1^{(2)} : \left\{a^2, a'\right\}, \tag{2.23c}$$

$$C_3^{(0,1)} : \left\{a', a, a^2 a'^2\right\}, \tag{2.23d}$$

$$C_3^{(0,2)} : \left\{a'^2, a^2, aa'\right\}, \tag{2.23e}$$

$$C_3^{(1,p)} : \left\{ba^p, ba^{p-1}a', ba^{p-2}a'^2\right\}, \tag{2.23f}$$

$$C_3^{(2,p)} : \left\{ba^p, ba^{p-1}a', ba^{p-2}a'^2\right\}. \tag{2.23g}$$

The nine one-dimensional representations are written as $\mathbf{1}_{r,s}$ for $r, s = 0, 1, 2$ and the two triplets are called $\mathbf{3}_{[0][1]}$ and $\mathbf{3}_{[0][2]}$. At this point it is worth noting that there is a certain ambiguity in the labeling of the triplets because of the conjugation property of the semidirect product. In fact, representations obtained by conjugation with the elements b and b^2 are equivalent. Due to this, the square bracket used to label the triplets is defined as

$$[k][l] = (k, l) \vee (-k - l, k) \vee (l, -k - l). \tag{2.24}$$

The generators of the three-dimensional representations are

$$\mathsf{D}_{\mathbf{3}}(b) = \begin{pmatrix} 0 & 1 & 0 \\ 0 & 0 & 1 \\ 1 & 0 & 0 \end{pmatrix}, \tag{2.25a}$$

$$\mathsf{D}_{\mathbf{3}}(a) = \begin{pmatrix} \omega^{l} & 0 & 0 \\ 0 & \omega^{k} & 0 \\ 0 & 0 & \omega^{-k-l} \end{pmatrix}, \tag{2.25b}$$

$$\mathsf{D}_{\mathbf{3}}(a') = \begin{pmatrix} \omega^{-k-l} & 0 & 0 \\ 0 & \omega^{l} & 0 \\ 0 & 0 & \omega^{k} \end{pmatrix}, \tag{2.25c}$$

where $k, l = 0, 1, 2$ and $\omega \equiv \exp(2\pi i/3)$. The indices k and l represent the charges under Z_3 and Z_3' respectively. Due to this there is not only an ambiguity encoded in the bracket notation of equation (2.24) but also in the cyclic nature of the Z_3 charges. For example, an equivalent set of generators that can be used includes b^2 as the permuting generator and swaps the placement of ω^l and ω^k in $\mathsf{D}_{\mathbf{3}}(a)$[9]. Also note that for $k = l$ the matrices $\mathsf{D}_{\mathbf{3}}(a)$ and $\mathsf{D}_{\mathbf{3}}(a')$ are trivial and such triplet representations are actually reducible. The generators a and a' can be represented as diagonal matrices because they commute, as shown in equation (2.20b).

In the one-dimensional representations $\mathbf{1}_{r,s}$ for $r, s = 0, 1, 2$ the generators commute. By inspection of the definition of the generators in equations (2.19) and (2.20) the one-dimensional representations of the generators can be obtained:

$$\mathsf{D}_{\mathbf{1}}(b) = \omega^{r}, \tag{2.26a}$$

$$\mathsf{D}_{\mathbf{1}}(a) = \mathsf{D}_{\mathbf{1}}(a') = \omega^{s}. \tag{2.26b}$$

As can be seen in these expressions, the indices r and s refer to the charges under Z_3 and Z_3'. Consequently, the singlet of $\Delta(27)$ is $\mathbf{1}_{0,0}$.

In summary, the group $\Delta(27)$ has nine one-dimensional representations, labeled $\mathbf{1}_{r,s}$ for $r, s = 0, 1, 2$ and two three-dimensional representations $\mathbf{3}_{[0][1]}$ and $\mathbf{3}_{[0][2]}$.

[9] This set has the advantage of memorability, as the diagonal generator for $\mathbf{3}_{[0][1]}$ is $\mathrm{Diag}(\omega^0, \omega^1, \omega^2)$ and for $\mathbf{3}_{[0][2]}$ it is $\mathrm{Diag}(\omega^0, \omega^2, \omega^1)$, mimicking the subscript in the powers of the first two entries. However, due to consistency with the literature we stick to the notation of references [43, 49] at this point.

The tensor products of $\Delta(27)$ In order to construct invariants, the tensor products of the three-dimensional and one-dimensional representations have to be known. In general, three products are possible in $\Delta(27)$ [49]:

$$\mathbf{1}_{r,s} \otimes \mathbf{1}_{r',s'} = \mathbf{1}_{r+r',s+s'}, \tag{2.27a}$$

$$\mathbf{1}_{r,s} \otimes \mathbf{3}_{(k,l)} = \mathbf{3}_{[k+s][l+s]}, \tag{2.27b}$$

$$\begin{aligned}\mathbf{3}_{(k,l)} \otimes \mathbf{3}_{(k',l')} = &\sum_{s=0}^{2} \delta_{(k',l'),([-k+s][-l+s])} \left(\mathbf{1}_{0,s} \oplus \mathbf{1}_{1,s} \oplus \mathbf{1}_{2,s}\right) \\ &\oplus \mathbf{3}_{[k'+k][l'+l]} \oplus \mathbf{3}_{[k'-k-l][l'+k]} \oplus \mathbf{3}_{[k'+l][l'-k-l]}.\end{aligned} \tag{2.27c}$$

As can be seen in equation (2.27a), the product of two one-dimensional representations is determined by their behavior under the subgroup $\mathsf{Z}_3 \times \mathsf{Z}_3'$, where the charges are each added. The tensor product of two three-dimensional representations shown in equation (2.27c) is more complicated, as it can contain either the nine one-dimensional representations of $\Delta(27)$, including the singlet $\mathbf{1}_{0,0}$, or three-dimensional representations. In the cases where the Kronecker symbol allows for one-dimensional representations, the three-dimensional representations in the same product are always of the type $\mathbf{3}_{[k][k]}$, i.e. they are reducible. Following the notation of reference [43] the tensor products of equation (2.27) can be expressed in terms of the components of the representations. For reasons of clarity, the three different combinations of three-dimensional representations are considered separately:

$$\begin{pmatrix} x_{1,-1} \\ x_{0,1} \\ x_{-1,0} \end{pmatrix}_{\mathbf{3}_{[0][1]}} \otimes \begin{pmatrix} y_{1,-1} \\ y_{0,1} \\ y_{-1,0} \end{pmatrix}_{\mathbf{3}_{[0][1]}} = \begin{pmatrix} x_{1,-1}y_{1,-1} \\ x_{0,1}y_{0,1} \\ x_{-1,0}y_{-1,0} \end{pmatrix}_{\mathbf{3}_{[0][2]}} \oplus \begin{pmatrix} x_{-1,0}y_{1,-1} \\ x_{1,-1}y_{0,1} \\ x_{0,1}y_{-1,0} \end{pmatrix}_{\mathbf{3}_{[0][2]}} \oplus \begin{pmatrix} x_{1,-1}y_{-1,0} \\ x_{0,1}y_{1,-1} \\ x_{-1,0}y_{0,1} \end{pmatrix}_{\mathbf{3}_{[0][2]}}, \tag{2.28a}$$

$$\begin{pmatrix} x_{2,-2} \\ x_{0,2} \\ x_{-2,0} \end{pmatrix}_{\mathbf{3}_{[0][2]}} \otimes \begin{pmatrix} y_{2,-2} \\ y_{0,2} \\ y_{-2,0} \end{pmatrix}_{\mathbf{3}_{[0][2]}} = \begin{pmatrix} x_{2,-2}y_{2,-2} \\ x_{0,2}y_{0,2} \\ x_{-2,0}y_{-2,0} \end{pmatrix}_{\mathbf{3}_{[0][1]}} \oplus \begin{pmatrix} x_{-2,0}y_{2,-2} \\ x_{2,-2}y_{0,2} \\ x_{0,2}y_{-2,0} \end{pmatrix}_{\mathbf{3}_{[0][1]}} \oplus \begin{pmatrix} x_{2,-2}y_{-2,0} \\ x_{0,2}y_{2,-2} \\ x_{-2,0}y_{0,2} \end{pmatrix}_{\mathbf{3}_{[0][1]}}. \tag{2.28b}$$

In the case of multiplying two three-dimensional representations to produce the nine one-dimensional representations of $\Delta(27)$, the reducible three-dimensional representations shown in equation (2.27c) are omitted as they contain no unique physical content:

$$\begin{aligned}\begin{pmatrix} x_{1,-1} \\ x_{0,1} \\ x_{-1,0} \end{pmatrix}_{\mathbf{3}_{[0][1]}} \otimes \begin{pmatrix} y_{-1,1} \\ y_{0,-1} \\ y_{1,0} \end{pmatrix}_{\mathbf{3}_{[0][2]}} &= \sum_{r=0}^{2} \left(x_{1,-1}y_{-1,1} + \omega^{2r} x_{0,1}y_{0,-1} + \omega^{r} x_{-1,0}y_{1,0} \right)_{\mathbf{1}_{r,0}} \\ &\oplus \sum_{r=0}^{2} \left(x_{1,-1}y_{0,-1} + \omega^{2r} x_{0,1}y_{1,0} + \omega^{r} x_{-1,0}y_{-1,1} \right)_{\mathbf{1}_{r,1}} \\ &\oplus \sum_{r=0}^{2} \left(x_{1,-1}y_{1,0} + \omega^{2r} x_{0,1}y_{-1,1} + \omega^{r} x_{-1,0}y_{0,-1} \right)_{\mathbf{1}_{r,2}}.\end{aligned} \tag{2.28c}$$

Finally, the product of a three-dimensional representation and a one-dimensional representation (equation [2.27b]) can be computed as follows:

$$\begin{pmatrix} x_{1,-1} \\ x_{0,1} \\ x_{-1,0} \end{pmatrix}_{\mathbf{3}_{[0][1]}} \otimes \left(z_{r,s} \right)_{\mathbf{1}_{r,s}} = \begin{pmatrix} x_{1,-1}z_{r,s} \\ \omega^{r} x_{0,1}z_{r,s} \\ \omega^{2r} x_{-1,0}z_{r,s} \end{pmatrix}_{\mathbf{3}_{[s][1+s]}}, \tag{2.28d}$$

$$\begin{pmatrix} x_{2,-2} \\ x_{0,2} \\ x_{-2,0} \end{pmatrix}_{\mathbf{3}_{[0][2]}} \otimes \left(z_{r,s} \right)_{\mathbf{1}_{r,s}} = \begin{pmatrix} x_{2,-2}z_{r,s} \\ \omega^{r} x_{0,2}z_{r,s} \\ \omega^{2r} x_{-2,0}z_{r,s} \end{pmatrix}_{\mathbf{3}_{[s][2+s]}}. \tag{2.28e}$$

3 Signatures of a flavor model based on the permutation group S_3

In section 1.3.2 the flavor puzzle was introduced, one piece of it being the failure of the standard model to predict the mixing angles of quarks and leptons. The approach of using symmetry groups to explain and unify phenomena in particle physics has been vindicated by the success of the standard model and that success has lead to a similar approach being used to attempt to solve the flavor puzzle as well. Early attempts were made starting in the 1960s, using the continuous symmetry groups known from the dynamic sector of the standard model [50–53], however these models were not very successful [49].

The discovery of the nonzero neutrino mass [38–40] and the subsequent measurements of the mixing angles have changed the picture considerably: Finite discrete groups often provide matrices with large mixing angles, mimicking the large mixing angles found in the neutrino sector. For reviews of the use of discrete flavor symmetries in neutrino model building, see e.g. references [54–57].

In most cases when using discrete flavor symmetries to model the masses and mixing of matter particles additional fields in nontrivial representations have to be introduced. The mechanism of SSB is then used to break the symmetry, but the scale at which that happens can vary: In many cases additional fields called *familons* or *flavons*[1] are used, which are assigned to a nontrivial representation of the symmetry group and acquire a VEV a a high energy scale (cf. reference [60]). This breaking scheme is separated from the Higgs mechanism and due to their high masses, the flavons are invisible experimentally.

An alternative approach is using an extended electroweak breaking sector with nontrivial charges under the family group. Interesting experimental signatures such as nonstandard decays involving scalars and gauge bosons and/or large flavor changing neutral currents (FCNCs) often arise in such scenarios. The models discussed in this work fall into this category.

[1] The term *familon* has been in use since the 1980s [58]. Originally, *flavon* stood for a completely unrelated concept, but the two terms have been used interchangeably since the 1990s [59].

The permutation group S_3 introduced in section 2.2.2 is a particularly attractive candidate. It was first used in the context of flavor physics in reference [61] and has been explored by many authors since [62–72].

A problem many models using discrete flavor symmetries to solve the flavor puzzle have is that while they provide well-motivated and well-working fits to the data, their predictive power is often low. In this chapter, we explore a specific model (introduced in reference [48]) in the context of the scalar sector, thus providing experimental signatures that can be used to test the model. We specifically concentrate on the extended scalar sector compared to the standard model.

3.1 Building blocks of the model

The attractiveness of the group S_3 is based on the fact that it is the smallest discrete symmetry group having a two-dimensional irreducible representation. It is thus a good candidate for the description of the maximal mixing of two generations, which is a good approximation for the atmospheric neutrino mixing angle $\theta_{23} \approx 40.0°$ [18]. This result remains attractive after the discovery of a nonzero mixing angle θ_{13} [73–75]. That the group has two nonequivalent one-dimensional representations (see equation [2.17]) is also crucial for the correct reproduction of the fermion masses and mixing.

In the model proposed in reference [48] three scalar $SU(2)$ doublets are introduced with couplings to the gauge and fermion sectors as dictated by their charges under S_3. It is an interesting result that the same mixing mechanism that produces the large angle in the neutrino sector is responsible for producing an almost diagonal mixing in the quark sector by cancellation. The neutrino mass generation is treated separately using a type II seesaw mechanism (cf. section 1.3.1). By construction the neutrino mass matrix emerging from that mechanism is diagonal in this model, with the neutrino mixing angles encoded in the PMNS matrix stemming from the mismatch between this diagonal matrix and the off-diagonal nature of the charged lepton sector. The triplets used in the seesaw mechanism are heavy and are not dealt with in this work. Also, the exact mechanism by which the neutrino mixing angles and the CKM matrix are obtained is not repeated at this point. It can be found in reference [48].

In order to use the symmetry group S_3 to construct a Lagrangian the fields used have to be assigned to representations of the group. In the case of the model presented in [48] the assignments are presented in table 3.1. The VEVs of the three scalar doublet fields ϕ_1, ϕ_2, and ϕ_3 induce SSB in the electroweak sector, replacing the standard model Higgs mechanism.

Table 3.1: Assignments of particles to irreducible representations of S_3.

	2	**1′**	**1**
Leptons	$\begin{pmatrix} L_\mu \\ L_\tau \end{pmatrix}_{\mathbf{2}}$	τ^{C}	$L_e, e^{\mathsf{C}}, \mu^{\mathsf{C}}$
Quarks	$\begin{pmatrix} Q_2 \\ Q_3 \end{pmatrix}_{\mathbf{2}}$	$b^{\mathsf{C}}, t^{\mathsf{C}}$	$Q_1, u^{\mathsf{C}}, c^{\mathsf{C}}, d^{\mathsf{C}}, s^{\mathsf{C}}$
Scalars	$\begin{pmatrix} \phi_1 \\ \phi_2 \end{pmatrix}_{\mathbf{2}}$		ϕ_3

Note: The assignments are given as in reference [48]. L_e, L_μ, and L_τ are $\mathsf{SU}(2)$ doublets containing the charged leptons and neutrinos. Analogously Q_1, Q_2, and Q_3 contain the quarks. The charge-conjugated fields are $\mathsf{SU}(2)$ singlets and written using the C superscript. Finally, ϕ_1, ϕ_2, and ϕ_3 are $\mathsf{SU}(2)$ doublet scalar fields.

The addition of the scalar $\mathsf{SU}(2)$ doublet fields ϕ_1, ϕ_2, and ϕ_3 to the model leads to a scalar potential involving those fields. The most general scalar potential invariant under S_3 with the assignments of table 3.1 is given by references [48, 76]:

$$\begin{aligned} V = {} & m^2\left(\phi_1^\dagger\phi_1 + \phi_2^\dagger\phi_2\right) + m_3^2\phi_3^\dagger\phi_3 + \frac{\lambda_1}{2}\left(\phi_1^\dagger\phi_1 + \phi_2^\dagger\phi_2\right)^2 \\ & + \frac{\lambda_2}{2}\left(\phi_1^\dagger\phi_1 - \phi_2^\dagger\phi_2\right)^2 + \lambda_3\phi_1^\dagger\phi_2\phi_2^\dagger\phi_1 + \frac{\lambda_4}{2}\left(\phi_3^\dagger\phi_3\right)^2 + \lambda_5\left(\phi_3^\dagger\phi_3\right)\left(\phi_1^\dagger\phi_1 + \phi_2^\dagger\phi_2\right) \\ & + \lambda_6\phi_3^\dagger\left(\phi_1\phi_1^\dagger + \phi_2\phi_2^\dagger\right)\phi_3 + \left[\lambda_7\phi_3^\dagger\phi_1\phi_3^\dagger\phi_2 + \lambda_8\phi_3^\dagger\left(\phi_1\phi_2^\dagger\phi_1 + \phi_2\phi_1^\dagger\phi_2\right) + \text{H.c.}\right]. \end{aligned} \tag{3.1}$$

After the process of SSB, nine degrees of freedom are left in the scalar sector: three neutral scalars, two neutral pseudoscalars and two charged scalars with two degrees of freedom each. The remaining degrees of freedom are neutral (G^0) and charged ($G^\pm$) Goldstone bosons which are eaten up by Z^0 and $W^\pm$ respectively. Consequently, the

values of the VEVs are restricted by $v_1^2 + v_2^2 + v_3^2 = v_{SM}^2$, where $v_{SM} = 246\,\text{GeV}$. The remaining fields are labeled as follows:

$$\phi_1 \to \begin{pmatrix} 0 \\ h_1 \end{pmatrix}, \tag{3.2a}$$

$$\phi_2 \to \begin{pmatrix} h_2^+ \\ h_2 + i\chi_2 \end{pmatrix}, \tag{3.2b}$$

$$\phi_3 \to \begin{pmatrix} h_3^+ \\ h_3 + i\chi_3 \end{pmatrix}. \tag{3.2c}$$

The VEVs of the fields ϕ_1, ϕ_2, and ϕ_3 are labeled as v_1, v_2, and v_3. We assume that the scalar sector is not a source of CP violation, i.e. the couplings $\lambda_{\{1,\dots,8\}}$ and the VEVs v_1, v_2, and v_3 are real in this work.

Producing the maximal atmospheric mixing angle in the neutrino sector requires the specific vacuum alignment $v_1 = v_2 \equiv v$, as shown in reference [48]. This choice is not arbitrary, but is one of the solutions allowed by the minimization of the scalar potential of equation (3.1).

At this point we consider two different scenarios and their implications on collider signatures:

3.2 Scenario I: Light scalars and scalar three-point interactions

The following scenario was first explored in the diploma thesis in reference [77] and further expanded in reference [1]. As the second scenario builds upon it, it is repeated here with additional comments regarding the impact of the discovery of the Higgs.

3.2.1 Mass spectrum of the scalars

In this scenario, we only consider the CP-even scalars h_1, h_2, and h_3, assuming very high masses for all other degrees of freedom. When we impose the condition $v_1 = v_2$ it is

possible to minimize the potential (3.1) and derive conditions on the squared mass parameters m^2 and m_3^2:

$$-m^2 = \left(2\lambda_1 + \lambda_3\right)v^2 + \left(\lambda_5 + \lambda_6 + \lambda_7\right)v_3^2 + 3\lambda_8 v v_3, \tag{3.3a}$$

$$-m_3^2 = \lambda_4 v_3^2 + 2\left(\lambda_5 + \lambda_6 + \lambda_7\right)v^2 + 2\lambda_8 \frac{v^3}{v_3}. \tag{3.3b}$$

These conditions ensure an extremal point for the chosen vacuum alignment, but they do not guarantee that it corresponds to a minimum of the potential. This has to be checked separately by calculating the Hessian matrix, i.e. the square matrix of second order partial derivatives giving the local curvature of the potential. Coincidentally, the Hessian matrix in this case is the squared mass matrix of the scalars. Thus, the positivity of the eigenvalues of that matrix—which is necessary to obtain physical masses for the scalars—also ensures that the vacuum alignment $v_1 = v_2$ represents a minimum of the potential.

This procedure ensures a local minimum in $v_1 = v_2$, but it is still necessary to choose the potential parameters $\lambda_{\{1,\dots,8\}}$ in a way that guarantees the global, i.e. asymptotic, stability of the potential. After the process of SSB the potential is a polynomial of order four and its global stability in the asymptotic limit $\phi_{\{1,2,3\}} \to \pm\infty$ can be ensured by the following set of conditions:

$$\begin{aligned} &\lambda_1 + \lambda_2 > 0, \quad \lambda_1 + \lambda_3 > \lambda_2, \quad \lambda_4 > 0, \\ &\lambda_5 + \lambda_6 > 0, \qquad \lambda_7 > 0, \quad \lambda_8 > 0. \end{aligned} \tag{3.4}$$

These conditions keep the coefficients of the highest-order terms positive and thus define the asymptotic behavior of the potential. Note that this simple set of conditions is stricter than necessary as it cuts off parts of the parameter space that might still be viable. A more precise treatment of this problem can be found in the second scenario presented in section 3.3.

To calculate the masses and mixing of the three CP-even scalars, the SSB expansion $\phi_i^0 = v_i + h_i$ (with $i = 1, 2, 3$) is inserted into equation (3.1). The resulting matrix in the $(h_1, h_2, h_3)^T$ basis can be diagonalized to obtain the physical—i.e. mass basis—scalars h_a, h_b, and h_c. In terms of the mass basis scalars, h_1, h_2, and h_3 can be expressed as follows:

$$h_1 = U_{1b}h_b + U_{1c}h_c - \frac{1}{\sqrt{2}}h_a, \tag{3.5a}$$

$$h_2 = U_{1b}h_b + U_{1c}h_c + \frac{1}{\sqrt{2}}h_a, \tag{3.5b}$$

$$h_3 = U_{3b}h_b + U_{3c}h_c, \tag{3.5c}$$

where U_{ib} and U_{ic} (for $i = 1, 3$) are analytically tractable but complicated functions of $\lambda_{\{1,\dots,8\}}$ and the VEVs v and v_3, which are not shown here. Note that the equality of the mixing coefficients contained in h_1 and h_2 is a consequence of $v_1 = v_2$. It is also interesting that the mixing equation for h_a does not depend on any parameter of the potential or the VEVs:

$$h_a = \frac{1}{\sqrt{2}} \left(h_2 - h_1 \right). \tag{3.6}$$

This is a consequence of the S_3 symmetry, which generates a squared mass matrix of the pattern

$$\begin{pmatrix} A & B & C \\ B & A & C \\ C & C & D \end{pmatrix}, \tag{3.7}$$

which for arbitrary values of A, B, C, and D always yields $(-1, 1, 0)^\intercal$ as one eigenvector.

The squared masses of the three CP-even neutral scalars h_a, h_b, and h_c are

$$m^2_{h_a} = 4\lambda_2 v^2 - 2\lambda_3 v^2 - v_3 \left(2\lambda_7 v_3 + 5\lambda_8 v \right), \tag{3.8a}$$

$$m^2_{h_b} = \frac{1}{2v_3} \left[4\lambda_1 v^2 v_3 + 2\lambda_3 v^2 v_3 + 2\lambda_4 v_3^3 - 2\lambda_8 v^3 + 3\lambda_8 v v_3^2 - \Delta m^3 \right], \tag{3.8b}$$

$$m^2_{h_c} = \frac{1}{2v_3} \left[4\lambda_1 v^2 v_3 + 2\lambda_3 v^2 v_3 + 2\lambda_4 v_3^3 - 2\lambda_8 v^3 + 3\lambda_8 v v_3^2 + \Delta m^3 \right], \tag{3.8c}$$

where

$$\begin{aligned} \Delta m^3 = \Bigg[& 8 v v_3 \Bigg\{ 2 v v_3^3 \Big(2\big(\lambda_5 + \lambda_6 + \lambda_7\big)^2 - \lambda_4 \big(2\lambda_1 + \lambda_3\big) \Big) \\ & + 2\lambda_8 v^4 \big(2\lambda_1 + \lambda_3\big) - 3\lambda_4 \lambda_8 v_3^4 + 12 \lambda_8 v^2 v_3^2 \big(\lambda_5 + \lambda_6 + \lambda_7\big) + 12 \lambda_8^2 v^3 v_3 \Bigg\} \\ & + \Big\{ 2 v^2 v_3 \big(2\lambda_1 + \lambda_3\big) + 2\lambda_4 v_3^3 - 2\lambda_8 v^3 + 3\lambda_8 v v_3^2 \Big\}^2 \Bigg]^{\frac{1}{2}}. \end{aligned} \tag{3.9}$$

To assess the possible mass spectrum of the CP-even scalars h_a, h_b, and h_c a numerical approach is taken: The magnitude of the potential parameters $\lambda_{\{1,\dots,8\}}$ is chosen randomly in the range $[0, 1]$, while the ratio of v_3/v is kept fixed at 0.6 to ensure compliance with the CKM fit of reference [48]. Since h_b and h_c behave similarly with respect to their Yukawa and gauge interactions (as will be shown in the next section), only their mass splitting is shown in figure 3.1a. The relation between m_{h_b} and m_{h_a} is shown in figure 3.1b.

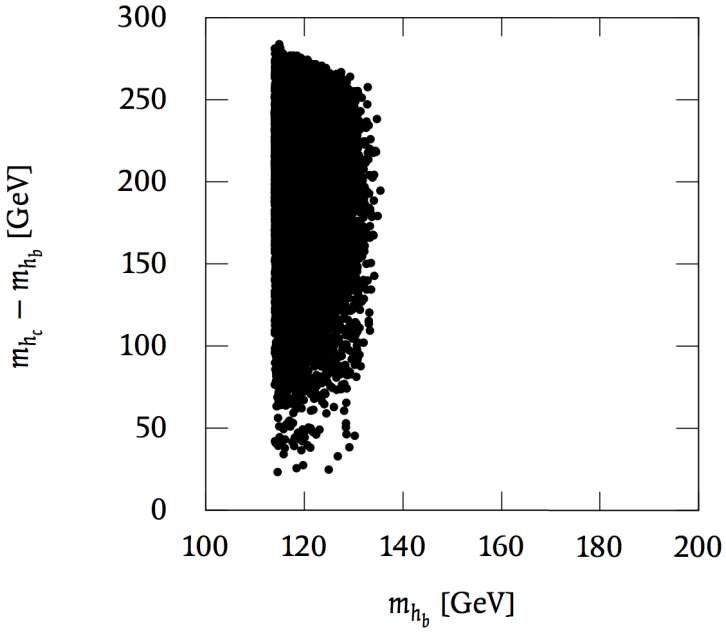

(a) Splitting $m_{h_c} - m_{h_b}$ against m_{h_b}.

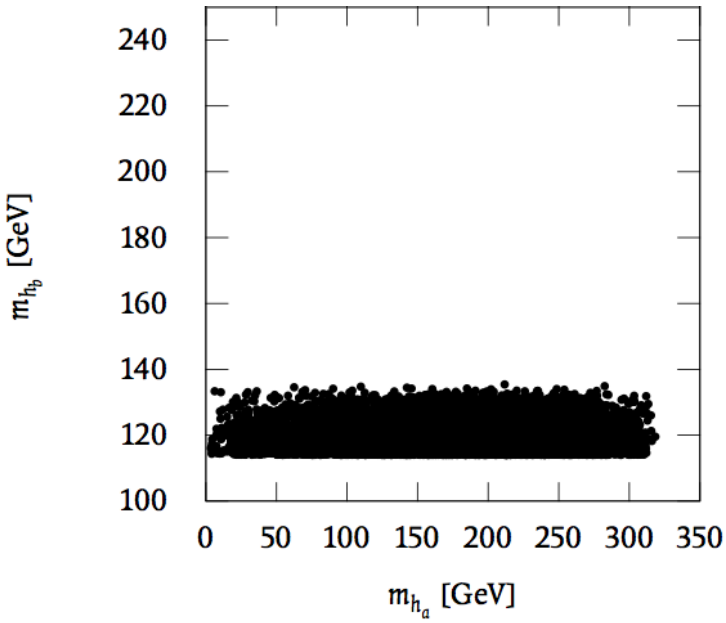

(b) Allowed range of m_{h_a}.

Figure 3.1: Results of a random numerical search for allowed scalar masses with a fixed $v_3/v = 0.6$ [1].

3.2.2 Scalar couplings to gauge and matter fields

When calculating the kinetic terms $|D_\mu \phi_i|^2$ (with $i = 1, 2, 3$), the couplings of the symmetry basis scalars $h_{\{1,2,3\}}$ to the gauge bosons $W^\pm$ and Z^0 are suppressed by a factor of $v_i/v_{SM} < 1$ for $i = 1, 2, 3$. Using equation (3.5a) to transform the kinetic terms into the mass basis of the scalars, two interesting changes compared to standard model physics emerge:

1. The physical scalars h_b and h_c both couple to W^+W^- and Z^0Z^0, but their couplings are modified by

$$\frac{1}{v_{SM}} \left(2vU_{1b} + v_3 U_{3b}\right) \quad \text{for } h_b, \tag{3.10a}$$

$$\frac{1}{v_{SM}} \left(2vU_{1c} + v_3 U_{3c}\right) \quad \text{for } h_c. \tag{3.10b}$$

2. The scalar h_a does not couple to Z^0Z^0 or W^+W^- through the three-point vertex, unlike the other scalars or the standard model Higgs. This is a consequence of the orthogonality of the $h_1 + h_2$ state (roughly h_b and h_c) and the $h_2 - h_1$ state, which was identified as h_a in equation (3.6). Note that the four-point vertices $h_a^2 Z^0 Z^0$ and $h_a^2 W^+ W^-$ still exist.

To obtain the couplings of the scalars to the quarks and leptons, the S_3 invariant Yukawa Lagrangian $\mathscr{L}_Y$ has to be considered:

$$\begin{aligned}\mathscr{L}_Y = {} & f_4 e e^C h_3 + f_5 e \mu^C h_3 + f_1 \mu^C (\mu h_2 + \tau h_1) + f_2 \tau^C (-\mu h_2 + \tau h_1) \\ & + g_4^u u u^C h_3 + g_5^u u c^C h_3 + g_1^u c^C (c h_2 + t h_1) + g_2^u t^C (-c h_2 + t h_1) \\ & + g_4^d d d^C h_3 + g_5^d d s^C h_3 + g_1^d s^C (s h_2 + b h_1) + g_2^d b^C (-s h_2 + b h_1) + \text{H.c.},\end{aligned} \tag{3.11}$$

where the $f_{\{1,2,4,5\}}$ are the leptonic and the $g^{u/d}_{\{1,2,4,5\}}$ are the quark Yukawa couplings for the up and down sectors.

The couplings of h_b and h_c to the quarks and leptons depend on the parameters $v, v_3, \lambda_{\{1,\ldots,8\}}$, and $f_{\{1,2,4,5\}}$ (or, $g^{u/d}_{\{1,2,4,5\}}$ for the quarks), while the couplings of the scalar h_a to fermions depend only on $f_{\{1,2,4,5\}}$ (or, $g^{u/d}_{\{1,2,4,5\}}$ for the quarks). This is clearly a consequence of equation (3.6). The full expressions for the couplings are complicated

functions of these parameters and are not given here, however the patterns in the Yukawa matrices deserve some attention[2]:

$$Y_{h_a} = \begin{pmatrix} 0 & 0 & Y^a_{e_L\tau_R} \\ 0 & 0 & Y^a_{\mu_L\tau_R} \\ Y^a_{\tau_L e_R} & Y^a_{\tau_L\mu_R} & 0 \end{pmatrix}, \tag{3.12a}$$

$$Y_{h_{b/c}} = \begin{pmatrix} Y^{b/c}_{e_L e_R} & Y^{b/c}_{e_L\mu_R} & 0 \\ Y^{b/c}_{\mu_L e_R} & Y^{b/c}_{\mu_L\mu_R} & 0 \\ 0 & 0 & Y^{b/c}_{\tau_L\tau_R} \end{pmatrix}. \tag{3.12b}$$

While $h_{b/c}$ show the diagonal Yukawa couplings similar to the standard model Higgs, they also have off-diagonal components. Due to the absence of natural flavor conservation [78], these lead to scalar-mediated flavor changing currents at tree level, with branching ratios determined by the Yukawa couplings f and g. However, numerically, these off-diagonal couplings are so small as to be insignificant.

The scalar h_a, interestingly, has no diagonal couplings to the quarks and leptons, but instead only features off-diagonal couplings involving a particle of the third generation.

The last two points require further clarification. In a theory with more than one $\mathsf{SU}(2)$ scalar doublet, tree level FCNCs generally exist in the scalar sector. For example, they exist in the ordinary two Higgs doublet model (2HDM), but in the supersymmetric standard model they are avoided by the arrangement that one doublet couples only to the up-type fermions and the other to only the down-types. In nonsupersymmetric scenarios—in the absence of any natural flavor conservation—symmetry arguments have been advanced in the context of multi-Higgs models to show that the off-diagonal Yukawa couplings of the neutral scalars are suppressed by their relation to the off-diagonal entries of the CKM matrix [79].

In the present case, S_3 symmetry, under which both scalars and fermions transform nontrivially, is instrumental in suppressing the off-diagonal couplings. To provide an intuitive understanding, we take—as an example—only the two-flavor μ–τ sector together with two neutral scalars h_1 and h_2. It is not difficult to see that the combination $(h_2 - h_1)$, which corresponds to h_a, couples only off-diagonally, as mentioned earlier. But the other combination $(h_2 + h_1)$, which corresponds to $h_{b/c}$ following equation (3.5a), couples only diagonally to physical μ or τ states. When we consider the quark sector, μ and τ

[2] We show the Yukawa matrices for the charged lepton sector as an example. The equivalent matrices for the quarks follow the same patterns, however.

would be replaced by second and third generation quarks which will have CKM mixing. This will yield off-diagonal entries for the $h_{b/c}$ couplings to quarks suppressed by the off-diagonal CKM elements. The same happens for off-diagonal couplings involving the first two generations as well. The tiny size of tree level FCNC rates in an S_3 flavor model has been noticed also earlier, where predictions for the branching ratios (BRs) BR($\tau \to 3\mu$), BR($K_L \to 2e$), and BR($B_s \to 2\mu$) have been given [80]. In some setups where the fermion transformations under S_3 are not appropriately adjusted, the off-diagonal Yukawa couplings may become order one which induce sizable neutral scalar mediated rare processes, like $K_L \to \mu e$ or $K_L \to 2\pi$ at tree level. This requires those neutral scalars to lie beyond several TeV [76, 81]. In our case, once we adjust the $f_i/g_i^{u,d}$ couplings (with $i = 1, 2, 4, 5$) to reproduce the fermion masses and mixing, the off-diagonal Yukawa couplings are determined too. The largest of them corresponds to $\bar{c}_L t_R h_a$, which is about 0.8. The second largest off-diagonal coupling is that for $\bar{s}_L b_R h_a$, and is about 0.02. The next in line is $\bar{\mu}_L \tau_R h_a$, whose coefficient is about 0.008. The others are orders of magnitude smaller, and are of no numerical significance. Although FCNC processes like B_d–$\bar{B}_d$ and B_s–$\bar{B}_s$ mixing proceed at tree level, the contributions are adequately suppressed even for light scalar mediators.

3.2.3 Collider signatures

The perturbativity condition $|\lambda_{\{1,\ldots,8\}}| \leq 1$ and the requirement $m_{h_b/h_c} \geq 114\,\text{GeV}$ (for which we set $v_3/v \simeq 0.6$) yields m_{h_b} in the neighbourhood of 125 GeV and m_{h_c} within 400 GeV—see the scatter plots in figure 3.1. Note that while the result for the mass of h_c is in tension with the Higgs data from the LHC [12, 13], the mass range can be extended easily by adjusting the allowed range for $\lambda_{\{1,\ldots,8\}}$ still within perturbative bounds. This is the approach taken in scenario II, presented in the next section. Both h_b and h_c would decay into the usual Z^0Z^0, W^+W^-, $b\bar{b}$, $\gamma\gamma$, etc. modes, but the dominant decay mode of h_b (or h_c) for the case of $m_{h_a} < m_{h_b}/2$ (or $m_{h_a} < m_{h_c}/2$) would be into $h_a h_a$. Since the $h_a Z^0 Z^0$ or $h_a W^+W^-$ couplings are nonexistent, the mass of h_a is not directly constrained by the experimental results of the Large Electron–Positron Collider (LEP) and LHC. We numerically calculate the strength of the $h_b h_a h_a$ coupling from the set of acceptable parameters characterizing the potential, and introduce a parameter k which is the ratio of the $h_b h_a h_a$ coupling and the $h_b W^+W^-$ coupling. The magnitude of k depends on the choice of $\lambda_{\{1,\ldots,8\}}$ and v_3. Assuming $m_{h_a} = 75\,\text{GeV}$, we obtain k in the range of 6–30. Just to compare with a 2HDM [82], the corresponding k value, when the heavier Higgs weighing around 400 GeV decays into two lighter Higgs (114 GeV each), is about 10.

In figure 3.2a we have plotted the branching ratio of $h_b \to h_a h_a$ as a function of m_{h_b} for two representative values $m_{h_a} = 50\,\text{GeV}$ and $m_{h_a} = 75\,\text{GeV}$, and for $k \sim 5$ and $k \sim 30$,

which correspond to the smallest and largest k obtained from the set of *accepted* scalar parameters. We observe that till the W^+W^- or Z^0Z^0 decay modes open up, the branching ratio $h_b \to h_a h_a$ is almost 100%. To calculate the decay widths into the usual modes (other than $h_a h_a$), we have used HDECAY [83] by appropriately modifying the gauge and Yukawa couplings. As figure 3.2b suggests, as long as $m_{h_a} < m_t$, h_a will dominantly decay into jets, and one of them can be identified as the b-jet. The branching ratio of $h_a \to \mu\bar{\tau}$ is, nevertheless, not negligible (about 0.1). As shown in figure 3.3, for $m_{h_a} \ll m_t$, the branching ratio of $t \to h_a c$ is quite sizable, which falls with increasing m_{h_a}. It may be possible to reconstruct h_a from $h_a \to \mu\bar{\tau}$. In fact, a light h_a would be copiously produced from the top decay at the LHC. On the other hand, if $m_{h_a} > m_t$, as can be seen again from figure 3.2b, h_a decays to $t\bar{c}$ with an almost 100% branching ratio.

A large k provides an interesting twist to the failed Higgs search at LEP. In this case, $h_b \to h_a h_a$ would overwhelm $h_b \to b\bar{b}$, and hence the conventional search for the SM-like scalar (h_b, as the lighter between h_b and h_c) would fail. This is similar to what happens in the next-to-minimal supersymmetric models, when the lightest scalar would dominantly decay into two pseudoscalars, and each pseudoscalar would then decay into $2b$ or 2τ final states. In view of these possible $4b$ or 4τ Higgs signals, LEP data have been reanalyzed putting constraints on the Higgs production cross section times the decay branching ratios [84, 85]. The possibility of the Higgs cascade decays into 4j (j standing for quark or gluon), $2j + 2$ photons and 4 photons has been studied too [86, 87]. From a study of $4b$ final states, a limit $m_h > 110$ GeV (for a standard model like Higgs) has been obtained [86]. From all other cascade decays the limit on m_h will be considerably weaker. Our h_a has the special feature that it has only off-diagonal Yukawa couplings involving one third-family fermion. If h_b is lighter than the top quark, it would decay as $h_b \to h_a h_a \to 2b + 2j$, and into $b + 1j + \mu + \tau$, the latter constituting a spectacular signal with two different lepton flavors μ and τ. The standard $2b$ and cascade $4b$ decay searches are not sensitive to our final states, and so a value of m_{h_b} much lighter than 110 GeV would have been compatible.

As a standard model like Higgs has been discovered at a mass of 125 GeV [12, 13], which corresponds to the scalar h_b in this scenario, the hidden decay into a nonstandard channel can be ruled out, although the total measured branching ratio is lower than expected as of now. This effectively places a lower mass limit on h_a, with $m_{h_a} > m_{h_b}/2$. Scenario II, which follows in the next section, takes this new result into account.

In summary, in the setup of scenario I there are two scalars which are standard model Higgs like, except that each of them can have a dominant decay into the third ($h_{b/c} \to h_a h_a$). The latter, i.e. h_a, has no $h_a VV$-type gauge interactions, and has only flavor off-diagonal Yukawa couplings with one fermion from the third generation. The measurement of the Higgs mass at the LHC places a lower bound on the mass of h_a.

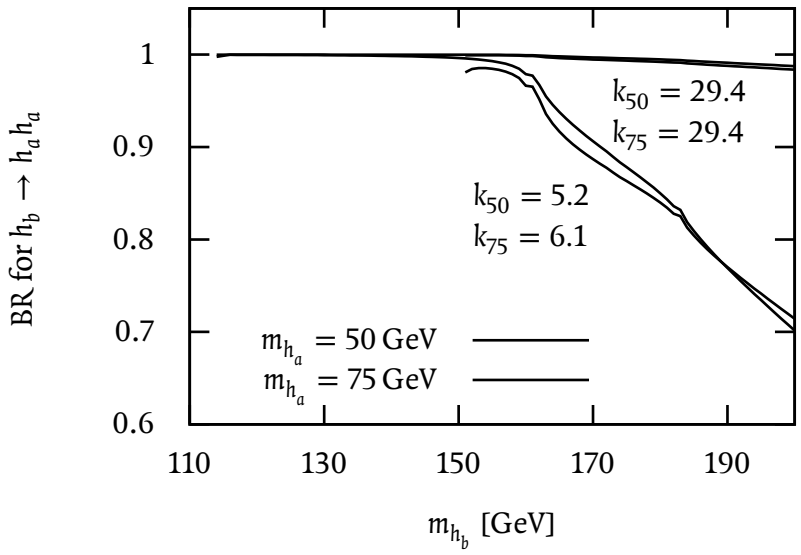

(a) Branching ratio of $h_b \to h_a h_a$ for two representative values of m_{h_a}, and in each case for smallest / largest values of k in the set of accepted scalar parameters.

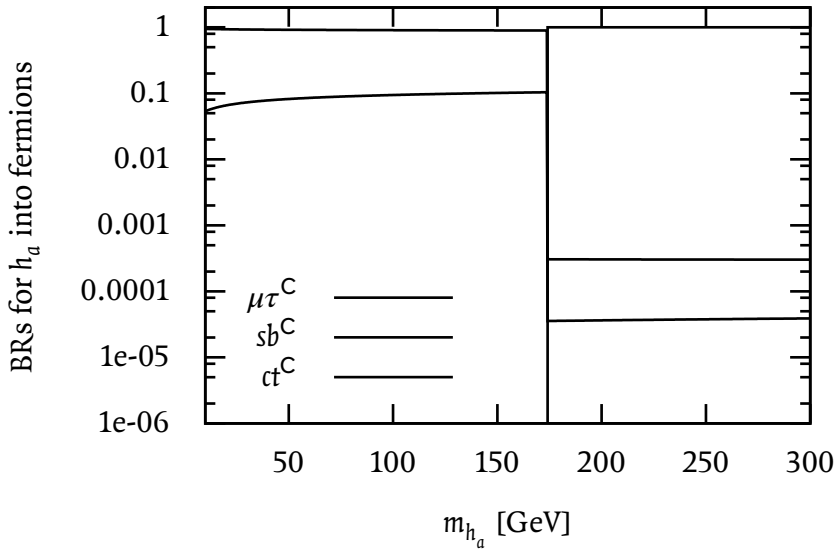

(b) Branching ratios for the decay of h_a into fermions.

Figure 3.2: Branching ratios for several scalar decay modes and the production of h_a through top decays. In (a), k compares the strength of the $h_b h_a h_a$ coupling to the strength of $h_b W^+ W^-$ coupling [1].

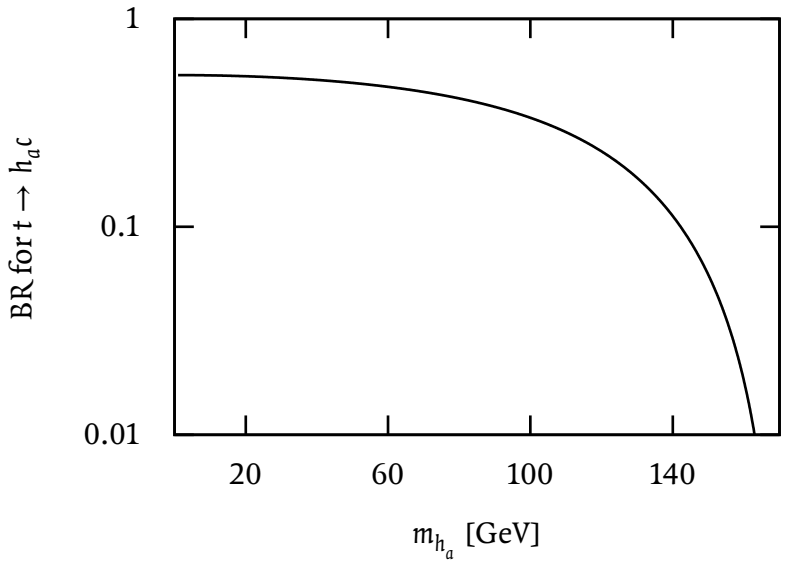

Figure 3.3: Branching ratio of the top quark decay into h_a and charm quark.

3.3 Scenario II: Light scalars and pseudoscalars

The first scenario dealt with only the CP-even scalars and concentrated on the decay $h_b \to h_a h_a$. In the scenario investigated in this section, presented in reference [4], the pseudoscalar degrees of freedom are taken into account as well and an experimental signature in the light of the Higgs discovery is discussed. The main properties dictating the collider signatures remain the same:

1. Two of the three CP-even scalars $h_{b/c}$ have standard model like couplings except that they can dominantly decay into the third scalar h_a, whose couplings are not standard model like.

2. The scalar h_a and pseudoscalar χ_a have no interactions of the type $(h_a/\chi_a)VV$, where $V \equiv W^{\pm}, Z^0$.

3. The scalars/pseudoscalars h_a/χ_a have only flavor off-diagonal Yukawa couplings with one fermion of the third generation.

More specifically, in this scenario we have extended the previous analysis by including not only the CP-even neutral scalars, but all scalar degrees of freedom: three CP-even neutral scalars, two CP-odd neutral scalars and two sets of charged scalars. In this section we will perform the following steps:

1. Determination of the mass spectrum of the neutral scalars/pseudoscalars and the charged scalars following an improved potential minimization technique,

2. Calculation of their couplings to the gauge bosons and matter fields, and

3. Identification of a novel channel of a scalar (pseudoscalar) decay within reach of the LHC.

3.3.1 Mass spectrum of the scalars/pseudoscalars and charged scalars

To obtain the mass spectrum for the physical scalars/pseudoscalars and charged scalars, the potential of equation (3.1) has to be minimized taking all of the fields into account. After diagonalizing the mass matrices the masses of the physical scalars/pseudoscalars are obtained. These are denoted by $h_{a,b,c}$, $\chi_{a,b}$, and $h^+_{a,b}$.

To keep the potential globally bounded from below the conventional approach is to arrange all the coefficients of the highest-power terms in the potential to be positive

definite. This was followed in the first scenario where only the CP-even degrees of freedom were considered. However, this strategy eliminates the allowed possibility of a large part of valid parameter space where the potential is bounded from below although some coefficients still stay negative.

The present scenario is now more complete in the sense that we deal with the complete spectrum including all neutral and charged degrees of freedom following the potential minimization. Moreover, some parts of the allowed parameter space that were cut off by the traditional method are now resurrected by our new approach. As a first step, to have an analytic feel we identify some simple-looking relations of the coefficients by inspection that allow the potential to stay positive and also provide the physical scalar masses. To do this the scalar potential in equation (3.1) is factorized into a simplified polynomial in ϕ_1, ϕ_2, and ϕ_3, treating them naively as real quantities for calculational ease. There remain three distinct types of terms of order four: ϕ_i^4, $\phi_i^2\phi_j^2$, and $\phi_i^2\phi_j\phi_k$, where $i, j, k = 1, 2, 3$. Out of the nine terms, only six have independent coefficients, called $c_{\{1,\dots,6\}}$:

$$c_1\phi_1^4 + c_1\phi_2^4 + c_2\phi_3^4 + c_3\phi_1^2\phi_2^2 + c_4\phi_1^2\phi_3^2 + c_4\phi_2^2\phi_3^2 + c_5\phi_1^2\phi_2\phi_3 + c_5\phi_1\phi_2^2\phi_3 + c_6\phi_1\phi_2\phi_3^2. \quad (3.13)$$

The coefficients $c_{\{1,\dots,6\}}$ can be expressed in terms of the potential parameters $\lambda_{\{1,\dots,8\}}$:

$$\begin{aligned} c_1 &= \frac{\lambda_1}{2} + \frac{\lambda_2}{2}, \quad c_2 = \frac{\lambda_4}{2}, \quad c_3 = \lambda_1 - \lambda_2 + \lambda_3, \\ c_4 &= \lambda_5 + \lambda_6, \quad c_5 = 2\lambda_8, \quad c_6 = 2\lambda_7. \end{aligned} \quad (3.14)$$

By inspection we found the following conditions on the coefficients $c_{\{1,\dots,6\}}$ from the analytic expressions:

$$\begin{gathered} c_1 > 0, \quad c_2 > 0, \\ 2c_3 \geq -c_1, \quad 2c_3 \geq -c_2, \quad 2c_4 \geq -c_1, \quad 2c_4 \geq -c_2, \\ -\frac{1}{2}c_1 \leq c_5 \leq c_1, \quad -\frac{1}{2}c_1 \leq c_6 \leq c_1, \quad -\frac{1}{2}c_2 \leq c_5 \leq c_2, \quad -\frac{1}{2}c_2 \leq c_6 \leq c_2. \end{gathered} \quad (3.15)$$

These conditions ensure an acceptable mass spectrum for the neutral scalars/pseudoscalars and charged scalars and keep the potential globally stable. However, this method renders a large part of the parameter space still inaccessible. Moreover, the masses obtained by employing equation (3.15) are generally quite light, none exceeding 300 GeV when $|\lambda_{\{1,\dots,8\}}| \leq \pi$.

To obtain a more complete picture we have transformed equation (3.13) into spherical coordinates (ρ, θ, ϕ). The potential then splits into a radial and an angular part. The

question of global stability is thus reduced to keeping the overall sign of the angular part of the potential positive definite in the limit of the radial part going to infinity:

$$\begin{aligned}\sin^4\theta\Big\{\left(2c_1-c_3\right)\cos(4\phi)+6c_1+c_3\Big\}+8c_2\cos^4\theta\\ +\sin^2(2\theta)\Big(2c_4\sin^2\phi+c_6\sin(2\phi)\Big)+8c_4\cos^2\phi\sin^2\theta\cos^2\theta\\ +4c_5\sin(2\phi)\sin^3\theta\cos\theta\Big(\sin\phi+\cos\phi\Big)>0\end{aligned}\tag{3.16}$$

As this is a transcendental inequality there is no analytically tractable and simple set of conditions that can be imposed on the coefficients $c_{\{1,\dots,6\}}$ to solve equation (3.16). We therefore decided to check the positivity of this function numerically at each point of the parameter space. This allows us to explore the until now inaccessible territory of the stable parameter space that could not be reached by the conditions of equation (3.15). Consequently, masses well beyond 300 GeV for the scalars/pseudoscalars can be reached even while keeping $|\lambda_{\{1,\dots,8\}}| \leq \pi$. To sum up, our equation (3.15) is an improvement over what we have done in scenario I and subsequently our numerical approach improves the size of the accessible parameter space even further.

Diagonalizing the mass matrix of the pseudoscalars gives the symmetry basis pseudoscalars $\chi_{1,2,3}$ in terms of the physical basis pseudoscalars $\chi_{a/b}$:

$$\chi_1 = \frac{v}{v_{\mathrm{SM}}}\mathrm{G}^0 - \left(\frac{1}{\sqrt{2}}\right)\chi_a - \frac{v_3}{\sqrt{2}v_{\mathrm{SM}}}\chi_b, \tag{3.17a}$$

$$\chi_2 = \frac{v}{v_{\mathrm{SM}}}\mathrm{G}^0 + \left(\frac{1}{\sqrt{2}}\right)\chi_a - \frac{v_3}{\sqrt{2}v_{\mathrm{SM}}}\chi_b, \tag{3.17b}$$

$$\chi_3 = \frac{v}{v_{\mathrm{SM}}}\mathrm{G}^0 + \sqrt{2}\frac{v_3}{v_{\mathrm{SM}}}\chi_b. \tag{3.17c}$$

It is interesting to note that the mixing coefficients are very simple and just depend on the ratio v_3/v_{SM}. This is in stark contrast to the mixing of $h_{1,2,3}$ and $h_{a,b,c}$ given in equation (3.5a), where the coefficients are complicated functions of the $\lambda_{\{1,\dots,8\}}$ parameters of equation (3.1).

The mixing relations for the charged scalars $h^+_{a/b}$ are obtained by substituting $\chi \to h^+$ and $\mathrm{G}^0 \to \mathrm{G}^+$ in equation (3.17).

We now derive the pseudoscalar squared masses as

$$m^2_{\chi_a} = -9\lambda_8 v v_3, \tag{3.18a}$$

$$m^2_{\chi_b} = -v^2_{\mathrm{SM}} \left(2\lambda_7 + \lambda_8 \frac{v}{v_3} \right). \tag{3.18b}$$

The corresponding squared masses for the charged scalars are

$$m^2_{h^+_a} = -2\lambda_3 v^2 - v_3^2 \left(\lambda_6 + \lambda_7 \right) + 5\lambda_8 v v_3, \tag{3.19a}$$

$$m^2_{h^+_b} = -v^2_{\mathrm{SM}} \left(\lambda_6 + \lambda_7 + \lambda_8 \frac{v}{v_3} \right). \tag{3.19b}$$

The allowed ranges for the masses can be found by a random scattering in the parameter space where the couplings in the potential are varied within $\lambda_{\{1,\ldots,8\}} \in [-\pi, \pi]$ and the ratio v_3/v is fixed to 0.6. The allowed range for the couplings $\lambda_{\{1,\ldots,8\}}$ has been increased with respect to scenario I to admit a broader mass spectrum. The values are still very much within perturbative bounds. This leads to a CP-even mass spectrum similar to scenario I, but with higher allowed ranges. The scalar h_a can be as massive as roughly 800 GeV or arbitrarily light as it evades the LEP bound due to its maximally nonstandard couplings. The mass of the standard model like scalar h_b is limited within 114–500 GeV, while h_c is still heavier. Both h_b and h_c masses should however satisfy the LEP lower bound of 114 GeV (See figure 3.5 for details).

In view of the recent LHC results [12, 13] that hint towards a standard model like Higgs boson at around 125 GeV with a large excluded region above and below, the mass spectrum in this model is compatible with the following scenario:

1. The scalar h_b plays the role of the standard model like Higgs boson with a mass of roughly 125 GeV. The Yukawa and gauge couplings of h_b and h_c are standard model like with numerically negligible flavor off-diagonal couplings, as in scenario I [1].

2. The scalars/pseudoscalars h_a and χ_a have nonstandard interactions that hide them from standard searches, as will be discussed in the following sections. In particular, h_a and χ_a can be very light.

3. All other scalar/pseudoscalar masses, including the charged scalars, can have masses above 550 GeV. We however note that the existing limits on charged scalar masses are not so stringent and the parameters of our potential can be arranged to admit a much smaller mass for them, though this is not the main focus of our present work.

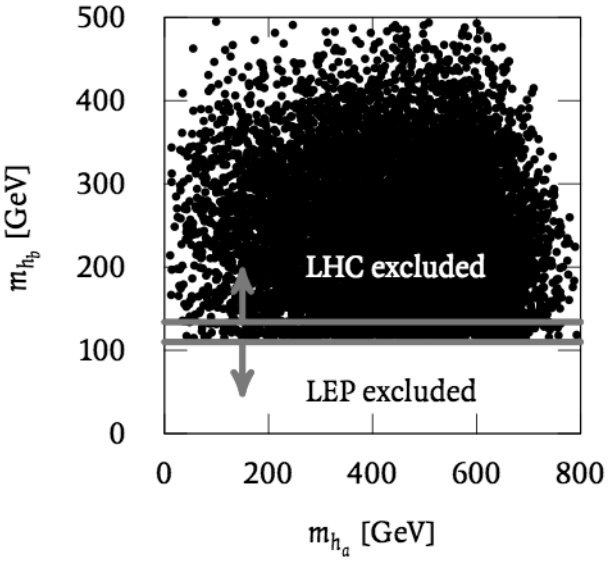

(a) Masses of CP-even scalars h_a and h_b.

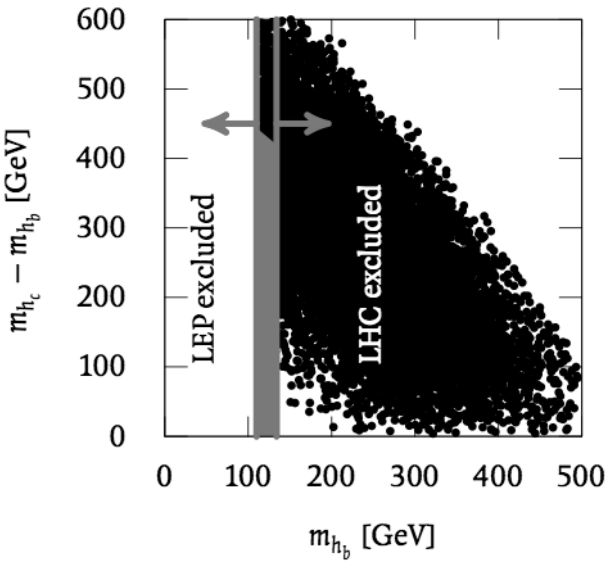

(b) Mass of CP-even scalar h_b plotted against the mass difference of h_c and h_b, the red-shaded strip is also disfavored by LHC which rules out a second standard model like Higgs within 550 GeV.

Figure 3.5: Scatter plots of masses of h_a, h_b, h_c, and χ_a, where $v_3/v = 0.6$. The lines give the current interesting window between 114 GeV (LEP) and 130 GeV (LHC) [12, 13]. (*continued on next page*)

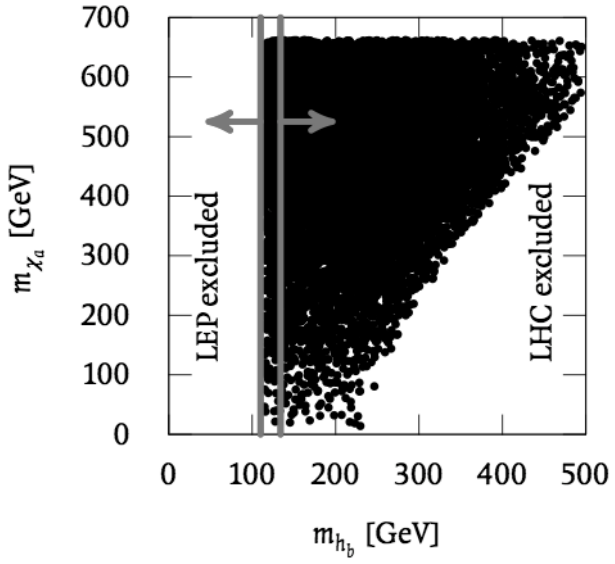

(a) Mass of h_b compared to that of the CP-odd scalar χ_a.

Figure 3.5: Scatter plots of masses of h_a, h_b, h_c, and χ_a, where $v_3/v = 0.6$. The lines give the current interesting window between 114 GeV (LEP) and 130 GeV (LHC) [12, 13].

Table 3.2: Three-point vertices involving at least one neutral scalar/pseudoscalar and gauge bosons. A black square indicates that the vertex exists.

	$h_a^\pm W^\mp$	$h_b^\pm W^\mp$	$\chi_a Z$	$\chi_b Z$	$W^\pm W^\mp$	ZZ
h_a	■	—	■	—	—	—
h_b	—	■	—	■	■	■
h_c	—	■	—	■	■	■
χ_a	■	—	—	—	—	—
χ_b	—	■	—	—	—	—

3.3.2 Scalar/pseudoscalar couplings to gauge and matter fields

It is worth noting that among the couplings listed in table 3.2 the ones involving h_a do not depend on any parameters of the scalar potential, while the couplings of h_b and h_c to the gauge bosons are complicated functions of the scalar mixing parameters, which we refer to in our tables by black squares without displaying their explicit forms. The $h_a \chi_a Z$ coupling has a simple form

$$h_a \chi_a Z: \qquad -\frac{i}{2} G q_\mu, \tag{3.20}$$

where $G = \sqrt{g^2 + g'^2}$ is an electroweak coupling constant and q_μ is the momentum transfer. As stated in the first scenario, h_a stands out because it does not couple to pairs of gauge bosons via the three-point vertex. As a result, neither the LEP lower limit of 114 GeV nor the electroweak precision test upper limit of around 200 GeV applies on it. The same is true for the pseudoscalar χ_a. For certain kinematic regions, the coupling $h_a \chi_a Z$ is important for collider searches as we shall see later. Table 3.3 contains the other gauge-scalar-scalar and the triple-scalar vertices. Note that h_a couples only off-diagonally to the other scalars/pseudoscalars. The $h_a h_a^\pm h_b^\mp$ couplings depend only on v_3/v, while the other triple scalar couplings are complicated functions of the scalar mixing parameters.

The Yukawa Lagrangian of the CP-even scalars in the basis (h_1, h_2, h_3) was given in equation (3.11) and is still correct in this scenario. Rotating the scalars to their physical

Table 3.3: Other three-point vertices. A black square indicates that the vertex exists.

(a) Charged scalars and gauge bosons.

	$h_a^\mp\gamma$	$h_a^\mp Z$	$h_b^\mp\gamma$	$h_b^\mp Z$
$h_a^\pm$	■	■	—	—
$h_b^\pm$	—	—	■	■

(b) Three-scalar/pseudoscalar couplings.

	$h_a h_a$	$h_a h_b$	$h_a h_c$	$h_a^\pm h_a^\mp$	$h_b^\pm h_b^\mp$	$h_a^\pm h_b^\mp$	$\chi_a\chi_a$	$\chi_b\chi_b$	$\chi_a\chi_b$
h_a	—	■	■	—	—	■	—	—	■
h_b	■	—	—	■	■	—	■	■	—
h_c	■	—	—	■	■	—	■	■	—

basis (h_a, h_b, h_c) gives the Yukawa matrices $Y_{\{a,b,c\}}$, shown in equation (3.12). In general, there are two generic textures of Yukawa couplings in this model [1]:

$$Y_a = \begin{pmatrix} 0 & 0 & Y_{13} \\ 0 & 0 & Y_{23} \\ Y_{31} & Y_{32} & 0 \end{pmatrix}, \quad Y_{b,c} = \begin{pmatrix} Y_{11} & Y_{12} & 0 \\ Y_{21} & Y_{22} & 0 \\ 0 & 0 & Y_{33} \end{pmatrix}. \tag{3.21}$$

Here Y_a symbolically describes the Yukawa couplings for h_a, χ_a, and h_a^+, while $Y_{b,c}$ describe the couplings for h_b, h_c, χ_b, and h_b^+. The pattern holds both for leptons and quarks, as in scenario I, and reproduces the observed masses and mixing [48]. The off-diagonal couplings in $Y_{b,c}$ remain numerically small and can be controlled by one free parameter which keeps processes like $\mu \to e\gamma$ and meson mixing well under control. The largest off-diagonal coupling in Y_a is $(h_a/\chi_a)ct$ which is about 0.8 that leads to viable production channel of h_a via t decays as described in the next section. The next largest couplings are $(h_a/\chi_a)sb \approx 0.02$ and $(h_a/\chi_a)\mu\tau \approx 0.008$. The $\chi_a\mu\tau$ coupling induces an interesting decay channel potentially observable at the LHC. Note that since the h_a^+tb coupling does not exist the mass of h_a^+ is not constrained by the LHC searches in the $t \to h^+b$ channel in the mass window of 80 to 160 GeV [88, 89].

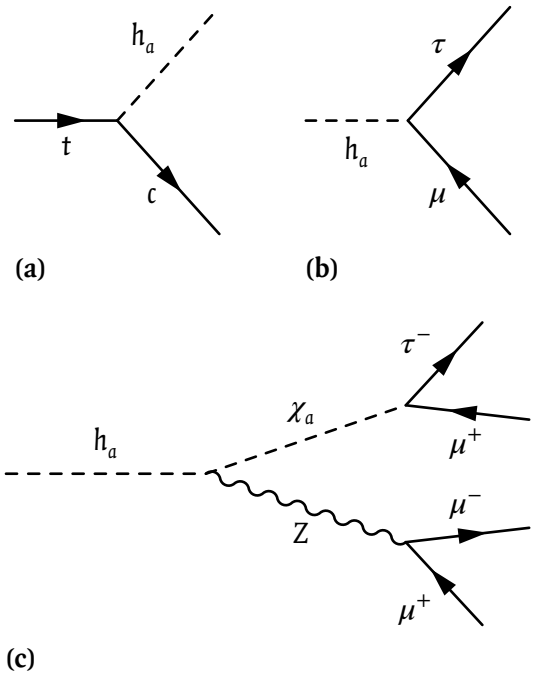

Figure 3.6: Feynman graphs for dominant sources of h_a production and decays which might be relevant at the LHC.

3.3.3 Collider signatures

If kinematically allowed the dominant production of h_a occurs through $t \to h_a c$ (figure 3.6a). The subsequent decay channels depend crucially on the mass of the pseudoscalar χ_a: if $m_{h_a} < m_{\chi_a}$, h_a decays dominantly into b and s quarks, or τ and μ (see figure 3.6b). The BR for $t \to h_a c$ is about 0.17(0.06) for $m_{h_a} = 130(150)$ GeV. Then $h_a \to \mu\tau$ proceeds with a BR of 10% and $h_a \to bs$ with 90%.

A spectacular channel opens up when $h_a \to \chi_a Z$ is kinematically accessible (figure 3.6c). The BR of $h_a \to Z\chi_a$ is almost 100% due to the numerical dominance of the gauge coupling over the Yukawa couplings involving light fermions, followed by $\chi_a \to \tau\mu$ with a BR of about 10%, and a $Z \to \mu\mu$ BR of about 3%. If two h_a are produced from $t\bar{t}$ pairs, this could lead to a characteristic signal with up to six muons with the tau tags. The BRs for $t \to ch_a$ and subsequently $h_a \to \chi_a Z \to \tau\mu\mu\mu$ are plotted in figures 3.8. For these plots $m_{\chi_a} = 20$ GeV has been assumed, which is allowed by current data. The BR peaks for $m_{h_a} = 110$ GeV once the kinematic threshold is crossed and then falls sharply for larger masses due to phase space constraints.

In summary, this is a natural extension of the work [1] presented as scenario I in section 3.2, where only the CP-even scalars were studied, assuming the pseudoscalars to

be too heavy to be relevant. In this scenario we have analyzed the complete scalar/pseudoscalar sector of the S_3 flavor model. We deal with three CP-even, two CP-odd and two sets of charged scalar particles. In this scenario we have improved the potential minimization technique which enabled us to explore a larger region of the allowed parameter space. It is possible to arrange the mass spectrum in full compatibility with the current LHC data, with the scalar h_b mimicking the Higgs-like object lurking around 125 GeV. The specific scalar (pseudoscalar) with prominent nonstandard gauge and Yukawa interactions, namely h_a (χ_a), evade standard searches at LEP/Tevatron/LHC and hence can be rather light. The other scalars/pseudoscalars can be arranged to stay beyond the current LHC reach (e.g. 550 GeV). In particular, we have identified a promising channel for h_a search involving up to six muons in the final state with the tau tags.

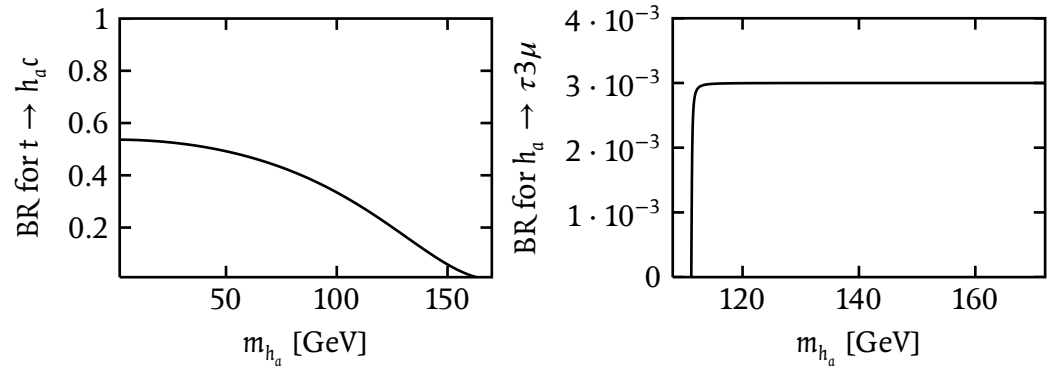

(a) **(b)**

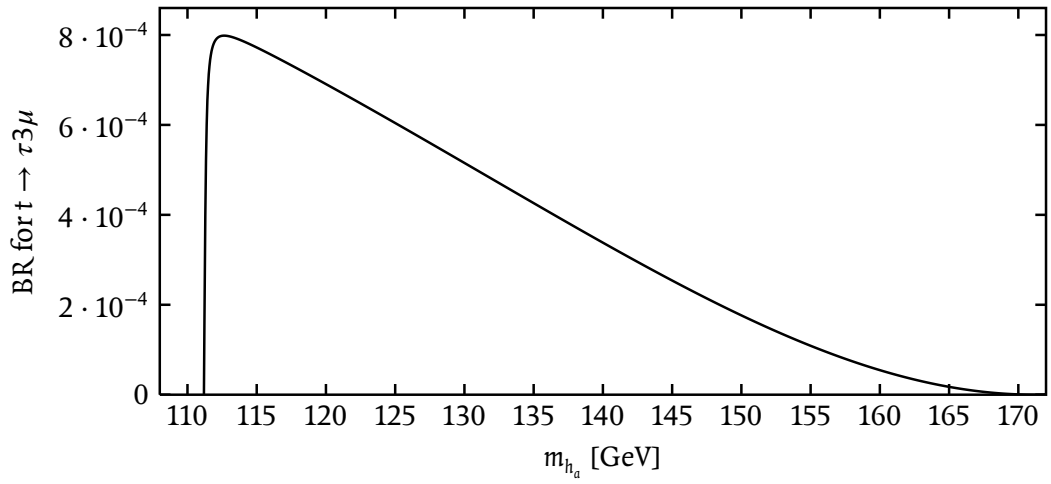

(c)

Figure 3.8: Different branching ratios involving the production and decay of h_a. In all cases, $m_{\chi_a} = 20$ GeV is assumed.

4 Geometrical CP violation and the flavor puzzle

The model based on S_3 presented in chapter 3 is a successful demonstration of a discrete symmetry's ability to produce the mixing of particles in a geometrical way. In particular, the doublet structure of S_3 makes it a suitable candidate for the explanation of the maximal atmospheric neutrino mixing angle θ_{23}. We have shown that such a model can also have significant impact on the electroweak breaking sector which leads to nonstandard collider signatures. It is reasonable to assume that such a behavior should appear in all models based on discrete symmetries where there is no separate and hidden flavon sector.

In this chapter we concentrate on a model that aims to reproduce the quark mixing data, which is known at a precision level, as well as the lepton mixing data. At the same time, a new ingredient is introduced: The model also includes a geometrical and calculable source of CP violation that enters the CKM matrix and is determined by the vacuum of the model[1].

4.1 Introduction to the idea of geometrical CP violation

In the 1970s the idea that CP might be a spontaneously broken symmetry was introduced [90, 91]. In this work we refer to this idea as spontaneous CP violation (SCPV). It has remarkable physical consequences: Starting from a Lagrangian that is CP invariant CP is broken through specific complex phases that appear in the Higgs VEVs breaking the gauge symmetry[2]. This SCPV mechanism provides an elegant solution to the strong CP problem, as was explored in references [92–99]. It is also helpful in alleviating the supersymmetric CP problem [100]. Furthermore, SCPV is the only mechanism that allows for a CP asymmetry to appear in perturbative string theory [101–103].

[1] The model was analyzed in reference [5].

[2] One has to make sure that no field redefinition can be found that evades the SCPV phases.

Table 4.1: Assignments of the scalar fields to $\Delta(27)$ representations.

	$\mathbf{3}_{[0][1]}$	$\mathbf{3}_{[0][2]}$
H	$\begin{pmatrix} H^1 \\ H^2 \\ H^3 \end{pmatrix}$	
$H^\dagger$		$\begin{pmatrix} H_1^\dagger \\ H_2^\dagger \\ H_3^\dagger \end{pmatrix}$

Note: The representations of $\Delta(27)$ can be reviewed in section 2.2.3. The fields H^i, with $i = 1, 2, 3$, are scalar doublets of SU(2).

In general, the CP violating phase appearing in SCPV can depend on the parameters of the Higgs potential, which makes it tunable. An interesting subclass of SCPV appears when the CP phases do not depend on the potential parameters, but are instead *calculable* [104]. This is referred to as geometrical CP violation (GCPV) in this work, because the source of CP violation is a geometrical property of the underlying symmetry group. It was only recently realized by imposing the non-Abelian discrete symmetry group $\Delta(27)$—which was introduced in section 2.2.3—on the full Lagrangian [104]. More recently, GCPV in the context of the group $\Delta(54)$ (cf. references [43, 105]) was also considered [106], which leads to the same scalar potential as $\Delta(27)$. One of the main features of GCPV is that the phases of the VEVs are stable against radiative corrections due to the presence of the non-Abelian discrete symmetry [107, 108].

In reference [106] a promising leading order fermion mass structure was presented. However, viable Yukawa structures require taking terms at the nonrenormalizable level into account. Naturally, the scalar potential acquires higher-order terms at the same time and the compatibility with GCPV is not guaranteed. In this chapter we present an analysis of the scalar potential invariant under $\Delta(27)$ (or $\Delta(54)$, which has the same scalar sector) that leads to GCPV by allowing higher order terms in the scalar potential.

4.2 Geometrical CP violation from the scalar potential of Δ(27)

It is possible to classify the terms allowed in the potential and their effect on the previously obtained vacuum solutions using the properties of the underlying symmetry. Both Δ(27) and Δ(54) can be considered here, as their differences do not manifest themselves in the scalar potential: Due to the SU(2) doublet nature of the scalars an even number of Δ(27)/Δ(54) triplets and their conjugates is needed to form an invariant. Compared to Δ(27), Δ(54) has an additional generator that swaps two components of a triplet. This generator then combines two separate Δ(27) invariants that are related by this transformation into a single invariant of Δ(54). However, this does not affect the analysis of the scalar potential, because the cyclic permutation of all three components is a generator shared by both groups.

4.2.1 The renormalizable potential

The renormalizable potential V_{ren} consists of the scalar fields defined in table 4.1. In this chapter, the Δ(27) triplets H and $H^\dagger$ will usually be shown in terms of their components H^i and $H_i^\dagger$ (where $i = 1, 2, 3$). To make the representations easier to distinguish, the superscript H^i denotes that the fields belongs to a $\mathbf{3}_{[0][1]}$ representation, while its conjugate $H_i^\dagger$—where a subscript i is used—belongs to the $\mathbf{3}_{[0][2]}$ representation of Δ(27). The potential V_{ren} is then given as

$$V_{\text{ren}} = H^i H_i^\dagger + (H^i H_i^\dagger)(H^j H_j^\dagger) + (H^i H_i^\dagger H^i H_i^\dagger) + c_\theta \left[\sum_{i \neq j \neq k} (H^i)^2 H_j^\dagger H_k^\dagger + \text{H.c} \right]. \tag{4.1}$$

Here, repeated indices denote a sum, and we have omitted the arbitrary parameters of each term except for the single phase-dependent term that is inside the square brackets.

As the phase-dependence of the VEVs is relevant for this analysis, it is given as an explicit imaginary exponential function:

$$\begin{aligned} \left\langle H^1 \right\rangle &= v_1 e^{i\varphi_1}, \\ \left\langle H^2 \right\rangle &= v_2 e^{i\varphi_2}, \\ \left\langle H^3 \right\rangle &= v_3 e^{i\varphi_3}. \end{aligned} \tag{4.2}$$

In particular, when the vacuum expectation values are inserted into the potential V_{ren}, the exponentials compensate each other in all terms of the sum except for the last. There the following combination of angles appears in the combined exponential:

$$\theta_i \equiv -2\varphi_i + \varphi_j + \varphi_k, \tag{4.3}$$

where $i \neq j \neq k$.

The VEVs that can be obtained from the minimization of V_{ren} were first presented in reference [104] and further used in reference [106]. Two classes can be distinguished depending on the sign of c_θ in equation (4.1):

$$\langle H \rangle = \frac{v}{\sqrt{3}} \begin{pmatrix} 1 \\ \omega \\ \omega^2 \end{pmatrix}, \text{ or} \tag{4.4a}$$

$$\langle H \rangle = \frac{v}{\sqrt{3}} \begin{pmatrix} \omega^2 \\ 1 \\ 1 \end{pmatrix}, \tag{4.4b}$$

with the calculable phase $\omega \equiv \exp(2\pi i/3)$. Within each class it is possible to obtain equivalent VEVs by taking cyclic permutations of the components, e.g. $(1, 1, \omega^2)^T$, or by swapping the powers of ω, e.g. $(\omega, 1, 1)^T$.

This ω appearing in the VEV is the core ingredient of GCPV. It can serve as the only source of CP violation and is entirely determined by the minimization of the potential V_{ren} of equation (4.1).

4.2.2 Higher-order terms in the potential

When introducing higher-order terms, the number of such terms in the nonrenormalizable potential V increases steeply with the order considered. We use properties of the underlying symmetries to classify this large number of terms in a smaller number of categories that remains manageable up to a certain point. A very important question that arises when adding such terms is whether the property of GCPV survives at higher orders, that is whether the structure of the VEVs presented in equation (4.4) remains valid. It is especially important to assess if $v_1 = v_2 = v_3$ can be maintained. First, note that this equality property of the VEVs is fundamentally connected to the underlying Z_3 cyclic permutation generator introduced in section 2.2.3 (cf. equation [2.25]), which is contained

in both Δ(27) and Δ(54). In the symmetry basis of the scalars, this generator forces any invariant term to be a cyclically permuting combination of the three scalar doublets contained in H. In equations, we denote the cyclic permutation by the shorthand c.p. and only give one instance, i.e. $H^1H_2^\dagger + \text{c.p.}$ stands for $H^1H_2^\dagger + H^2H_3^\dagger + H^3H_1^\dagger$.

Phase-independent contributions

Starting with the phase-independent combinations we observe that they appear only in three different types. Specifically, the distinguishing property of these three types is how many of the components of the triplets are included in a single part of the combination. We have either

$$v_1^n + \text{c.p.}, \text{ or} \tag{4.5a}$$
$$v_1^m v_2^n + \text{c.p.}, \text{ or} \tag{4.5b}$$
$$v_1^l v_2^m v_3^n + \text{c.p.}, \tag{4.5c}$$

where l, m, n are different powers depending on the order of the term. Each of these terms has a different effect on the VEVs. At the renormalizable level of V_{ren}, only the first two types are allowed (cf. equations [4.5a] and [4.5b]):

$$\left(H^1H_1^\dagger\right)^2 + \left(H^2H_2^\dagger\right)^2 + \left(H^3H_3^\dagger\right)^2, \tag{4.6a}$$
$$\left(H^1H_1^\dagger\right)\left(H^2H_2^\dagger\right) + \text{c.p.} \tag{4.6b}$$

The last type—corresponding to the type of equation (4.5c)—appears at order six:

$$\left(H^1H_1^\dagger\right)\left(H^2H_2^\dagger\right)\left(H^3H_3^\dagger\right). \tag{4.7}$$

Table 4.2 summarizes the type of VEVs that each phase-independent combination type favors, depending on the coefficient of that combination being positive or negative.

When considering the triplet tensor products of higher order than two, each invariant can contain more than one type of combination. However, it is always possible to rewrite the potential in such a way that all terms belonging to one combination are grouped. The coefficient for that group is then a linear combination involving the $\mathcal{O}(1)$ coefficients of all the invariants that contain that cyclic combination as well as group theoretical factors and mass scale suppression factors.

In order to obtain a $(0, 0, 1)^\intercal$ or a $(1, 1, 1)^\intercal$ VEV, ultimately the requirement turns out to be that the combined importance of terms favoring one or the other VEV is stronger. This holds even when there is a large number of terms favoring each type of VEV. At arbitrarily

Table 4.2: Types of combinations and preferred VEVs according to the sign of their coefficient.

	+	−
$v_1^n + \text{c.p.}$	$\begin{pmatrix}1\\1\\1\end{pmatrix}$	$\begin{pmatrix}0\\0\\1\end{pmatrix}$
$v_1^m v_2^n + \text{c.p.}$	$\begin{pmatrix}0\\0\\1\end{pmatrix}$	$\begin{pmatrix}0\\1\\1\end{pmatrix}$
$v_1^l v_2^m v_3^n + \text{c.p.}$	$\begin{pmatrix}0\\0\\1\end{pmatrix} \Big/ \begin{pmatrix}0\\1\\1\end{pmatrix}$	$\begin{pmatrix}1\\1\\1\end{pmatrix}$

Note: The combinations displayed in equation (4.5) prefer different VEVs, shown here. The phases ω and ω^2 are omitted, as the terms are phase-independent.

high orders in the scalar potential V, the symmetry generically predicts either a $(0,0,1)^T$ or $(1,1,1)^T$ type of VEV due to its underlying cyclic structure. There are exceptions to this generic prediction, related with the appearance of a $(0,1,1)^T$ VEV or a VEV with the hybrid form $(x,y,y)^T$ with the ratio x/y depending on the values of the combined coefficients, but we have observed that to obtain those fine-tuning of the coefficients is required. The reason is that at each order, the v_i^n type is naturally dominating (and this effect increases with the order). On the other hand, there are also more combinations of the other types, particularly the $v_1^l v_2^m v_3^n$ type which appears most frequently in invariants. Therefore in a typical situation, with similarly valued coefficients for all invariants, the sign of the combined coefficients of v_i^n and $v_1^l v_2^m v_3^n$ determines the VEV, with the $v_i^m v_j^n$ terms not affecting things unless one enhances their contributions—which would be the fine-tuning we referred to previously. So to obtain either $(0,0,1)^T$ or $(1,1,1)^T$ VEVs is quite natural and there are huge regions of parameter space that lead to them.

To better illustrate this we have parametrized a VEV of constant unit magnitude:

$$v_1 = \sin(\alpha \cdot \pi)\cos(\beta \cdot \pi), \tag{4.8a}$$

$$v_2 = \sin(\alpha \cdot \pi)\sin(\beta \cdot \pi), \tag{4.8b}$$

$$v_3 = \cos(\alpha \cdot \pi). \tag{4.8c}$$

In this parametrization, the $(1,1,1)^\intercal$ direction corresponds to $\beta = 1/4$ and $\alpha \simeq 0.30$ (strictly, $\cos(\alpha \cdot \pi) = 1/\sqrt{3}$). Due to the periodicity we focus on the region between zero and 1/2 for α and β. In the case in figure 4.1a, the v_i^n (positive coefficient) and $v_1^l v_2^m v_3^n$ (negative coefficient) terms work together to easily produce a $(1,1,1)^\intercal$ VEV. In the case in figure 4.1b, v_i^n (positive coefficient) overpowers $v_1^l v_2^m v_3^n$ (positive coefficient) to produce a $(1,1,1)^\intercal$ VEV, even though the coefficient of the v_i^n is only 2/7 of the coefficient of $v_1^l v_2^m v_3^n$. The effect of the terms $v_i^m v_j^n$ only becomes relevant if their coefficients are significantly enhanced. The plots shown were created for order six, but they are representative of what happens at higher orders. Note that in both cases reversing the signs of all the coefficients would invert the plot and would lead to the $(0,0,1)^\intercal$ type of VEVs as expected.

Phase-dependent contributions

We have shown that only the last term of equation (4.1) depends on the phase of the VEV. At higher order, new phase dependencies emerge. Again, the large number of new terms that are possible at higher orders can be classified using the fundamental properties of the symmetries. The remaining generators that are shared by the groups Δ(27) and Δ(54) are also Z_3 factors and are fundamentally connected to the allowed phase-dependent invariants.

One such phase-dependent expression was identified in reference [106]: When the powers of the renormalizable—order four—phase-dependent invariant are doubled, another invariant with a distinctly different phase-dependency appears:

$$\sum_{i\neq j\neq k} \left(H^i\right)^4 \left(H_j^\dagger H_k^\dagger\right)^2, \tag{4.9}$$

where $i,j,k = 1,2,3$. This works not only when doubling the powers, but with any integer multiple n. At a given order new combined phases θ_i^n are thus enabled:

$$\theta_i^n \equiv -2n\varphi_i + n\varphi_j + n\varphi_k \qquad (i \neq j \neq k). \tag{4.10}$$

Yet a different phase dependency pattern η_i arises at order six:

$$\eta_i \equiv 3\varphi_i - 3\varphi_j + 0\varphi_k \qquad (i \neq j \neq k). \tag{4.11}$$

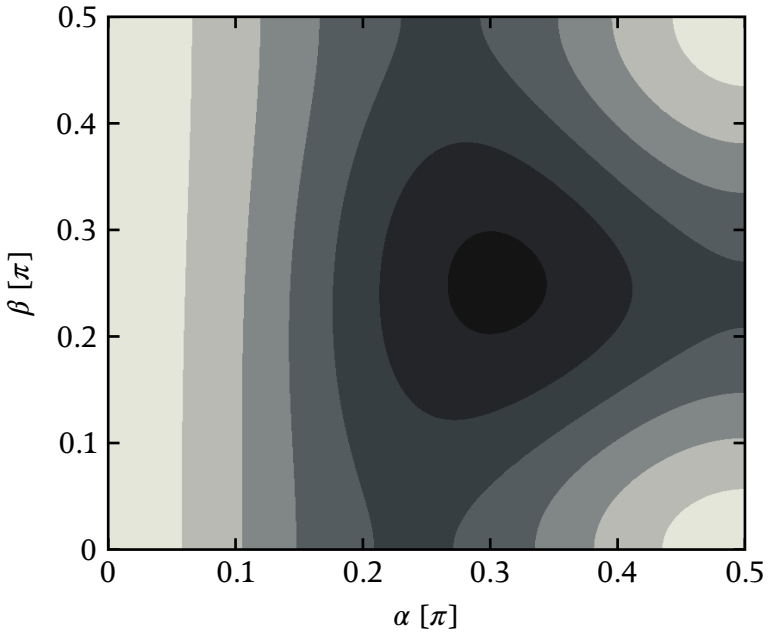

(a) (1, 1, 1) arises from cooperating terms.

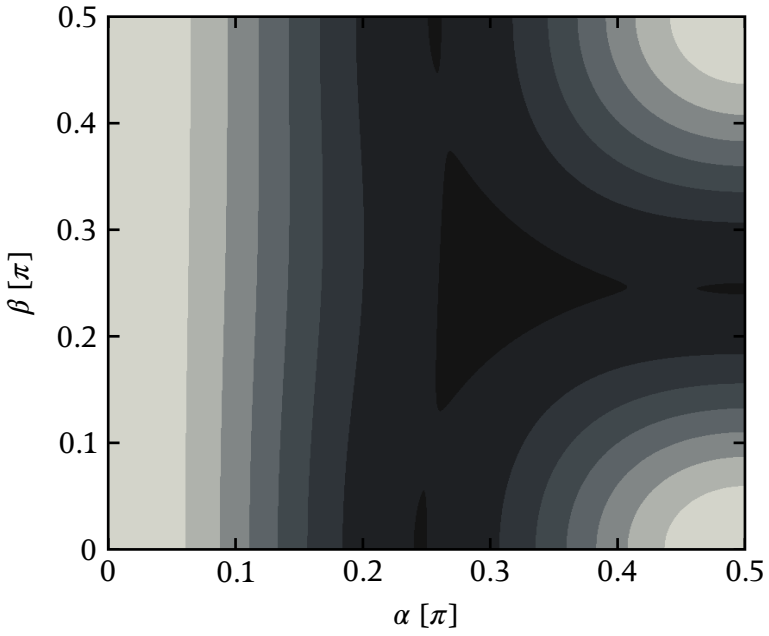

(b) (1, 1, 1) arises from dominant term.

Figure 4.1: Potential strength for cases of different dominating combinations shown in equation (4.5). Deep areas of the potential are darker than light areas.

Like in equation (4.10), this expression can be generalized using integer multiples n that appear at higher orders:

$$\eta_i^n \equiv 3n\varphi_i - 3n\varphi_j + 0\varphi_k \qquad (i \neq j \neq k). \tag{4.12}$$

Remarkably, as there is a link between the allowed phase-dependencies and the generators of the group $\Delta(27)$, it can be concluded that the combinations in equations (4.10) and (4.12) are all allowed possibilities. This can be verified by explicitly computing all possible invariant products and sorting them according to the phase-dependencies. We found that beyond order twelve the number of invariants is too large for this approach to be effective, but it remains possible to verify certain properties about the θ_i^n and η_i^n combinations: They first appear through the respective powers of the lowest order terms with the θ and η dependencies. For example θ^3 and η^2 appear at order twelve respectively from

$$\sum_{i\neq j\neq k} \left(H^i\right)^8 \left(H_j^\dagger H_k^\dagger\right)^4, \tag{4.13}$$

and

$$\sum_{i\neq j} \left(H^i\right)^6 \left(H_j^\dagger\right)^6. \tag{4.14}$$

As with the phase-independent terms discussed already, distinct invariants may include more than one type of phase-dependence, but we can rewrite the potential V in terms of the unique combinations. The effective combined coefficient of each combination is a weighted sum of the $\mathcal{O}(1)$ coefficients of the invariants containing it, with group theoretical factors and the appropriate number of mass scale suppressions for the nonrenormalizable invariants. As an illustration of this, in $\Delta(27)$ the product

$$\left(H \otimes H^\dagger\right) \otimes \left(H \otimes H^\dagger \otimes H^\dagger \otimes H\right), \tag{4.15}$$

contains an invariant

$$\left[\left(H^1H_3^\dagger\right)^3 + \text{c.p.}\right] + 3\left[\left(H^1H_3^\dagger\right)^2\left(H^2H_1^\dagger\right) + \text{c.p.}\right] + 3\left[\left(H^1H_3^\dagger\right)^2\left(H^3H_2^\dagger\right) + \text{c.p.}\right] + 6H^1H^2H^3H_1^\dagger H_2^\dagger H_3^\dagger. \tag{4.16}$$

Going back to the types of VEVs listed in table 4.2, the $(0,0,1)^\intercal$ VEV loses the phase-dependency, so from here on we consider only the $(1,1,1)^\intercal$ class of VEVs. The phase-dependent combinations also preserve the $(1,1,1)^\intercal$ VEVs naturally (as a direct consequence of the nondiagonal cyclic generator). We can now take different combinations

that share the same phase-dependence and further reduce the number of independent combined coefficients: we only need a single one for each unique phase-dependency. A demonstration of this is possible at order six, where one can obtain the θ_i phase dependence that appears first at order four in two distinct ways:

1. By combining the θ_1 portion of the invariant with a matched additional $H^1H_1^\dagger$ to obtain
$$\left[\left(H^1\right)^2 H_2^\dagger H_3^\dagger \left(H^1 H_1^\dagger\right) + \text{c.p.}\right] + \text{H.c.}, \tag{4.17}$$

2. or by combining the θ_1 portion of the invariant with either unmatched $H^2H_2^\dagger/H^3H_3^\dagger$, to obtain
$$\left[\left(H^1\right)^2 H_2^\dagger H_3^\dagger \left(H^{2,3} H_{2,3}^\dagger\right) + \text{c.p.}\right] + \text{H.c.} \tag{4.18}$$

Given a $(1,1,1)^\intercal$ type of VEV, any $H^iH_i^\dagger = v^2/3$ so they all become equivalent. They are also equivalent to the already existing order four term with the same θ_i dependency and we can absorb their effect into a suitable redefinition of the lowest order coefficient (which is naturally dominant, given the higher order terms all have mass scale suppressions). This procedure greatly reduces the number of relevant parameters, particularly when considering high orders where the number of invariants is huge, and allows us to treat the minimization of the potential when a numerical approach would not be feasible.

The effect of all θ_i dependent terms is therefore already known—with a positive combined coefficient c_θ the favored VEV is $(\omega,1,1)^\intercal$, contributing $-3c_\theta v_i^4$ to the potential, otherwise with a negative coefficient the $(1,\omega,\omega^2)^\intercal$ type of VEV is favored contributing $6c_\theta v_i^4$ ($c_\theta < 0$).

We must now consider the effect of the phase dependencies that appear only at the nonrenormalizable level:

$$\theta^n, \qquad \eta, \qquad \eta^n. \tag{4.19}$$

It turns out they all preserve the existing GCPV VEVs, given suitable signs of their respective combined coefficients. Starting with θ^n, we conclude for any n that a positive combined coefficient c_θ^n favors the $(\omega,1,1)^\intercal$ class of VEVs, contributing $-3c_\theta^n v_i^{4n}/M^{(4n-4)}$ to the potential. For a negative combined coefficient the $(1,\omega,\omega^2)^\intercal$ class of VEVs is favored with the potential contribution $6c_\theta^n v_i^{4n}/M^{(4n-4)}$, where M is a generic mass scale associated with the completion of the theory.

Consider next η. These terms do not distinguish the two classes of VEVs and a negative combined coefficient c_η would preserve both classes of VEVs with a potential contribution $6c_\eta v_i^6/M^2$. Finally, for η^n phase-dependencies the effect is the same, with negative combined coefficients c_η^n preserving either class of VEVs with $6c_\eta^n v_i^{6n}/M^{(6n-4)}$.

The conclusion is that it is possible to exactly preserve both the $(1,1,1)^T$ type of VEV together with calculable phases to an arbitrarily high order if one is willing to choose the appropriate signs of the respective combined coefficients. Note also that the θ^n or η^n phase-dependencies get a minimum of either four or six additional v/M suppressions respectively.

To summarize, Δ(27) and Δ(54) are the smallest groups that lead to complex VEVs with calculable phases stable against radiative corrections with the minimum number of three Higgs SU(2) doublets. We have investigated their nonrenormalizable potentials. We described a procedure that allows to classify the possible invariants and greatly reduce the number of relevant parameters. Following this procedure we could treat the minimization of the potential and concluded that the calculable phases can be naturally preserved to arbitrarily high order.

4.3 Fermion masses and mixing

In the last section it was shown that a model based on the discrete symmetry $\Delta(27)$ can have VEVs that contain phases of geometric origin. These VEVs are acquired during the process of electroweak SSB in which the scalar fields contained in the triplet H take part. Astonishingly, the GCPV VEVs are stable even when higher orders in the scalar fields H are considered.

In this section, we extend the model and present for the first time a viable flavor model of fermion masses and mixing that is able to account for all currently observed data[3]. We require a Lagrangian which is invariant under the standard model gauge group, the non-Abelian discrete symmetry $\Delta(27)$ and CP, that is the scalar sector discussed in the last section is the only source of CP violation in this model. We shall show that in this model novel phenomenology—similar to the model presented in chapter 3—emerges, which makes it testable at the LHC.

The origin of CP violation is currently an open question in particle physics. In the standard model, CP is broken due to complex Yukawa couplings and CP violation manifests itself in charged weak interactions through the CKM matrix. Going beyond the standard model it is possible to explore the origin of CP violation, and breaking CP spontaneously is particularly appealing [90, 91]. In the framework of SCPV, CP is a symmetry of the Lagrangian and therefore its parameters are real. CP violation can then arise from complex VEVs of the Higgs multiplets, provided the unitary transformation, U, given by

$$\left\langle H_i \right\rangle \to \left\langle H_i \right\rangle^* = U_{ij} \left\langle H_j \right\rangle, \tag{4.20}$$

acting on the H_i and relating the VEV to its complex conjugate, is *not* a symmetry of the Lagrangian. If it is, then CP is conserved even though the VEVs are complex.

In this model, the calculable phase arising from GCPV is uniquely determined independently of the arbitrary parameters of the scalar potential. GCPV requires at least three Higgs doublets and a non-Abelian symmetry [104]. $\Delta(27)$ is known to be the smallest group for producing geometrical phases. In reference [106] this was generalized to larger groups obtaining the same calculable phases. Recently, several new phase solutions were advanced and expressed in terms of the number of scalars and the group [109].

So far, viable models of fermion masses and mixing within the GCPV framework have not been constructed, although promising leading order structures have been proposed [106]. Motivated by these previous works, we attempt here to produce for the first time the *minimal* model of GCPV which can fit all data in the quark sector, which is

[3] The results of this section were presented in reference [6].

known to great accuracy, including the complex phase. For this purpose we add only the minimal amount of additional matter to the $\Delta(27)$ model introduced.

As in the last section, we assume—without any loss of generality—that the three Higgs doublets, H^i, transform as a $\Delta(27)$ triplet with an assignment to a $\mathbf{3}_{[0][1]}$ irreducible representation with an *upper* index. Their Hermitian conjugates $H_i^\dagger$ transform as the conjugate representation $\mathbf{3}_{[0][2]}$ with a *lower* index, constituting the antitriplet. We now clarify our notation and illustrate some group properties. We deviate somewhat from the notation of section 2.2.3 by using an equivalent representation of the generators of $\Delta(27)$. The generator that performs cyclic permutation is defined as

$$\mathsf{D}'_{\mathbf{3}}(b)\begin{pmatrix} H^1 \\ H^2 \\ H^3 \end{pmatrix} = \begin{pmatrix} H^2 \\ H^3 \\ H^1 \end{pmatrix}, \tag{4.21a}$$

$$\mathsf{D}'_{\mathbf{3}}(b)\begin{pmatrix} H_1^\dagger \\ H_2^\dagger \\ H_3^\dagger \end{pmatrix} = \begin{pmatrix} H_2^\dagger \\ H_3^\dagger \\ H_1^\dagger \end{pmatrix}, \tag{4.21b}$$

where $\omega \equiv \exp(2\pi \mathrm{i}/3)$. The action of the first diagonal generator is given as

$$\mathsf{D}'_{\mathbf{3}}(a)\begin{pmatrix} H^1 \\ H^2 \\ H^3 \end{pmatrix} = \begin{pmatrix} H^1 \\ \omega H^2 \\ \omega^2 H^3 \end{pmatrix}, \tag{4.21c}$$

$$\mathsf{D}'_{\mathbf{3}}(a)\begin{pmatrix} H_1^\dagger \\ H_2^\dagger \\ H_3^\dagger \end{pmatrix} = \begin{pmatrix} H_1^\dagger \\ \omega^2 H_2^\dagger \\ \omega H_3^\dagger \end{pmatrix}. \tag{4.21d}$$

The one-dimensional representations $\mathbf{1}_{i,j}$ transform as given in equation (2.26), i.e. the first index corresponds to the b generator, the second index to the a generator.

We have shown in the last section that the renormalizable scalar potential in the $\Delta(27)$ context can lead to a complex VEV of the type:

$$\langle H \rangle = v \begin{pmatrix} \omega \\ 1 \\ 1 \end{pmatrix}, \tag{4.22}$$

that necessarily violates CP, as the corresponding U (cf. equation [4.20]) is not a symmetry of the potential. We will revisit the scalar potential in greater detail later, but now it is important to focus on the Yukawa interactions.

When focusing on the Yukawa interactions, we start with the quarks and recall the results of reference [106]: In order to make invariant Yukawa terms some of the quarks must transform as triplet or antitriplet under $\Delta(27)$ [104]. We write the invariants symbolically as

$$QH^i d^C, \tag{4.23}$$

and

$$QH_i^\dagger u^C, \tag{4.24}$$

where we omit the SU(2) indices, with Q the left-handed quark doublets and u^C, d^C as the up and down right-handed SU(2) singlets. As described in reference [106], by choosing Q^i as a $\mathbf{3}_{[0][1]}$ we would necessarily require the $(d^C)^i$ to transform also as a $\mathbf{3}_{[0][1]}$. Instead, if Q_i is a $\mathbf{3}_{[0][2]}$, the u_i^C is forced to be a $\mathbf{3}_{[0][2]}$. The end result is at least one sector has a leading order Yukawa structure given by the $\Delta(27)$ invariant $\mathbf{3}_{[0][i]} \otimes \mathbf{3}_{[0][i]} \otimes \mathbf{3}_{[0][i]}$. With the VEV in equation (4.22), this structure leads to a mass matrix with three degenerate quark masses. We therefore conclude that Q cannot be assigned as a triplet or an antitriplet.

We are thus forced to choose instead u^C and d^C as $\Delta(27)$ triplets yielding

$$QH^i d_j^C, \tag{4.25}$$

and

$$QH_i^\dagger (u^C)^j, \tag{4.26}$$

with Q as one-dimensional representations. Both sectors have Yukawas arising as the $\Delta(27)$ invariants

$$\mathbf{1}_{i,j} \otimes \left(\mathbf{3}_{[0][1]} \otimes \mathbf{3}_{[0][2]} \right). \tag{4.27}$$

Although $\mathbf{3}_{[0][1]} \otimes \mathbf{3}_{[0][2]}$ results in nine distinct one-dimensional representations, the group properties are such that any $\mathbf{3}_{[0][1]} \otimes \mathbf{3}_{[0][2]} \to \mathbf{1}_{i,j}$ with $i \neq 0$ explicitly involves

powers of the complex ω, so these possibilities are not allowed by CP invariance of the Lagrangian. To generate a renormalizable Yukawa interaction we are then restricted to assign Q_1, Q_2 and Q_3 each as one or the other of the three $\mathbf{1}_{0,i}$ one-dimensional representations. The remaining possibilities are then assigning

1. all three Q in the same one-dimensional representations, or
2. assigning two in the same, or
3. all three Q in different representations.

All three structures lead to mass matrices that have a special structure distinguished by rows. The choice of Q as $\mathbf{1}_{0,0}$, $\mathbf{1}_{0,1}$ or $\mathbf{1}_{0,2}$ forces the respective $H^i d_j^C$ or $H_i^\dagger (u^C)^j$ product to be $\mathbf{1}_{0,0}$, $\mathbf{1}_{0,2}$ or $\mathbf{1}_{0,1}$ respectively, which essentially amounts to a shift in the position of the ω in the mass matrix. More explicitly the corresponding down mass matrix $\tilde{M}_d$ looks like:

$$\tilde{M}_d = v \begin{pmatrix} y_1\omega & y_1 & y_1 \\ y_2 & y_2\omega & y_2 \\ y_3 & y_3 & y_3\omega \end{pmatrix}, \tag{4.28}$$

and the associated up quark mass matrix looks very similar (ω^2 instead of ω and the second and third rows swapped). Conversely, if Q_1, Q_2, and Q_3 are assigned to $\mathbf{1}_{0,0}$, $\mathbf{1}_{0,0}$, and $\mathbf{1}_{0,2}$ respectively, we get:

$$M_d = v \begin{pmatrix} y_1\omega & y_1 & y_1 \\ y_2\omega & y_2 & y_2 \\ y_3 & y_3 & y_3\omega \end{pmatrix}. \tag{4.29}$$

We recall that due to the explicit CP invariance of the Lagrangian, the Yukawa couplings are all real, and the phase appears only through the complex VEV. At this point it is instructive to show the Hermitian matrices $MM^\dagger$:

$$\tilde{M}_d \tilde{M}_d^\dagger = 3v^2 \begin{pmatrix} y_1^2 & 0 & 0 \\ 0 & y_2^2 & 0 \\ 0 & 0 & y_3^2 \end{pmatrix}. \tag{4.30}$$

Vanishing off-diagonal entries follow from $1 + \omega + \omega^2 = 0$.

Finally, for M_d we have:

$$M_d M_d^\dagger = 3v^2 \begin{pmatrix} y_1^2 & y_1 y_2 & 0 \\ y_1 y_2 & y_2^2 & 0 \\ 0 & 0 & y_3^2 \end{pmatrix}. \tag{4.31}$$

Note that the determinant of this structure is zero but it has two nonvanishing masses. The last choice—all generations of Q in the same one-dimensional representation—leads to a rank one structure with a single nonvanishing mass. Another relevant observation is that the complex phase is entirely absent in all these Hermitian structures.

In order to obtain a viable CKM matrix it is necessary to generate additional off-diagonal terms. The minimal way to do this is to add a gauge singlet scalar that is assigned to a nontrivial $\Delta(27)$ one-dimensional representation, which we denote as ϕ. Without any loss of generality we place ϕ in the representation $\mathbf{1}_{0,1}$. This enables a new nonrenormalizable Yukawa coefficient per row, associated with terms of the type $QH^i d_j^C \phi$. For Q_1, Q_2, and Q_3 in $\mathbf{1}_{0,0}$, $\mathbf{1}_{0,0}$, and $\mathbf{1}_{0,2}$ respectively, we have to add to M_d the corresponding mass matrix:

$$M_\phi = v \begin{pmatrix} y_{\phi 1} & y_{\phi 1}\omega & y_{\phi 1} \\ y_{\phi 2} & y_{\phi 2}\omega & y_{\phi 2} \\ y_{\phi 3}\omega & y_{\phi 3} & y_{\phi 3} \end{pmatrix}. \tag{4.32}$$

From the interference $M_d M_\phi^\dagger + M_\phi M_d^\dagger$ we obtain the required off-diagonal entries whereas the effect of $M_\phi M_\phi^\dagger$ can be absorbed within the structure of $M_d M_d^\dagger$.

A complex phase in the CKM matrix requires that the Hermitian matrices of the $MM^\dagger$ type are complex, which is not the case up to now. To preserve the complex phase in the Hermitian matrices requires a further augmentation. The minimal possibility is to consider the nonrenormalizable interactions that contain higher powers of H, e.g. $QH^i d_j^C (H^k H_l^\dagger)$. The only nontrivial structure that we extract from the last nonrenormalizable combination is:

$$M_H = v \begin{pmatrix} y_{H1} & y_{H1}\omega^2 & y_{H1}\omega^2 \\ y_{H2} & y_{H2}\omega^2 & y_{H2}\omega^2 \\ y_{H3}\omega^2 & y_{H3}\omega^2 & y_{H3} \end{pmatrix}, \tag{4.33}$$

where the identity $1 + \omega + \omega^2 = 0$ was used and the existing coefficients were redefined to absorb similar entries in the mass matrix. From the interference $M_d M_H^\dagger + M_H M_d^\dagger$ we

Table 4.3: Comparison of experimental results for the Wolfenstein parameters with a model fit.

Wolfenstein parameter	Experimental value	Model value
λ	0.22535 ± 0.00065	0.22534
A	$0.811^{+0.022}_{-0.012}$	0.810
$\bar{\rho}$	$0.131^{+0.026}_{-0.013}$	0.129
$\bar{\eta}$	$0.345^{+0.013}_{-0.014}$	0.344

Note: The experimental values for the Wolfenstein parameters are from reference [16].

obtain the phases that enable complex CKM elements, whereas both $M_\phi M_H^\dagger + M_H M_\phi^\dagger$ and $M_H M_H^\dagger$ give structures that do not qualitatively change the analysis. The essential point is that the presence of M_H is crucial to generate the phase.

Note that M_ϕ and M_H are the minimal mandatory additions that are necessary for a perfect fit to the existing data. Following the above chain of arguments, we finally write the relevant Lagrangian, explicitly showing the $\Delta(27)$ multiplet indices, as:

$$\mathscr{L}_{\text{Yuk}} = Q\left(H^{\dagger i} u_j^c + H_i d^{cj} + H_i d^{cj}\phi + H_i d^{cj}\left[H_k H^{\dagger l}\right]\right). \tag{4.34}$$

The assignments of the particles to the irreducible representations of $\Delta(27)$ are summarized in table 4.4.

In fact we found that the only choice that favorably accounts for the precision flavor data is when Q_1, Q_2, and Q_3 are chosen as $\mathbf{1}_{0,0}$, $\mathbf{1}_{0,0}$, and $\mathbf{1}_{0,2}$ respectively. Concerning the up quark sector, $M_u M_u^\dagger$ can be considered to be diagonal, and we need only one additional nonrenormalizable Yukawa coupling in order to generate the small up quark mass. In figure 4.2 we show that with this choice we can successfully reproduce the Wolfenstein parameters from reference [16], which are given in table 4.3.

The lepton sector is experimentally less constrained than the quark sector. The possible invariants depend on what is responsible for the generation of neutrino masses, e.g. the type of seesaw mechanism, as discussed in reference [110]. In addition to the

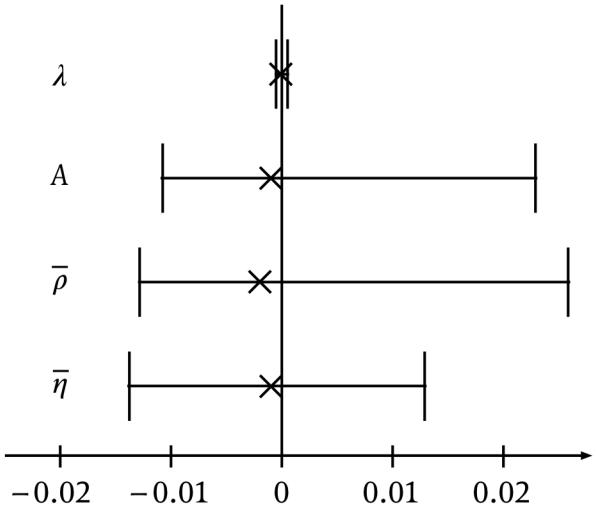

Figure 4.2: The experimental spread of the Wolfenstein parameters λ, A, $\bar{\rho}$ and $\bar{\eta}$ around their central values [16]. Each experimental value is shifted in such a way that their central values line up with the y axis. Crosses denote our model values.

structures that fit the quark sector, other representation choices can also work in the lepton sector. A leptonic model based on the $\mathbf{3}_{[0][i]} \otimes \mathbf{3}_{[0][i]} \otimes \mathbf{3}_{[0][i]}$ invariants in $\Delta(27)$ has been discussed in reference [111] (for the A_4 group see the detailed analysis in references [112, 113]).

We now turn our attention to the scalar potential which contains the $\Delta(27)$ triplet H_i as well as ϕ and is thus more complex than the one shown in equation (4.1). The full renormalizable potential is (recalling that all couplings are real):

$$\begin{aligned} V(H,\phi) = {} & m_1^2 \left[H_1 H_1^\dagger + \text{c.p.}\right] + m_2^2 \phi\phi^\dagger + m_3 \left[\phi^3 + \text{H.c.}\right] + \lambda_1 \Big[\left(H_1 H_1^\dagger\right)^2 \\ & + \text{c.p.}\Big] + \lambda_2 \left[H_1 H_1^\dagger H_2 H_2^\dagger + \text{c.p.}\right] + \lambda_3 \left[H_1 H_2^\dagger H_1 H_3^\dagger + \text{H.c.} + \text{c.p.}\right] + \lambda_4 \left[\phi\phi^\dagger\right]^2 \\ & + \lambda_5 \left[\phi\left(H_1 H_2^\dagger\right) + \text{H.c.} + \text{c.p.}\right] + \lambda_6 \left[\phi\phi\left(H_1 H_3^\dagger\right) + \text{H.c.} + \text{c.p.}\right], \end{aligned} \tag{4.35}$$

where we write c.p. to denote the cyclic permutations on the $\Delta(27)$ indices which we do not explicitly show. The geometrical phase solution in equations (4.22) is not affected by $\phi\phi^\dagger$. When λ_5 and λ_6 are small, equation (4.22) holds, and otherwise one can add a Z_4 symmetry acting on ϕ to trivially enforce them to vanish (in this case equation (4.32) arises from a ϕ^4 insertion instead of ϕ, all conclusions remaining unchanged). For illustration we display only the CP-even scalar components (in this class of models, one

can separately identify scalars and pseudoscalars [114]). Following the minimization of the potential and determination of the mass eigenvalues, we observed these features:

1. The field ϕ is much heavier (beyond 1 TeV) and decouples from the $\mathsf{SU}(2)$ doublets. More specifically, the mass of ϕ is determined by $\lambda_{\{4,5,6\}}$, while those of $h_{\{a,b,c\}}$ are controlled by $\lambda_{\{1,2,3\}}$.

2. The physical scalars h_a, h_b and h_c mix in a very specific way as witnessed in chapter 3 in the S_3 context [1, 4, 70, 115]. The scalar mass squared matrix has the structure

$$\begin{pmatrix} A & B & C \\ B & A & C \\ C & C & D \end{pmatrix}, \tag{4.36}$$

   which leads to one physical scalar h_a that is orthogonal to the other scalars and has no $h_a VV$-type gauge couplings (where $V = W^{\pm}, Z^0$). Its Yukawa couplings to up- and down-type quarks are strongly suppressed, except that the $h_a cc$ and $h_a uc$ couplings are about 0.25. The other physical scalars, h_b and h_c, have almost standard model like gauge and Yukawa couplings.

Adjusting the scalar potential couplings, two viable scenarios can be identified:

1. There is only one light scalar, h_b, that plays the role of the standard model like Higgs found near 125 GeV. In this case all other scalars are beyond the current exclusion range of the LHC.

2. A scenario which has richer collider consequences emerges when the exotic scalar h_a is light enough to be produced (either through $h_a uc$, $h_a cc$ interactions or through heavy scalar decays) at the LHC. Under the reasonable assumption that m_ϕ is greater than 1 TeV or so we can obtain the following analytic relations:

$$m^2_{h_a} = \frac{2}{3}\left(2\lambda_1 v^2 - 2\lambda_2 v^2 + 3\lambda_3 v^2\right), \tag{4.37a}$$

$$\begin{aligned} m^2_{h_b} = \frac{1}{6}\Big(&5\lambda_1 v^2 + 4\lambda_2 v^2 - \sqrt{3}\Big[v^4\big(3\lambda_1^2 + 8\lambda_1\lambda_2 \\ &- 16\lambda_1\lambda_3 + 16\lambda_2^2 - 64\lambda_2\lambda_3 + 64\lambda_3^2\big)\Big]^{\frac{1}{2}}\Big), \end{aligned} \tag{4.37b}$$

$$\begin{aligned} m^2_{h_c} = \frac{1}{6}\Big(&5\lambda_1 v^2 + 4\lambda_2 v^2 + \sqrt{3}\Big[v^4\big(3\lambda_1^2 + 8\lambda_1\lambda_2 \\ &- 16\lambda_1\lambda_3 + 16\lambda_2^2 - 64\lambda_2\lambda_3 + 64\lambda_3^2\big)\Big]^{\frac{1}{2}}\Big). \end{aligned} \tag{4.37c}$$

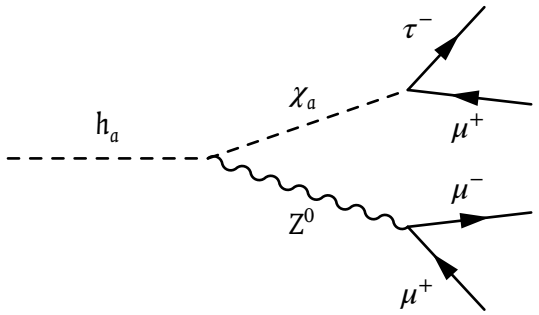

Figure 4.3: Example of a decay mode of the exotic scalar h_a that can be tested at the LHC.

> It is possible to adjust the potential couplings λ_i to yield m_{h_a} around or perhaps slightly larger than the mass 125 GeV of the standard model like h_b, with h_c heavier than 600 GeV.

In this case, a spectacular decay channel opens through $h_a \to \chi_a Z$, fixing $m_{\chi_a} \approx 20$ GeV, with subsequent decays of the pseudoscalar χ_a to charged leptons of different flavors (e.g. $\mu\tau$) and of the Z^0 boson to leptons—see figure 4.3. There is enough freedom in the lepton sector to boost this χ_a coupling, which may generate a sizable branching ratio in this channel. However, a more specific prediction requires a detailed numerical study of the lepton Yukawa sector which we do not delve into here.

In summary, we have for the first time reproduced the CKM mixing matrix in a minimal $\Delta(27)$ flavor model, which is the smallest group where one can implement spontaneous CP violation of geometrical origin. Since quark mixing can be tested in several different independent channels, to reproduce the CKM matrix in a minimal scenario is often more difficult than fitting the lepton mixing. Within the framework of a large class of discrete symmetries it is usually difficult to exclude different choices of representations from data. But our scenario is quite falsifiable, in the sense that only two choices broadly worked, out of which only one set of matter and Higgs representations fits the ever growing precision of flavor data. The scalar sector of the model inherits enough symmetries of the flavor group which induce exotic scalar decays into multi-lepton of different flavors, constituting a smoking gun signal of the model testable at the LHC.

Table 4.4: Assignments of the scalar and fermion fields to $\Delta(27)$ representations.

	$\mathbf{3}_{[0][1]}$	$\mathbf{3}_{[0][2]}$	$\mathbf{1}_{0,0}$	$\mathbf{1}_{0,1}$	$\mathbf{1}_{0,2}$
$\mathsf{SU}(2)_\mathbf{2}$ scalars	$\begin{pmatrix} H^1 \\ H^2 \\ H^3 \end{pmatrix}$				
		$\begin{pmatrix} H_1^\dagger \\ H_2^\dagger \\ H_3^\dagger \end{pmatrix}$			
$\mathsf{SU}(2)_\mathbf{1}$ scalar				ϕ	
$\mathsf{SU}(2)_\mathbf{1}$ fermions	u^C				
		d^C			
$\mathsf{SU}(2)_\mathbf{2}$ fermions			Q_1		
					Q_2
					Q_3

Note: The representations of $\Delta(27)$ can be reviewed in section 2.2.3. The fields H^i, with $i = 1, 2, 3$, are scalar $\mathsf{SU}(2)$ doublets, ϕ is an $\mathsf{SU}(2)$ singlet scalar.

5 Neutrino mixing from the right-handed sector

In the absence of light right-handed neutrinos, neutrino masses can be generated through the effective Weinberg dimension-five-operator [35]

$$-\mathscr{L}_{\phi\phi} = \frac{C}{m}\left(\bar{\ell}_L\tilde{\phi}\right)\left(\phi^\dagger\tilde{\ell}_R\right) + \text{H.c.}, \tag{5.1}$$

where C is a coupling, m a mass scale suppressing the operator and

$$\ell_L \equiv \begin{pmatrix} \nu_L \\ e_L \end{pmatrix}, \qquad \tilde{\ell}_r \equiv \begin{pmatrix} e_R^C \\ -\nu_r^C \end{pmatrix}, \qquad \phi \equiv \begin{pmatrix} \phi^+ \\ \phi^0 \end{pmatrix}, \qquad \tilde{\phi} \equiv \begin{pmatrix} \phi^{0\dagger} \\ -\phi^- \end{pmatrix}. \tag{5.2}$$

A simple realization of this operator is through the low energy limit of the seesaw mechanism introduced in section 1.3.

In the quark sector the mixing is described by the CKM matrix, which is approximately diagonal, i.e. quark mixing is small. The fact that the mixing effects can be treated as perturbations to a mostly diagonal mixing matrix is the idea that lead to the Wolfenstein parametrization [37] of the CKM matrix, which is an expansion in the Cabbibo angle θ_C and was used in the last chapter.

The situation in the neutrino sector is entirely different: The PMNS matrix, which describes neutrino mixing, can be experimentally determined to be, at the 3σ level [18],

$$V_{\text{PMNS}} = \begin{pmatrix} [0.795, 0.846] & [0.513, 0.585] & [0.126, 0.178] \\ [0.205, 0.543] & [0.416, 0.730] & [0.579, 0.808] \\ [0.215, 0.548] & [0.409, 0.725] & [0.567, 0.800] \end{pmatrix}. \tag{5.3}$$

The nonzero nature of θ_{13} is now an experimental fact. However, it is still a reasonable assumption to treat it as deviation from zero, considering that the two other angles

are much larger than θ_{13}. In this approximation, the tribimaximal pattern [41, 42] still serves as a starting point:

$$V_{\text{PMNS}} \approx V_{\text{TBM}} = \begin{pmatrix} -\frac{2}{\sqrt{6}} & \frac{1}{\sqrt{3}} & 0 \\ \frac{1}{\sqrt{6}} & \frac{1}{\sqrt{3}} & \frac{1}{\sqrt{2}} \\ \frac{1}{\sqrt{6}} & \frac{1}{\sqrt{3}} & -\frac{1}{\sqrt{2}} \end{pmatrix}. \tag{5.4}$$

5.1 Generic assumptions for the left- and right-handed sectors

At this point we assume that all leptonic mixing originates from a heavy Majorana sector while the Dirac mass matrices of the neutrinos and charged leptons are diagonal[1]. This point of view is motivated by the fact that the CKM mixing is generated in absence of a high-energy mechanism like the seesaw mechanism and is quite small. Assuming that the quark and lepton sectors are related in general, it is reasonable to assume that a source of mixing in the low-energy neutrino sector would be similar to the one producing the CKM sector, i.e. it would produce small angles. The observed big angles are then the consequence of an additional sector not present for quarks, i.e. the right-handed Majorana sector.

The postulated relationship between quarks and leptons is quite a natural consequence of SO(10) GUTs. With all quarks and leptons unified in a **16** multiplet of SO(10), the GUT will cause the mass matrices of the quarks and leptons to be very similar. This means that they could at least approximately all be brought into a diagonal form. The experimentally obvious differences between the CKM quark mixing matrix and the PMNS lepton mixing matrix have to be explained by an additional mechanism, which can be the seesaw mechanism used here.

With respect to the seesaw formula in equation (1.19), the model investigated here can be written as

$$m_{\text{D}} = \begin{pmatrix} m_1^{\text{D}} & 0 & 0 \\ 0 & m_2^{\text{D}} & 0 \\ 0 & 0 & m_3^{\text{D}} \end{pmatrix}, \tag{5.5}$$

[1] This section and the numerical analysis are based on reference [2], updated for $\theta_{13} > 0$.

and $M \in \mathbb{R}^{3\times3}$ symmetric and arbitrary. After applying equation (1.19), the mass matrix in the flavor basis is given by

$$M^{\nu}_{\text{flv}} = \frac{1}{\Delta^3}\begin{pmatrix} \left[M_{22}M_{33} - \left(M_{23}\right)^2\right]\left(m_1^{\text{D}}\right)^2 & (M_{13}M_{23} - M_{33}M_{12})m_1^{\text{D}}m_2^{\text{D}} & (M_{12}M_{23} - M_{22}M_{13})m_1^{\text{D}}m_3^{\text{D}} \\ (M_{13}M_{23} - M_{33}M_{12})m_1^{\text{D}}m_2^{\text{D}} & \left[M_{11}M_{33} - \left(M_{13}\right)^2\right]\left(m_2^{\text{D}}\right)^2 & (M_{12}M_{13} - M_{11}M_{23})m_2^{\text{D}}m_3^{\text{D}} \\ (M_{12}M_{23} - M_{22}M_{13})m_1^{\text{D}}m_3^{\text{D}} & (M_{12}M_{13} - M_{11}M_{23})m_2^{\text{D}}m_3^{\text{D}} & \left[M_{11}M_{22} - \left(M_{12}\right)^2\right]\left(m_3^{\text{D}}\right)^2 \end{pmatrix}, \tag{5.6}$$

where the common factor of mass dimension three is given by

$$\Delta^3 = -M_{33}\left(M_{12}\right)^2 + 2M_{12}M_{13}M_{23} - M_{22}\left(M_{13}\right)^2 - M_{11}\left(M_{23}\right)^2 + M_{11}M_{22}M_{33}. \tag{5.7}$$

It is obvious that the structure of the matrix depends crucially on the differences of the Majorana masses M_{ij}.

The $(1,1)$ element of equation (5.6) is the effective mass $m_{\beta\beta}$ observed in neutrinoless double beta decays. In order to make statements about the neutrino mixing angles and mass squared differences, the mass matrix has to be diagonalized using an eigenvalue decomposition, yielding the mixing matrix U. We use the ordering scheme of reference [116] in which the labels m_1 and m_2 are assigned to the pair of eigenvalues whose absolute mass squared difference is minimal. Out of these two the eigenvalue whose corresponding eigenvector has the smaller modulus in the first component is labeled m_2. The hierarchy of the neutrino masses is then given by the sign of the mass squared differences Δm^2_{31} or Δm^2_{32}. The mixing angles can then be determined using [19]

$$\theta_{13} = \arcsin\left(\left|U_{13}\right|\right), \tag{5.8a}$$

$$\theta_{12} = \begin{cases} \arctan\left(\frac{|U_{12}|}{|U_{11}|}\right) & \text{if } U_{11} \neq 0 \\ \frac{\pi}{2} & \text{else} \end{cases}, \tag{5.8b}$$

$$\theta_{23} = \begin{cases} \arctan\left(\frac{|U_{23}|}{|U_{33}|}\right) & \text{if } U_{33} \neq 0 \\ \frac{\pi}{2} & \text{else} \end{cases}. \tag{5.8c}$$

If the mass matrix in equation (5.6) is supposed to represent neutrino data, it needs to be able to generate neutrino mixing that is close to being tribimaximal [41, 42]. A

general class of flavor space mass matrices that leads to tribimaximal mixing is given by the following pattern [65]:

$$M_\nu^{\mathrm{TBM,flv}} = \begin{pmatrix} x & y & y \\ y & x+v & y-v \\ y & y-v & x+v \end{pmatrix}, \tag{5.9}$$

where x, y, and v are real numbers. It is useful to compare the entries of this matrix to equation (5.6) for the two important mass hierarchies, illustrated in figure 5.1:

1. **Inverted hierarchy:** In this case we approximate an inverted mass hierarchy by two neutrino masses at a higher scale $\tilde{m}$ and one neutrino mass set to zero—i.e., the diagonal mass matrix becomes $\mathrm{Diag}(\tilde{m}, \tilde{m}, 0)$. Equation (5.9) can then be written as

$$\tilde{m} \cdot \begin{pmatrix} 1 & 0 & 0 \\ 0 & \frac{1}{2} & \frac{1}{2} \\ 0 & \frac{1}{2} & \frac{1}{2} \end{pmatrix}, \tag{5.10}$$

   which is equivalent to setting $x = 1, y = 0$, and $v = -½$ in equation (5.9). Comparing equation (5.10) with the mass matrix of equation (5.6) leads to a set of equations whose solutions determine if an inverted neutrino mass hierarchy is possible in this model:

$$\begin{aligned} \frac{1}{\Delta^3}\left(M_{23}^2 - M_{22}M_{33}\right)\left(m_1^{\mathrm{D}}\right)^2 &= \tilde{m}, \\ \frac{1}{\Delta^3}\left(M_{13}^2 - M_{11}M_{33}\right)\left(m_2^{\mathrm{D}}\right)^2 &= \frac{\tilde{m}}{2}, \\ \frac{1}{\Delta^3}\left(M_{12}^2 - M_{11}M_{22}\right)\left(m_3^{\mathrm{D}}\right)^2 &= \frac{\tilde{m}}{2}, \\ \frac{1}{\Delta^3}\left(M_{33}M_{12} - M_{13}M_{23}\right) m_1^{\mathrm{D}} m_2^{\mathrm{D}} &= 0, \\ \frac{1}{\Delta^3}\left(M_{22}M_{13} - M_{12}M_{23}\right) m_1^{\mathrm{D}} m_3^{\mathrm{D}} &= 0, \\ \frac{1}{\Delta^3}\left(M_{11}M_{23} - M_{12}M_{13}\right) m_2^{\mathrm{D}} m_3^{\mathrm{D}} &= \frac{\tilde{m}}{2}. \end{aligned} \tag{5.11}$$

   Trying to solve this set of equations immediately leads to a condition

$$\tilde{m} = 0, \tag{5.12}$$

which means that in this approximation it is not possible to generate an inverted neutrino mass hierarchy. Translated to a realistic scenario where the facts that tribimaximal mixing is only an approximation and that the smaller mass squared difference is not zero are taken into account, one can conclude that in this model the inverted mass hierarchy should be strongly disfavored.

2. **Normal hierarchy:** A normal neutrino mass hierarchy is approximated by two vanishing neutrino masses and one neutrino mass at a higher scale $\tilde{m}$—i.e., a diagonal mass matrix of $\mathrm{Diag}(0, 0, \tilde{m})$. This leads to a flavor space mass matrix of the form

$$\tilde{m} \cdot \begin{pmatrix} 0 & 0 & 0 \\ 0 & \frac{1}{2} & -\frac{1}{2} \\ 0 & -\frac{1}{2} & \frac{1}{2} \end{pmatrix}. \tag{5.13}$$

Again, comparing this matrix with equation (5.6) gives a set of equations. Note that in this case the $(1, 1)$ element of the matrix is zero instead of $\tilde{m}$. This eliminates the suppressive condition of equation (5.12). The rest of the set of equations is solvable and just restricts the parameter space of the mass matrix.

5.2 Numerical analysis

In this section we present the results of a numerical analysis to determine the general allowed ranges for the following observables:

1. The neutrinoless double beta decay parameter $m_{\beta\beta}$, given by the $(1, 1)$-entry of the mass matrix in equation (5.6),
2. The lightest neutrino mass m_0,
3. The neutrino mixing angle θ_{13}, as it is the mixing angle with the largest relative experimental uncertainty.

The Dirac masses m_i^D are mostly responsible for the mass eigenvalues of the neutrinos, while the mixing angles are dominantly determined by the Majorana mass matrix entries M_{ij}.

Because of this, the numerical analysis of each point in the parameter space is performed in two steps: First, random starting points of the electroweak scale are chosen

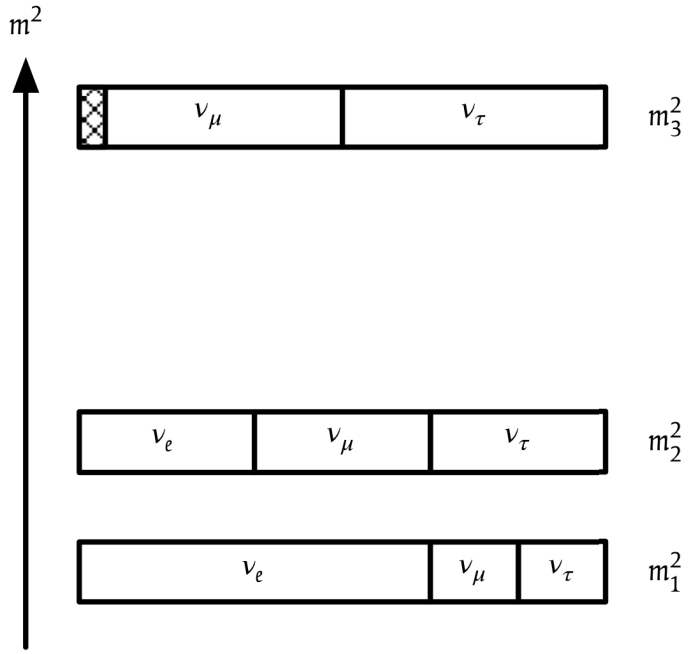

(a) Normal hierarchy.

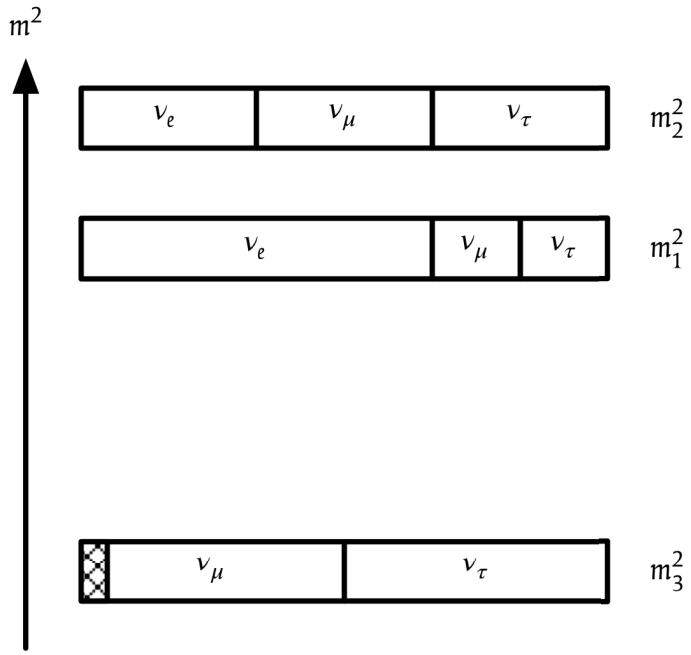

(b) Inverted hierarchy.

Figure 5.1: Illustration of neutrino mass hierarchies. The mixing in terms of ν_e, ν_μ, and ν_τ is based on a tribimaximal mixing scheme, however $\theta_{13} > 0$ is indicated using the shaded area.

Table 5.1: Experimental neutrino data from the global fit of reference [18].

Parameter	Best fit	1σ range	3σ range
θ_{12} [°]	33.8	± 0.8	31–36
$\theta_{23}^{\text{norm}}$ [°]	40.0	$+2.1/-1.5$	36–55
θ_{23}^{inv} [°]	50.4	$+1.2/-1.3$	36–55
θ_{13} [°]	8.6	$+0.44/-0.46$	7.2–9.5

Note: The 1σ ranges of θ_{12}, $\theta_{23}^{\text{norm}}$, and θ_{13} are used in the numerical analysis.

for the Dirac masses m_i^D, which are then varied. The Majorana parameters M_{ij} are also chosen randomly at a scale of up to 100×10^{14} GeV, but are not varied in this step. We have ignored the possibility of CP violation here and assigned real valued numbers to all parameters. A χ_M^2 function for the mass squared differences can be calculated using the diagonalized mass matrix and comparison values from a global fit of all experimental data [18] (the uncertainties refer to 1σ and 3σ ranges respectively):

$$\left(\Delta m_{21}^2\right)^{\text{exp}} = 7.50 \pm 0.185(7.00 \to 8.09) \times 10^{-5}\,\text{eV}^2, \tag{5.14}$$

$$\left(\Delta m_{31}^2\right)^{\text{exp,norm}} = 2.47 + \begin{pmatrix} +0.069 \\ -0.067 \end{pmatrix} (2.27 \to 2.69) \times 10^{-3}\,\text{eV}^2, \tag{5.15}$$

$$\left(\Delta m_{32}^2\right)^{\text{exp,inv}} = -2.43 + \begin{pmatrix} +0.042 \\ -0.065 \end{pmatrix} (-2.65 \to -2.24) \times 10^{-3}\,\text{eV}^2. \tag{5.16}$$

This χ_M^2 function is numerically minimized using a multidimensional minimization algorithm [117]. At this point, if the minimum is above the threshold value for χ_M^2, the data point is discarded. For the accepted points, the second step consists of calculating the mixing angles [116]. The χ_A^2 function for the angles is then analyzed and compared to the data obtained from the global fit of experimental results [18], shown in table 5.1.

For the number of degrees of freedom considered, the threshold value for χ_A^2 is at 16.8 for a significance of 0.99. The scan covering roughly 16×10^6 data points finds 5470 acceptable samples that lead to a normal neutrino mass hierarchy and just 6 samples with an inverted neutrino mass hierarchy. This meets the expectation of the inverted

mass hierarchy being strongly suppressed in the model. The best fit point lies in the regime of normal mass ordering with $\chi^2_A = 0.15$. This low value is possible because we do not fit a specific model, but a large class of models. The parameters leading to this best fit are

$$\begin{aligned} M_{11} &= 57 \times 10^{13}\,\text{GeV}, & M_{22} &= 50 \times 10^{13}\,\text{GeV}, & M_{33} &= 34 \times 10^{13}\,\text{GeV}, \\ M_{12} &= 33 \times 10^{13}\,\text{GeV}, & M_{13} &= 19 \times 10^{13}\,\text{GeV}, & M_{23} &= 47 \times 10^{13}\,\text{GeV}, \\ m_1^D &= 17\,\text{GeV}, & m_2^D &= 16\,\text{GeV}, & m_3^D &= 19\,\text{GeV}. \end{aligned} \tag{5.17}$$

For all acceptable points, the values for the lightest neutrino mass m_0 are displayed in figure 5.2 for a normal mass hierarchy. For the inverted hierarchy case the small number of successful samples does not warrant a plot.

For both hierarchies, the best fit lightest neutrino mass m_0 is below 0.005 eV (cf. figure 5.2). Both values lead to summed neutrino masses $M_\nu = \sum m_i$ below the current bound of roughly $M_\nu \approx 0.5$ eV[24–33].

As the contribution from m_0 is negligible and θ_{13} is still small, the neutrinoless double beta decay observables for the cases of normal or inverted hierarchies are given by (see e.g. references [118–121] and the references therein)

$$m_{\beta\beta} \approx \begin{cases} \sqrt{\Delta m^2_{12}}\,\sin^2\left(\theta_{12}\right) & \text{for normal hierarchy} \\ \sqrt{\Delta m^2_{23}} \quad \text{resp.} \quad \sqrt{\Delta m^2_{23}}\,\cos\left(2\theta_{12}\right) & \text{for inverted hierarchy} \end{cases}, \tag{5.18}$$

where $\Delta m_{12} \ll \Delta m_{23}$ and CP conservation has been assumed. The two values given for the case of an inverted mass hierarchy stem from the sign ambiguity of the $\pm \sin^2\left(\theta_{12}\right)$ term in the sum of masses. Using these formulas, the mass squared differences and mixing angles given in the global fit of reference [18] lead to $m_{\beta\beta}^{\text{normal}} \approx 0.003$ eV for the case of a normal mass hierarchy. The two possible values for the inverted mass hierarchy case are $m_{\beta\beta}^{\text{inv/b}} \approx 0.05$ eV and $m_{\beta\beta}^{\text{inv/a}} \approx 0.04$ eV. As the model discussed here reproduces the mixing angles and mass parameters of the global fit, it also reproduces the global fit values for the mass parameter of the neutrinoless double beta decay $m_{\beta\beta}$ as given by equation (5.18).

All angles can be fitted to the experimental data of reference [18]. However, as the PMNS sector features a mixing pattern that can still be considered to be a deviation from tribimaximal, it is instructive to take a look at the case where θ_{13} is not part of the fit. In that case, only the mass squared differences and the angles θ_{12} and θ_{23} are fitted. The allowed ranges for the angle θ_{13} can then be seen as a prediction of the model. In the case of a normal mass hierarchy, there is a clear preference for $\theta_{13} \approx 0$, however we have seen that the experimental data including a nonzero θ_{13} can be fitted. In the case of an

inverted mass hierarchy, the preferred value of θ_{13} is clearly close to a maximal mixing angle. This means that the model with a solely right-handed mixing origin is a natural candidate for a tribimaximal mixing pattern. While the deviation from zero that has been found in θ_{13} can be fitted, a more natural explanation would be to generate it using a small mixing parameter in the left-handed mass matrix.

In summary, a generic model based on a seesaw type I mechanism with diagonal Dirac mass matrices for both the charged leptons and the neutrinos has been considered in this section. All contributions to the observed neutrino mixing originate from the heavy Majorana masses through a generic Majorana mass matrix that allows for off-diagonal components. It has been shown that models of that kind—which are well-motivated by GUTs—generate a small mixing angle θ_{13} naturally and that a normal neutrino mass hierarchy is preferred. Even though the current value for θ_{13} can be fitted using this model, it may be more sensible from a model-building standpoint to separate the generation of the small deviation from zero from the generation of the other angles by considering θ_{13} as a correction to the diagonal Dirac mass matrix.

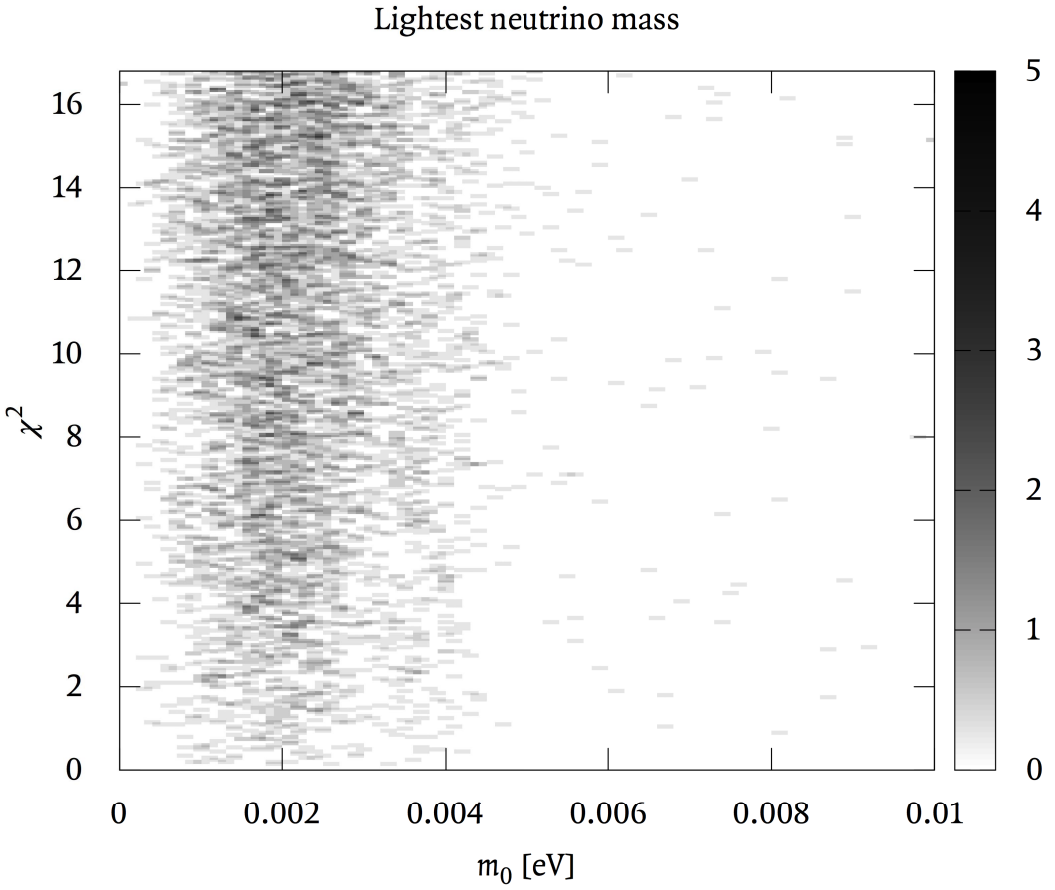

Figure 5.2: The lightest neutrino mass in the case of normal neutrino mass hierarchy. The bin sizes are $\Delta x = 0.0001$ eV and $\Delta y = 0.05$. The shade is proportional to the number of hits that lie in the shaded bin.

5.3 An exemplary realization inspired by knot theory

When considering parameters as in equation (5.6), patterns are often enforced using discrete symmetries, as we have done in chapters 2, 3, and 4 in similar contexts. Another possibility is to assume as little structure as possible and let the parameters assume random values. This concept is called *anarchy* [122–125] and the numerical analysis of the right-handed sector presented in the last section uses a similar approach.

In this section we demonstrate that there may exist structure in the right-handed sector that is not governed by a discrete flavor symmetry. More precisely, we will propose that the leptonic flavor structure could arise from the topological configurations of closed strings.

Closed strings are a fundamental ingredient of string theory, including in particular the graviton and its anti–de Sitter (adS)/QCD dual, the glueball, as well as dilaton superfields with fermionic degrees of freedom having the correct quantum numbers of a right-handed neutrino (a fact used extensively e.g. in neutrino mass models with large extra dimensions, see e.g. reference [126]).

It thus seems well-motivated that topologically nontrivial string configurations such as knots and links can contribute to the mass of closed string states, and may even dominate it. As string tension tends to minimize the string length, the knot or link length can be assumed to be directly proportional to the mass. For example, it has been shown in references [127–129] that the experimental spectrum of glueball candidates can be fitted very nicely by knot and link energies.

Here we exploit another interesting feature of the knot and link spectrum. Typically there exist different close-to-degenerate states with very small energy gaps. If right-handed neutrino masses are dominated by the knots and links of closed strings in a seesaw framework, large and maximal leptonic mixing may result naturally from the knot and link spectrum without the need for any flavor symmetry.

Consider the Dirac mass matrix of equation (5.6) and a right-handed Majorana mass matrix

$$M = \begin{pmatrix} m_1^K & m_1^L & m_2^L \\ m_1^L & m_2^K & m_3^L \\ m_2^L & m_3^L & m_3^K \end{pmatrix}. \tag{5.19}$$

Instead of populating the entries anarchically as in the last section, we now assume that the heavy masses $m_i^{K/L}$ take on values according to the spectrum of characteristic

lengths of knots and links [130], multiplied by a common high-energy scale m_S at which knotted string configurations can exist:

$$m_i^{K/L} = \ell_i^{K/L} \cdot m_S, \tag{5.20}$$

where the $\ell_i^{K/L}$ refer to the characteristic lengths of table 5.3. The diagonal entries of the mass matrix are generated by the knots' lengths, while the off-diagonal entries are related to the characteristic lengths of the links.

The characteristic lengths of knots and links are derived in reference [130] using an algorithm to minimize the lengths of polygons with fixed thickness. It turns out that the the characteristic length of a knot or link is a function of the number of crossings.

The mass matrix of the three light left-handed neutrinos in the flavor basis is given in equation (5.6) with the substitutions

$$M_{ii} \to m_i^K, \quad M_{12} \to m_1^L, \quad M_{13} \to m_2^L, \quad M_{23} \to m_3^L. \tag{5.21}$$

In the last section, approximative conditions on the entries of equation (5.6) were derived for the case of normal and inverted neutrino mass hierarchies. It is interesting to apply these conditions to the a knot-generated right-handed sector.

For a normal neutrino mass hierarchy, the comparison yields a set of relations between the Majorana parameters m_i^K, m_i^L and the other parameters:

$$m_3^K/m_2^K = \left(m_2^D\right)^2 \Big/ \left(m_3^D\right)^2, \tag{5.22a}$$

$$m_2^L/m_1^L = m_3^D/m_2^D, \tag{5.22b}$$

$$m_2^K m_2^L = m_1^L m_3^L, \tag{5.22c}$$

$$m_1^K m_2^K \neq \left(m_1^L\right)^2, \tag{5.22d}$$

$$\tilde{m} = 2\left(m_3^D\right)^2 \left(\left(m_1^L\right)^2 - m_1^K m_2^K\right)/\Delta^3, \tag{5.22e}$$

where Δ^3 is given in equation (5.7). If the Dirac masses m_i^D are assumed to be roughly equal the first three conditions can be fulfilled if the selected lengths ℓ_i^K and ℓ_i^L are close to each other. In general, as the order (crossing number) of the knots increases, the spacing decreases since the length grows roughly linearly with crossing number, but the number of knots grows faster than exponentially with crossing number.

As the neutrino mass scale $\tilde{m}$ is small due to the seesaw mechanism, the electroweak scale m_3^D factor in the condition $\tilde{m} = 2(m_3^D)^2[(m_1^L)^2 - m_1^K m_2^K]/\Delta^3$ needs to be compensated by making the expression in the parentheses small. This can again be achieved by having

an almost degenerate spectrum for ℓ_i^K and ℓ_i^L. Since the spectrum of knots and links features almost degenerate lengths, it is thus expected that it will provide a better fit to the leptonic flavor structure than random numbers.

The corresponding condition for an inverted hierarchy, which is approximated as two neutrino masses at a higher scale $\tilde{m}$ and one neutrino mass set to zero—i.e., the diagonal mass matrix $\mathrm{Diag}(\tilde{m}, \tilde{m}, 0)$, gives a system of equations that can only be solved if $\tilde{m} = 0$. Thus, in this approximation it is not possible to generate an inverted neutrino mass hierarchy. Taking into account that the tribimaximal pattern is only an approximation and that the smaller mass difference is not zero, one would expect that in this model the inverted mass hierarchy should be suppressed.

Finally we analyze the compatibility of the model with a degenerate neutrino mass spectrum. Assuming a diagonal mass matrix $\mathrm{Diag}(\tilde{m}, \tilde{m}, \tilde{m})$ the conditions that follow from equation (5.6) read:

$$m_1^D m_3^D \neq 0, \tag{5.23a}$$

$$m_2^K = m_1^K \left(m_2^D\right)^2 \Big/ \left(m_1^D\right)^2, \tag{5.23b}$$

$$m_3^K = m_1^K \left(m_3^D\right)^2 \Big/ \left(m_1^D\right)^2, \tag{5.23c}$$

$$m_3^K \neq 0, \tag{5.23d}$$

$$m_1^K m_2^K \neq 0, \tag{5.23e}$$

$$m_1^K \neq 0, \tag{5.23f}$$

$$m_1^L = m_2^L = m_3^L = 0, \tag{5.23g}$$

$$m_1^K m_2^K \left(m_3^D\right)^2 + \tilde{m} \cdot \Delta^3 = 0. \tag{5.23h}$$

Out of these conditions, the last two are in contradiction with the framework of the model: The m_i^L and m_i^K parameters cannot be zero or close to zero. The model investigated in this paper thus cannot be used to explain a degenerate neutrino mass hierarchy.

In order to investigate the viability of the models, we turn to a numerical analysis similar to the once performed in the last section. Now, however, instead of random numbers, every possible combination of characteristic lengths up to a given knot order is used as an input for the right-handed Majorana masses. No duplicate lengths of knots or links are allowed.

The parameters m_i^D for $i = 1, 2, 3$ as well as the overall scale of the Majorana masses are not fixed by the model. As the scope of this analysis is the viability of the choice of knots and links as a source of Majorana masses, the Dirac masses are chosen in a way

as to minimize the χ^2 value of the squared mass differences of the neutrinos compared to experimental data [18]. This way, no potentially viable combinations of knots and links are discarded due to a wrong choice for the Dirac masses. The overall Majorana scale factor that is multiplied with the characteristic lengths of the knots and links is fixed at 10^{12} GeV.

If the characteristic string spectrum is realized by cosmic strings, one has to respect bounds obtained by the effect of such cosmological defects on the power law index of primordial density perturbations as measured in cosmic microwave background (CMB) probes such as the Wilkinson Microwave Anisotropy Probe (WMAP) experiment [131].

Such cosmological defects arise in the phase transitions associated with the spontaneous breakdown of non-Abelian gauge symmetries. The string tension, which is Newton's constant times the mass per unit length, is then related to the symmetry breaking scale. If strings are formed at the GUT scale 10^{16} GeV, then the string tension is approximately 10^{-6}, which is below the constraint from CMB observations [131]. Even stronger constraints result from the contribution of cosmic strings to the stochastic background of gravitational waves which can be constrained from pulsar timing observations [132]. These constraints require a string tension below 10^{-9} corresponding to a symmetry breaking scale of about 10^{13} GeV. Consequently we adopt this value as an upper bound for the scale confinement $m_{\text{conf}} = m_S$.

For the subset of models that have acceptable squared mass differences the mixing angles are calculated and also compared to the experimental values. All models with a $\chi^2 < 16.8$ for the mixing angles are considered viable. This corresponds to a P value of 0.01 and six degrees of freedom.

The scan covering 10692864 possible combinations of knots' and links' lengths results in 10930 models with normal neutrino mass hierarchy and no models with an inverted neutrino mass hierarchy that fall below the χ^2 limit of 16.8. This means that about 0.07% of all possible combinations yield phenomenologically acceptable results. The best fit lies in the regime of normal hierarchy with a $\chi^2_{\text{best}} = 0.07$. The best fit model is described by the parameters in table 5.2.

This can be compared with the case of an anarchic right-handed Majorana matrix discussed in the last section, where the same number of combinations was tested, but using random numbers instead of characteristic lengths. We recall that the scan yielded 5470 successful hits with a best fit result in the regime of normal hierarchy. The relative number of viable models with a normal neutrino mass hierarchy is even larger in the case of knots and links. This can be explained by the conditions that follow from equation (5.6), which lead to the spectrum of knots and links being able to fit the requirements for a normal mass hierarchy easier than random numbers.

In the anarchy case the total number of acceptable models is lower than the total number of acceptable models in the case of knots and links. This means that the models using the characteristic lengths of knots and links are more suitable to fit the neutrino data than a fit using anarchy.

Table 5.2: The model parameters giving the best fit for normal and inverted hierarchies. The knots and links indices refer to table 5.3.

K_1	K_2	K_3	L_1	L_2	L_3	m_1^D [GeV]	m_2^D [GeV]	m_3^D [GeV]
01	06	11	08	16	06	11.47	12.48	12.69

To determine the phenomenological consequences of the allowed models, the following observables are calculated: the double beta decay parameter $m_{\beta\beta}$, the lightest neutrino mass m_0 and the neutrino mixing angle θ_{13}. In the normal hierarchy case, $m_{\beta\beta}$ tends to be small, i.e. between 0.001 eV and 0.008 eV. Note that most of the viable models have $m_{\beta\beta}$ around 0.005 eV and 0.007 eV.

The lightest neutrino mass in the normal hierarchy case is below 0.001 eV, illustrated in figure 5.3, well below the current bound on the sum of the neutrino masses obtained from cosmological observations $\sum m_i \lesssim 0.5$ eV [24–33].

As in the last section, we have repeated the numerical analysis omitting θ_{13} from the fit. We have then surveyed the model prediction for the angle and compared that to the global fit. The results for a normal mass hierarchy are shown in figure 5.4. A small angle θ_{13} close to zero is preferred, again pointing towards an origin of a nonzero θ_{13} that is not in the right-handed Majorana sector.

We would like to stress that the scenario we are pursuing here is an effective model which may result from various ultraviolet completions. In the following we sketch some qualitative ideas about such completions. First, fundamental closed strings could be considered, but it is not clear if these can have tight knots because of their vanishingly small cross section. Another option to generate massive knots near the GUT scale are cosmic strings. If a collapsing loop of nontrivial topology K tightens before it decays, then the tight knot configuration will have mass

$$M_K \sim L_K \langle \phi \rangle \tag{5.24}$$

near the symmetry breaking scale $\langle \phi \rangle$, where the $U(1)$ is broken that gives rise to the cosmic string. Here L_K is the dimensionless length of the knot K, i.e. the length of the knot divided by the radius of the cosmic string.

If a knot is bosonic above the supersymmetry breaking scale, then it will also have a fermionic partner of the same mass. Furthermore, If the fermionic knots are gauge singlets, then they can serve as the heavy right-handed neutrinos needed for the seesaw mechanism to generate the very light observed neutrino states.

The stability of various knot types will be model dependent, hence the lightest knots may not be stable and so may not be the ones that mix with the light neutrinos.

In summary, in this section we have provided an example for a right-handed sector that is neither governed by anarchy nor by a discrete flavor symmetry: A seesaw type I model whose Majorana mass structure is determined by the discrete spectrum of tight knots and links. We have not given an ultraviolet completion of this model, but have given some hints to what such a completion might look like. Based on the general structure of the mass matrices of the last section, we have shown that the model fits the current experimental neutrino data on squared mass differences and mixing angles, including a nonzero angle θ_{13}. It has also been shown that the spectrum of knots and links produces a larger number of viable models than a spectrum of random numbers. The model favors a normal neutrino mass hierarchy and predicts a small mixing angle θ_{13}.

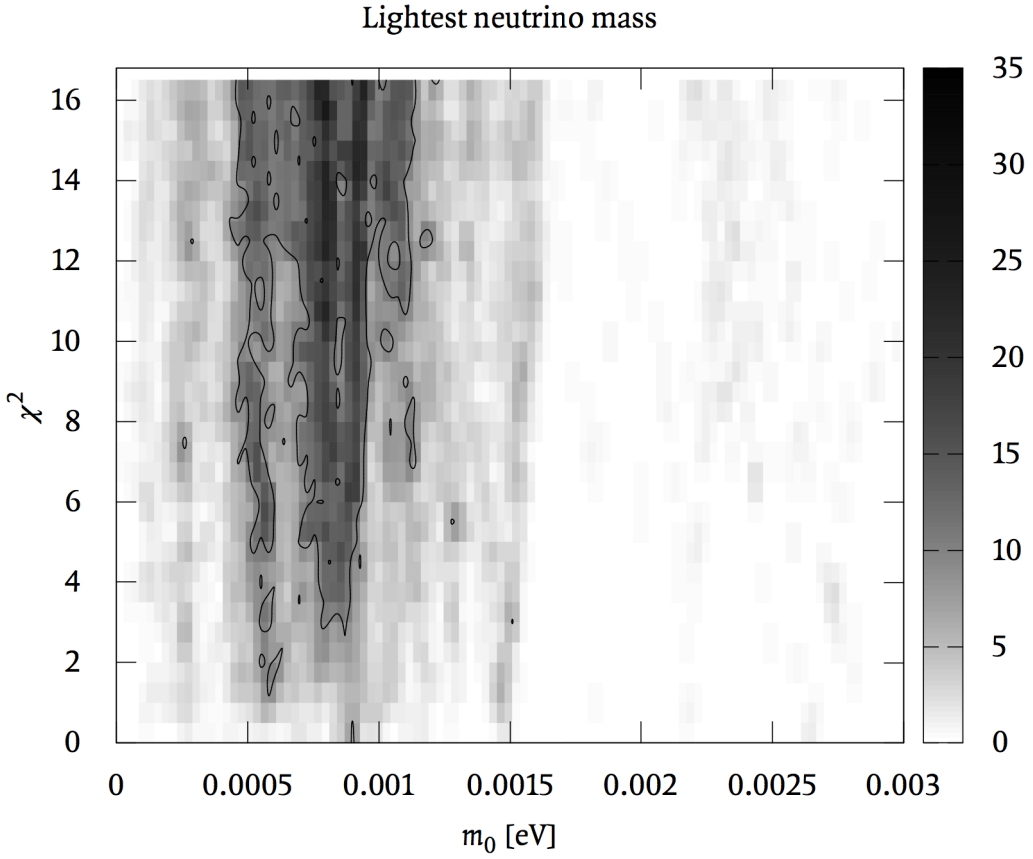

Figure 5.3: The lightest neutrino mass m_0 for the models using the characteristic lengths of knots and links. The plot has been divided into 106 bins along the x-axis and 35 bins along the y-axis. The shade of the rectangles represents the number of models found in that area. Outside of the boundary line, less than ten hits per rectangle were recorded.

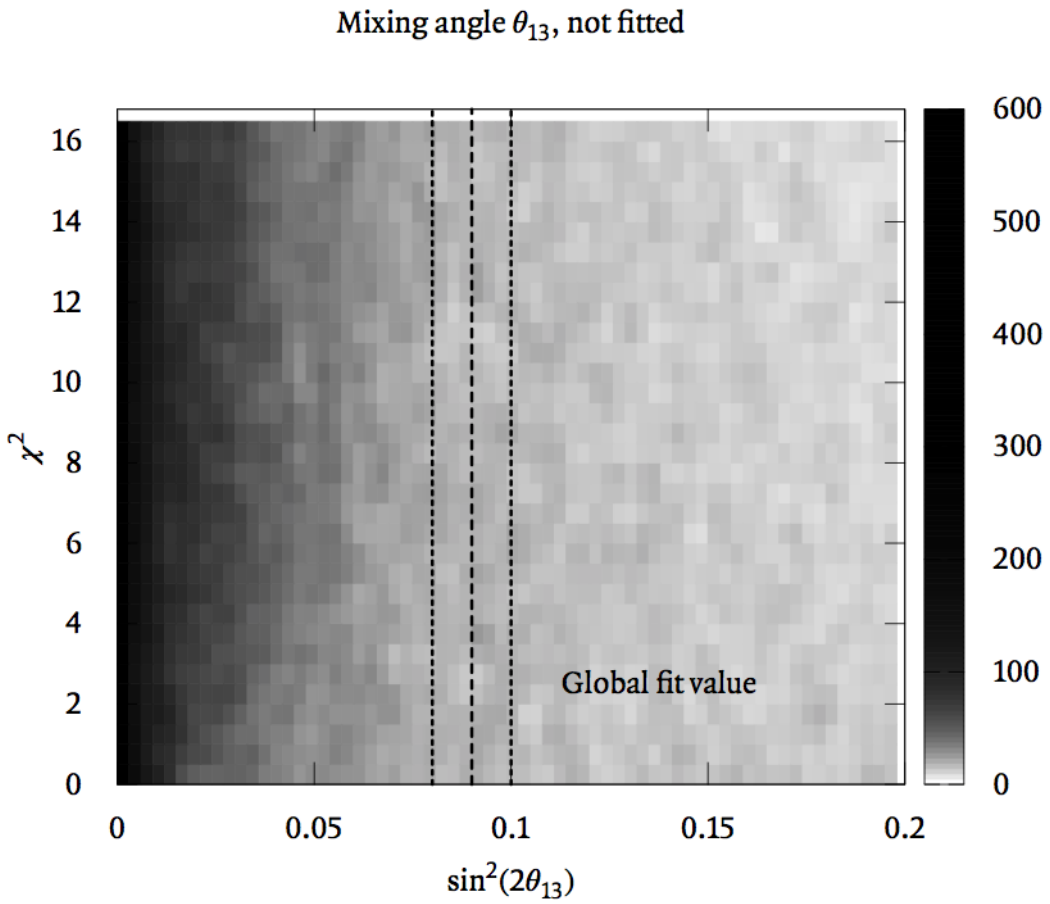

Figure 5.4: The quantity $\sin^2\left(2\theta_{13}\right)$ for the models with a normal mass hierarchy. θ_{13} was excluded from the fit for this plot. The plot has been divided into 334 bins along the x-axis for the range $0, \ldots, 1$ and 35 bins along the y-axis. The shade of the rectangles represents the number of models found in that area. The global fit value for $\sin^2(2\theta_{13})$ including 1σ uncertainties given by reference [18] is indicated by a dashed line.

Table 5.3: Characteristic lengths of knots and links up to knot order seven, taken from reference [130].

Index	Knot length [a.u.]	Link length [a.u.]
00	32.7436	25.1334
01	42.0887	40.0122
02	47.2016	49.7716
03	49.4701	54.3768
04	56.7058	56.7000
05	57.0235	58.1013
06	57.8392	57.8141
07	61.4067	58.0070
08	63.8556	50.5539
09	63.9285	64.2345
10	64.2687	65.0204
11	65.2560	65.3257
12	65.6924	65.0602
13	65.6086	66.1915
14		66.3147
15		55.5095
16		57.7631
17		65.8062

Acronyms

2HDM two Higgs doublet model.

adS anti–de Sitter.

BR branching ratio.

CKM Cabbibo-Kobayashi-Maskawa.

CMB cosmic microwave background.

FCNC flavor changing neutral current.

GCPV geometrical CP violation.

GUT grand unified theory.

GWS Glashow-Weinberg-Salam.

LEP Large Electron–Positron Collider.

LHC Large Hadron Collider.

PMNS Pontecorvo-Maki-Nakagawa–Sakata.

QCD quantum chromodynamics.

QED quantum electrodynamics.

SCPV spontaneous CP violation.

SSB spontaneous symmetry breaking.

VEV vacuum expectation value.

WMAP Wilkinson Microwave Anisotropy Probe.

Bibliography

[1] G. Bhattacharyya, P. Leser, and H. Päs, "Exotic Higgs boson decay modes as a harbinger of S_3 flavor symmetry," Phys. Rev. **D83**, 011701(R), arXiv: 1006.5597 [hep-ph] (2011) (cit. on pp. 2, 30, 33, 38, 43, 47, 48, 69).

[2] P. Leser and H. Päs, "Neutrino mass hierarchy and the origin of leptonic flavor mixing from the righthanded sector," Phys. Rev. **D84**, 017303, arXiv: 1104.2448 [hep-ph] (2011) (cit. on pp. 2, 74).

[3] T. W. Kephart, P. Leser, and H. Päs, "Knotted strings and leptonic flavor structure," Mod. Phys. Lett. **A27**, 1250224, arXiv: 1106.6201 [hep-ph] (2012) (cit. on p. 2).

[4] G. Bhattacharyya, P. Leser, and H. Päs, "Novel signatures of the Higgs sector from S3 flavor symmetry," Phys. Rev. **D86**, 036009, arXiv: 1206.4202 [hep-ph] (2012) (cit. on pp. 2, 40, 69).

[5] I. d. M. Varzielas, D. Emmanuel-Costa, and P. Leser, "Geometrical CP violation from non-renormalisable scalar potentials," Phys. Lett. **B716**, 193, arXiv: 1204.3633 [hep-ph] (2012) (cit. on pp. 2, 51).

[6] G. Bhattacharyya, I. d. M. Varzielas, and P. Leser, "Common origin of fermion mixing and geometrical CP violation, and its test through Higgs physics at the LHC," Phys. Rev. Lett. **109**, 241603, arXiv: 1210.0545 [hep-ph] (2012) (cit. on pp. 2, 62).

[7] S. Glashow, "Partial symmetries of weak interactions," Nucl. Phys. **22**, 579 (1961) (cit. on p. 2).

[8] S. Weinberg, "A model of leptons," Phys. Rev. Lett. **19**, 1264 (1967) (cit. on p. 2).

[9] D. Gross and F. Wilczek, "Asymptotically free gauge theories 1," Phys. Rev. **D8**, 3633 (1973) (cit. on p. 2).

[10] D. Gross and F. Wilczek, "Asymptotically free gauge theories 2," Phys. Rev. **D9**, 980 (1974) (cit. on p. 2).

[11] G. Altarelli and M. W. Grünewald, "Precision electroweak tests of the standard model," Phys. Rept. **403-404**, 189, arXiv: hep-ph/0404165 [hep-ph] (2004) (cit. on pp. 2, 3).

[12] G. Aad et al., "Observation of a new particle in the search for the Standard Model Higgs boson with the ATLAS detector at the LHC," Phys. Lett. **B716**, 1, arXiv: 1207.7214 [hep-ex] (2012) (cit. on pp. 2, 36, 37, 43–45).

[13] S. Chatrchyan et al., "Observation of a new boson at a mass of 125 GeV with the CMS experiment at the LHC," Phys. Lett. **B716**, 30, arXiv: 1207.7235 [hep-ex] (2012) (cit. on pp. 2, 36, 37, 43–45).

[14] P. W. Higgs, "Broken symmetries and the masses of gauge bosons," Phys. Rev. Lett. **13**, 508 (1964) (cit. on pp. 2, 6).

[15] N. Cabibbo, "Unitary symmetry and leptonic decays," Phys. Rev. Lett. **10**, 531 (1963) (cit. on p. 7).

[16] J. Beringer et al., "Review of particle physics," Phys. Rev. **D86**, 010001 (2012) (cit. on pp. 7, 12, 67, 68).

[17] S. Bilenky, "Neutrino. History of a unique particle," arXiv: 1210.3065 [hep-ph] (2012) (cit. on p. 8).

[18] M. Gonzalez-Garcia, M. Maltoni, J. Salvado, and T. Schwetz, "Global fit to three neutrino mixing: critical look at present precision," arXiv: 1209.3023 [hep-ph] (2012) (cit. on pp. 8, 13, 28, 73, 79, 80, 86, 90).

[19] T. Ohlsson and H. Snellman, "Three flavor neutrino oscillations in matter," J. Math. Phys. **41**, 2768, arXiv: hep-ph/9910546 [hep-ph] (2000) (cit. on pp. 8, 75).

[20] B. Cleveland, T. Daily, J. Davis, Raymond, J. R. Distel, K. Lande, et al., "Measurement of the solar electron neutrino flux with the Homestake chlorine detector," Astrophys. J. **496**, 505 (1998) (cit. on p. 9).

[21] W. Hampel et al., "GALLEX solar neutrino observations: Results for GALLEX IV," Phys. Lett. **B447**, 127 (1999) (cit. on p. 9).

[22] S. Fukuda et al., "Tau neutrinos favored over sterile neutrinos in atmospheric muon-neutrino oscillations," Phys. Rev. Lett. **85**, 3999, arXiv: hep-ex/0009001 [hep-ex] (2000) (cit. on p. 9).

[23] M. Ambrosio et al., "Matter effects in upward going muons and sterile neutrino oscillations," Phys. Lett. **B517**, 59, arXiv: hep-ex/0106049 [hep-ex] (2001) (cit. on p. 9).

[24] M. Steidl, "Experiments for the absolute neutrino mass measurement," arXiv: 0906.0454 [nucl-ex] (2009) (cit. on pp. 9, 80, 87).

[25] O. Elgaroy, O. Lahav, W. Percival, J. Peacock, D. Madgwick, et al., "A new limit on the total neutrino mass from the 2dF galaxy redshift survey," Phys. Rev. Lett. **89**, 061301, arXiv: astro-ph/0204152 [astro-ph] (2002) (cit. on pp. 9, 80, 87).

[26] M. Tegmark et al., "Cosmological constraints from the SDSS luminous red galaxies," Phys. Rev. **D74**, 123507, arXiv: astro-ph/0608632 [astro-ph] (2006) (cit. on pp. 9, 80, 87).

[27] S. Hannestad and G. G. Raffelt, "Neutrino masses and cosmic radiation density: combined analysis," JCAP **0611**, 016, arXiv: astro-ph/0607101 [astro-ph] (2006) (cit. on pp. 9, 80, 87).

[28] D. Spergel et al., "Wilkinson Microwave Anisotropy Probe (WMAP) three year results: implications for cosmology," Astrophys. J. Suppl. **170**, 377, arXiv: astro-ph/0603449 [astro-ph] (2007) (cit. on pp. 9, 80, 87).

[29] U. Seljak, A. Slosar, and P. McDonald, "Cosmological parameters from combining the Lyman-alpha forest with CMB, galaxy clustering and SN constraints," JCAP **0610**, 014, arXiv: astro-ph/0604335 [astro-ph] (2006) (cit. on pp. 9, 80, 87).

[30] S. Allen, R. Schmidt, and S. Bridle, "A preference for a nonzero neutrino mass from cosmological data," Mon. Not. Roy. Astron. Soc. **346**, 593, arXiv: astro-ph/0306386 [astro-ph] (2003) (cit. on pp. 9, 80, 87).

[31] S. Hannestad, H. Tu, and Y. Y. Wong, "Measuring neutrino masses and dark energy with weak lensing tomography," JCAP **0606**, 025, arXiv: astro-ph/0603019 [astro-ph] (2006) (cit. on pp. 9, 80, 87).

[32] S. Hannestad and Y. Y. Wong, "Neutrino mass from future high redshift galaxy surveys: sensitivity and detection threshold," JCAP **0707**, 004, arXiv: astro-ph/0703031 [astro-ph] (2007) (cit. on pp. 9, 80, 87).

[33] J. Lesgourgues, S. Pastor, and L. Perotto, "Probing neutrino masses with future galaxy redshift surveys," Phys. Rev. **D70**, 045016, arXiv: hep-ph/0403296 [hep-ph] (2004) (cit. on pp. 9, 80, 87).

[34] E. Majorana, "Theory of the Symmetry of Electrons and Positrons," Nuovo Cim. **14**, 171 (1937) (cit. on p. 9).

[35] P. Langacker, "Neutrino masses from the top down," arXiv: 1112.5992 [hep-ph] (2011) (cit. on pp. 9, 73).

[36] C. Aalseth, H. Back, L. J. Dauwe, D. Dean, G. Drexlin, et al., "Neutrinoless double beta decay and direct searches for neutrino mass," arXiv: hep-ph/0412300 [hep-ph] (2004) (cit. on p. 10).

[37] L. Wolfenstein, "Parametrization of the Kobayashi-Maskawa Matrix," Phys. Rev. Lett. **51**, 1945 (1983) (cit. on pp. 12, 73).

[38] K. Abe et al., "Indication of electron neutrino appearance from an accelerator-produced off-axis muon neutrino beam," Phys. Rev. Lett. **107**, 041801, arXiv: 1106.2822 [hep-ex] (2011) (cit. on pp. 13, 27).

[39] F. An et al., "Observation of electron-antineutrino disappearance at Daya Bay," Phys. Rev. Lett. **108**, 171803, arXiv: 1203.1669 [hep-ex] (2012) (cit. on pp. 13, 27).

[40] J. Ahn et al., "Observation of reactor electron antineutrino disappearance in the RENO experiment," Phys. Rev. Lett. **108**, 191802, arXiv: 1204.0626 [hep-ex] (2012) (cit. on pp. 13, 27).

[41] P. Harrison, D. Perkins, and W. Scott, "A redetermination of the neutrino mass squared difference in tri-maximal mixing with terrestrial matter effects," Phys. Lett. **B458**, 79, arXiv: hep-ph/9904297 [hep-ph] (1999) (cit. on pp. 13, 74, 75).

[42] P. Harrison, D. Perkins, and W. Scott, "Tri-bimaximal mixing and the neutrino oscillation data," Phys. Lett. **B530**, 167, arXiv: hep-ph/0202074 [hep-ph] (2002) (cit. on pp. 13, 74, 75).

[43] H. Ishimori et al., "Non-Abelian discrete symmetries in particle physics," Prog. Theor. Phys.Suppl. **183**, 1, arXiv: 1003.3552 [hep-th] (2010) (cit. on pp. 15, 22–25, 52).

[44] P. O. Ludl, "Systematic analysis of finite family symmetry groups and their application to the lepton sector," arXiv: 0907.5587 [hep-ph] (2009) (cit. on p. 15).

[45] W. M. Fairbairn, T. Fulton, and W. H. Klink, "Finite and disconnected subgroups of SU_3 and their application to the elementary-particle spectrum," J. Math. Phys. **5**, 1038 (1964) (cit. on p. 17).

[46] P. O. Ludl, "On the finite subgroups of $U(3)$ of order smaller than 512," J. Phys. A **A43**, 395204, arXiv: 1006.1479 [math-ph] (2010) (cit. on p. 17).

[47] N. Deshpande, M. Gupta, and P. B. Pal, "Flavor changing processes and *CP* violation in $S_3 \times Z_3$ model," Phys. Rev. **D45**, 953 (1992) (cit. on p. 20).

[48] S.-L. Chen, M. Frigerio, and E. Ma, "Large neutrino mixing and normal mass hierarchy: a discrete understanding," Phys. Rev. **D70**, 073008, arXiv: hep-ph/0404084 [hep-ph] (2004) (cit. on pp. 21, 28–30, 32, 47).

[49] C. Luhn, S. Nasri, and P. Ramond, "The flavor group $\Delta(3n^2)$," J. Math. Phys. **48**, 073501, arXiv: hep-th/0701188 [hep-th] (2007) (cit. on pp. 22, 24, 25, 27).

[50] M. J. Bowick and P. Ramond, "Calculable masses in grand unified theories," Phys. Lett. **B103**, 338 (1981) (cit. on p. 27).

[51] G. Feinberg and F. Gursey, "Approximate symmetries in the two-neutrino theory," Phys. Rev. **128**, 378 (1962) (cit. on p. 27).

[52] S. Meshkov and S. P. Rosen, "Lepton symmetry," Phys. Rev. Lett. **29**, 1764 (1972) (cit. on p. 27).

[53] F. Wilczek and A. Zee, "Horizontal interaction and weak mixing angles," Phys. Rev. Lett. **42**, 421 (1979) (cit. on p. 27).

[54] E. Ma, "Non-Abelian discrete symmetries and neutrino masses: two examples," New J. Phys. **6**, 104, arXiv: hep-ph/0405152 [hep-ph] (2004) (cit. on p. 27).

[55] C. H. Albright and M.-C. Chen, "Model predictions for neutrino oscillation parameters," Phys. Rev. **D74**, 113006, arXiv: hep-ph/0608137 [hep-ph] (2006) (cit. on p. 27).

[56] E. Ma, 2007 (cit. on p. 27).

[57] G. Altarelli and F. Feruglio, "Discrete flavor symmetries and models of neutrino mixing," Rev. Mod. Phys. **82**, 2701, arXiv: 1002.0211 [hep-ph] (2010) (cit. on p. 27).

[58] D. B. Reiss, "Can the family group be a global symmetry?" Phys. Lett. **B115**, 217 (1982) (cit. on p. 27).

[59] R. Barbieri and L. Hall, "Flavon models for the 17 keV neutrino," Nucl. Phys. **B364**, 27 (1991) (cit. on p. 27).

[60] F. Feruglio et al., "Lepton flavour violation in a supersymmetric model with A_4 flavour symmetry," Nucl. Phys. **B832**, 251, arXiv: 0911.3874 [hep-ph] (2010) (cit. on p. 27).

[61] S. Pakvasa and H. Sugawara, "Discrete symmetry and Cabibbo angle," Phys. Lett. **B73**, 61 (1978) (cit. on p. 28).

[62] E. Ma, "Two derivable relationships among quark masses and mixing angles," Phys. Rev. **D43**, 2761 (1991) (cit. on p. 28).

[63] E. Ma, "Permutation symmetry for neutrino and charged lepton mass matrices," Phys. Rev. **D61**, 033012, arXiv: hep-ph/9909249 [hep-ph] (2000) (cit. on p. 28).

[64] R. Mohapatra, A. Perez-Lorenzana, and C. A. de Sousa Pires, "Type II seesaw and a gauge model for the bimaximal mixing explanation of neutrino puzzles," Phys. Lett. **B474**, 355, arXiv: hep-ph/9911395 [hep-ph] (2000) (cit. on p. 28).

[65] P. Harrison and W. Scott, "Permutation symmetry, tri-bimaximal neutrino mixing and the S_3 group characters," Phys. Lett. **B557**, 76, arXiv: hep-ph/0302025 [hep-ph] (2003) (cit. on pp. 28, 76).

[66] W. Grimus and L. Lavoura, "$S_3 \times Z_2$ model for neutrino mass matrices," JHEP **0508**, 013, arXiv: hep-ph/0504153 [hep-ph] (2005) (cit. on p. 28).

[67] S. Morisi and M. Picariello, "The flavor physics in unified gauge theory from an $S_3 \times P$ discrete symmetry," Int. J. Theor. Phys. **45**, 1267, arXiv: hep-ph/0505113 [hep-ph] (2006) (cit. on p. 28).

[68] T. Teshima, "Flavor mass and mixing and S_3 symmetry: an S_3 invariant model reasonable to all," Phys. Rev. **D73**, 045019, arXiv: hep-ph/0509094 [hep-ph] (2006) (cit. on p. 28).

[69] R. Mohapatra, S. Nasri, and H.-B. Yu, "S_3 symmetry and tri-bimaximal mixing," Phys. Lett. **B639**, 318, arXiv: hep-ph/0605020 [hep-ph] (2006) (cit. on p. 28).

[70] Q.-H. Cao et al., "Probing lepton flavor triality with Higgs boson decay," Phys. Rev. **D83**, 093012, arXiv: 1103.0008 [hep-ph] (2011) (cit. on pp. 28, 69).

[71] P. Dong et al., "The S_3 flavor symmetry in 3–3–1 models," Phys. Rev. **D85**, 053001, arXiv: 1111.6360 [hep-ph] (2012) (cit. on p. 28).

[72] T. Teshima, "Higgs potential in S_3 invariant model for quark/lepton mass and mixing," Phys. Rev. **D85**, 105013, arXiv: 1202.4528 [hep-ph] (2012) (cit. on p. 28).

[73] D. Meloni, "S_3 as a flavour symmetry for quarks and leptons after the Daya Bay result on θ_{13}," JHEP **1205**, 124, arXiv: 1203.3126 [hep-ph] (2012) (cit. on p. 28).

[74] S. Dev, R. R. Gautam, and L. Singh, "Broken S_3 symmetry in the neutrino mass matrix and nonzero θ_{13}," Phys. Lett. **B708**, 284, arXiv: 1201.3755 [hep-ph] (2012) (cit. on p. 28).

[75] S. Zhou, "Relatively large θ_{13} and nearly maximal θ_{23} from the approximate S_3 symmetry of lepton mass matrices," Phys. Lett. **B704**, 291, arXiv: 1106.4808 [hep-ph] (2011) (cit. on p. 28).

[76] J. Kubo, H. Okada, and F. Sakamaki, "Higgs potential in minimal S_3 invariant extension of the standard model," Phys. Rev. **D70**, 036007, arXiv: hep-ph/0402089 [hep-ph] (2004) (cit. on pp. 29, 36).

[77] P. Leser, "Phenomenological consequences of an S_3 flavor symmetric extension of the standard model," MA thesis (TU Dortmund, 2009) (cit. on p. 30).

[78] S. L. Glashow and S. Weinberg, "Natural conservation laws for neutral currents," Phys. Rev. **D15**, 1958 (1977) (cit. on p. 35).

[79] F. Botella, G. Branco, and M. Rebelo, "Minimal flavour violation and multi-Higgs models," Phys. Lett. **B687**, 194, arXiv: 0911.1753 [hep-ph] (2010) (cit. on p. 35).

[80] J. Kubo et al., "The flavor symmetry," Prog. Theor. Phys. **109**, 795, arXiv: hep-ph/0302196 [hep-ph] (2003) (cit. on p. 36).

[81] Y. Yamanaka, H. Sugawara, and S. Pakvasa, "Permutation symmetries and the fermion mass matrix," Phys. Rev. **D25**, 1895 (1982) (cit. on p. 36).

[82] D. Lopez-Val and J. Sola, "Neutral Higgs-pair production at linear colliders within the general 2HDM: quantum effects and triple Higgs boson self-interactions," Phys. Rev. **D81**, 033003, arXiv: 0908.2898 [hep-ph] (2010) (cit. on p. 36).

[83] A. Djouadi, J. Kalinowski, and M. Spira, "HDECAY: A program for Higgs boson decays in the standard model and its supersymmetric extension," Comput. Phys. Commun. **108**, 56, arXiv: hep-ph/9704448 [hep-ph] (1998) (cit. on p. 37).

[84] S. Schael et al., "Search for neutral MSSM Higgs bosons at LEP," Eur. Phys. J. **C47**, 547, arXiv: hep-ex/0602042 [hep-ex] (2006) (cit. on p. 37).

[85] S. Schael et al., "Search for neutral Higgs bosons decaying into four taus at LEP2," JHEP **1005**, 049, arXiv: 1003.0705 [hep-ex] (2010) (cit. on p. 37).

[86] S. Chang, P. J. Fox, and N. Weiner, "Naturalness and Higgs decays in the MSSM with a singlet," JHEP **0608**, 068, arXiv: hep-ph/0511250 [hep-ph] (2006) (cit. on p. 37).

[87] S. Chang, P. J. Fox, and N. Weiner, "Visible cascade Higgs decays to four photons at hadron colliders," Phys. Rev. Lett. **98**, 111802, arXiv: hep-ph/0608310 [hep-ph] (2007) (cit. on p. 37).

[88] S. Chatrchyan et al., arXiv: 1205.5736 [hep-ex] (2012) (cit. on p. 47).

[89] G. Aad et al., "Search for charged Higgs bosons decaying via $H^+ \to \tau\nu$ in top quark pair events using pp collision data at $\sqrt{(}s) = 7$ TeV with the ATLAS detector," JHEP **1206**, 039, arXiv: 1204.2760 [hep-ex] (2012) (cit. on p. 47).

[90] T. Lee, "A theory of spontaneous T violation," Phys. Rev. **D8**, 1226 (1973) (cit. on pp. 51, 62).

[91] G. C. Branco, "Spontaneous CP violation in theories with more than four quarks," Phys. Rev. Lett. **44**, 504 (1980) (cit. on pp. 51, 62).

[92] R. N. Mohapatra and G. Senjanovic, "Natural suppression of strong P and T noninvariance," Phys. Lett. **B79**, 283 (1978) (cit. on p. 51).

[93] H. Georgi, "A model of soft CP violation," Hadronic J. **1**, 155 (1978) (cit. on p. 51).

[94] S. M. Barr and P. Langacker, "A superweak gauge theory of CP violation," Phys. Rev. Lett. **42**, 1654 (1979) (cit. on p. 51).

[95] A. E. Nelson, "Naturally weak CP violation," Phys. Lett. **B136**, 387 (1984) (cit. on p. 51).

[96] S. M. Barr, "Solving the strong CP problem without the Peccei-Quinn symmetry," Phys. Rev. Lett. **53**, 329 (1984) (cit. on p. 51).

[97] J. E. Kim, "Light pseudoscalars, particle physics and cosmology," Phys. Rept. **150**, 1 (1987) (cit. on p. 51).

[98] R. Peccei, "The strong CP problem," Adv. Ser. Direct. High Energy Phys. **3**, 503 (1989) (cit. on p. 51).

[99] H.-Y. Cheng, "The strong CP problem revisited," Phys. Rept. **158**, 1 (1988) (cit. on p. 51).

[100] S. Abel, S. Khalil, and O. Lebedev, "EDM constraints in supersymmetric theories," Nucl. Phys. **B606**, 151, arXiv: hep-ph/0103320 [hep-ph] (2001) (cit. on p. 51).

[101] E. Witten, "Some properties of O(32) superstrings," Phys. Lett. **B149**, 351 (1984) (cit. on p. 51).

[102] A. Strominger and E. Witten, "New manifolds for superstring compactification," Commun. Math. Phys. **101**, 341 (1985) (cit. on p. 51).

[103] M. Dine, R. G. Leigh, and D. A. MacIntire, "Of CP and other gauge symmetries in string theory," Phys. Rev. Lett. **69**, 2030, arXiv: hep-th/9205011 [hep-th] (1992) (cit. on p. 51).

[104] G. Branco, J. Gerard, and W. Grimus, "Geometrical T violation," Phys. Lett. **B136**, 383 (1984) (cit. on pp. 52, 54, 62, 64).

[105] J. Escobar and C. Luhn, "The flavor group $\Delta(6n^2)$," J. Math. Phys. **50**, 013524, arXiv: 0809.0639 [hep-th] (2009) (cit. on p. 52).

[106] I. de Medeiros Varzielas and D. Emmanuel-Costa, "Geometrical CP violation," Phys. Rev. **D84**, 117901, arXiv: 1106.5477 [hep-ph] (2011) (cit. on pp. 52, 54, 57, 62, 64).

[107] S. Weinberg, "Perturbative calculations of symmetry breaking," Phys. Rev. **D7**, 2887 (1973) (cit. on p. 52).

[108] H. Georgi and A. Pais, "CP-violation as a quantum effect," Phys. Rev. **D10**, 1246 (1974) (cit. on p. 52).

[109] I. de Medeiros Varzielas, "Geometrical CP violation in multi-Higgs models," JHEP **1208**, 055, arXiv: 1205.3780 [hep-ph] (2012) (cit. on p. 62).

[110] I. de Medeiros Varzielas, R. Gonzalez Felipe, and H. Serodio, "Leptonic mixing, family symmetries and neutrino phenomenology," Phys. Rev. **D83**, 033007, arXiv: 1101.0602 [hep-ph] (2011) (cit. on p. 67).

[111] E. Ma, "Neutrino mass matrix from $\Delta(27)$ symmetry," Mod. Phys. Lett. **A21**, 1917, arXiv: hep-ph/0607056 [hep-ph] (2006) (cit. on p. 68).

[112] R. de Adelhart Toorop, F. Bazzocchi, L. Merlo, and A. Paris, "Constraining flavour symmetries at the EW scale I: The A_4 Higgs potential," JHEP **1103**, 035, arXiv: 1012.1791 [hep-ph] (2011) (cit. on p. 68).

[113] R. de Adelhart Toorop, F. Bazzocchi, L. Merlo, and A. Paris, "Constraining flavour symmetries at the EW scale II: The fermion processes," JHEP **1103**, 040, arXiv: 1012.2091 [hep-ph] (2011) (cit. on p. 68).

[114] L. Lavoura and J. P. Silva, "Fundamental CP violating quantities in a SU(2) × U(1) model with many Higgs doublets," Phys. Rev. **D50**, 4619, arXiv: hep-ph/9404276 [hep-ph] (1994) (cit. on p. 69).

[115] E. Ma, "Quark and lepton flavor triality," Phys. Rev. **D82**, 037301, arXiv: 1006.3524 [hep-ph] (2010) (cit. on p. 69).

[116] S. Antusch, J. Kersten, M. Lindner, and M. Ratz, "Running neutrino masses, mixings and CP phases: analytical results and phenomenological consequences," Nucl. Phys. **B674**, 401, arXiv: hep-ph/0305273 [hep-ph] (2003) (cit. on pp. 75, 79).

[117] M. Galassi, J. Davies, J. Theiler, B. Gough, G. Jungman, P. Alken, M. Booth, and F. Rossi, *GNU Scientific Library Reference Manual*, 3rd (Network Theory Limited, 2009) (cit. on p. 79).

[118] H. Klapdor-Kleingrothaus, H. Päs, and A. Smirnov, "Neutrino mass spectrum and neutrinoless double beta decay," Phys. Rev. **D63**, 073005, arXiv: hep-ph/0003219 [hep-ph] (2001) (cit. on p. 80).

[119] H. Päs and T. J. Weiler, "Absolute neutrino mass determination," Phys. Rev. **D63**, 113015, arXiv: hep-ph/0101091 [hep-ph] (2001) (cit. on p. 80).

[120] S. Petcov, "Neutrino masses, mixing, Majorana CP-violating phases and $\beta\beta0\nu$ decay," New J. Phys. **6**, 109 (2004) (cit. on p. 80).

[121] M. Lindner, A. Merle, and W. Rodejohann, "Improved limit on θ_{13} and implications for neutrino masses in neutrino-less double beta decay and cosmology," Phys. Rev. **D73**, 053005, arXiv: hep-ph/0512143 [hep-ph] (2006) (cit. on p. 80).

[122] L. J. Hall, H. Murayama, and N. Weiner, "Neutrino mass anarchy," Phys. Rev. Lett. **84**, 2572, arXiv: hep-ph/9911341 [hep-ph] (2000) (cit. on p. 83).

[123] M. Hirsch, "Comment on: neutrino mass anarchy," arXiv: hep-ph/0102102 [hep-ph] (2001) (cit. on p. 83).

[124] A. de Gouvea and H. Murayama, "Statistical test of anarchy," Phys. Lett. **B573**, 94, arXiv: hep-ph/0301050 [hep-ph] (2003) (cit. on p. 83).

[125] G. Altarelli, F. Feruglio, and I. Masina, "Models of neutrino masses: anarchy versus hierarchy," JHEP **0301**, 035, arXiv: hep-ph/0210342 [hep-ph] (2003) (cit. on p. 83).

[126] N. Arkani-Hamed, S. Dimopoulos, G. Dvali, and J. March-Russell, "Neutrino masses from large extra dimensions," Phys. Rev. **D65**, 024032, arXiv: hep-ph/9811448 [hep-ph] (2002) (cit. on p. 83).

[127] R. V. Buniy and T. W. Kephart, "A model of glueballs," Phys. Lett. **B576**, 127, arXiv: hep-ph/0209339 [hep-ph] (2003) (cit. on p. 83).

[128] R. V. Buniy and T. W. Kephart, "Glueballs and the universal energy spectrum of tight knots and links," Int. J. Mod. Phys. **A20**, 1252, arXiv: hep-ph/0408027 [hep-ph] (2005) (cit. on p. 83).

[129] R. V. Buniy, M. J. Holmes, and T. W. Kephart, "Knotting and higher order linking in physical systems," arXiv: 1010.5832 [hep-ph] (2010) (cit. on p. 83).

[130] T. Ashton, J. Cantarella, M. Piatek, and E. Rawdon, "Knot tightening by constrained gradient descent," Exp. Math. **20**, 57, arXiv: 1002.1723v1 [math.DG] (2011) (cit. on pp. 84, 91).

[131] J. Urrestilla, N. Bevis, M. Hindmarsh, and M. Kunz, "Cosmic string parameter constraints and model analysis using small scale cosmic microwave background data," JCAP **1112**, 021, arXiv: 1108.2730 [astro-ph.CO] (2011) (cit. on p. 86).

[132] S. Olmez, V. Mandic, and X. Siemens, "Gravitational-wave stochastic background from kinks and cusps on cosmic strings," Phys. Rev. **D81**, 104028, arXiv: 1004.0890 [astro-ph.CO] (2010) (cit. on p. 86).

Acknowledgments

I wish to express my gratitude to my advisor Prof. Dr. Heinrich Päs, who guided and supported this work throughout the years and gave me many opportunities to learn, travel, and collaborate.

I am also deeply grateful to Prof. Dr. Gautam Bhattacharyya for countless insightful discussions and successful collaboration on many projects during his visits in Dortmund and during my visit at the Saha Institute in Kolkata.

It was also a pleasure to work with Dr. Ivo de Medeiros Varzielas during the last two years. I am very thankful for his support and encouragement as well as for the opportunity to collaborate.

I would like to thank Prof. Dr. Tom Kephart and Dr. David Emmanuel-Costa for giving me the opportunity to collaborate.

This project would not have been possible without the support of the *Studienstiftung des deutschen Volkes*, represented by my liaison lecturer Prof. Dr. Bernhard Spaan.

Nicht zuletzt danke ich meinen Eltern, Christel und Heribert Leser, sowie meiner gesamten Familie, die mich während des Promotionsprojektes unterstützte.